

Design and Synthesis of Functionalized Mn(III) Dipyrrromethene Complexes as
Peroxynitrite Decomposition Catalysts

by Eliwaza Naomi Shadrack Msengi, Bachelor of Science

A Thesis Submitted in Partial
Fulfillment of the Requirements
for the Degree
Master of Science
in the field of Chemistry

Advisory Committee:

William L. Neumann, Chair

Yun Lu

Gium Kwon

Marcelo Nieto

Graduate School
Southern Illinois University Edwardsville
December, 2014

UMI Number: 1572743

All rights reserved

INFORMATION TO ALL USERS

The quality of this reproduction is dependent upon the quality of the copy submitted.

In the unlikely event that the author did not send a complete manuscript and there are missing pages, these will be noted. Also, if material had to be removed, a note will indicate the deletion.



UMI 1572743

Published by ProQuest LLC (2015). Copyright in the Dissertation held by the Author.

Microform Edition © ProQuest LLC.

All rights reserved. This work is protected against unauthorized copying under Title 17, United States Code



ProQuest LLC.
789 East Eisenhower Parkway
P.O. Box 1346
Ann Arbor, MI 48106 - 1346

ABSTRACT

DESIGN AND SYNTHESIS OF FUNCTIONALIZED MANGANESE(III) DIPYRROMETHENE COMPLEXES AS PEROXYNITRITE DECOMPOSITION CATALYSTS

by

ELIWAZA NAOMI SHADRACK MSENGI

Chairperson: Professor William L. Neumann

The excessive production of peroxynitrite (ONOO^-) anion is well-known to play a significant role in numerous diseases including chronic inflammation, Type II Diabetes Mellitus (T2DM), Alzheimer's, and Parkinson's. The highly reactive peroxynitrite (PN) is known to nitrate and oxidize proteins, lipids, and nucleotides thus generating toxicity. Thus, our objective was to design and synthesize complexes that can attenuate the toxic effects of PN *in vivo* for pharmacological studies and potential therapeutic strategies. Redox-active Manganese(III) complexes of bis(hydroxyphenyl)-dipyrromethenes (Mn(III)-DPMs) are able to catalytically destroy PN by converting PN to nitrite ion through a two electron mechanism. Herein, synthetic methods for preparing functionalized Mn(III)-DPMs with enhanced solubility and a conjugation site for the attachment of biomolecules were studied. Since both Mn(III)-DPMs and peroxisome proliferator-activated receptor γ (PPAR γ) agonist have been shown to be active and effective in treating T2DM, we hypothesized that the conjugate of our Mn(III)-DPM and a functional PPAR γ agonist may have a synergistic effect in this condition. In addition, if synergistic action is observed it may be possible to reduce to dose of PPAR γ agonist. Structure-activity studies using boronate oxidation and the prevention-of-nitration assays were used to determine catalytic activity and the characteristics of these assays were examined and improved. In addition, the development

oxidant-triggered aza-bis(hydroxylphenyl)dipyrromethene (*aza*-DPM) pro-catalyst systems was also explored.

ACKNOWLEDGEMENTS

First and foremost, I would like to acknowledge my research advisor, Dr. William L. Neumann for his guidance, patience and encouragement throughout my research endeavors and graduate studies.

A special thanks to my research committee, Dr. Yun Lu, Dr. Gium Kwon, Dr. Marcelo Nieto, and Dr. Timothy McPherson, for their valuable advice and support throughout the duration of this project.

Departments of pharmaceutical sciences, department of chemistry, and SIUE graduate school for giving me the opportunity and the resources to learn and grow intellectually.

My labmates, past and present, especially Maryam Imani Nejad and Lyle Pratt for their support.

Last but not least, all my friends who have been with me throughout my academic and personal journey, thank you.

DEDICATION

This thesis is dedicated to my loving parents, Shadrack and Neema Msengi for their words of wisdom, encouragement, and unconditional love and support. I am very grateful for all you have done and continue to do for me. In addition, a special thanks to my brothers Gabriel, Samuel, and Edward for continuing to bring me love, joy, and laughter into my life.

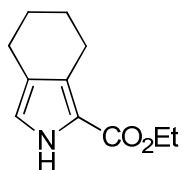
TABLE OF CONTENTS

ABSTRACT	ii	
ACKNOWLEDGENTS	iv	
DEDICATIONS.....	v	
LIST OF COMPOUNDS	ix	
LIST OF SCHEMES.....	xxi	
LIST OF FIGURES	xxiii	
LIST OF TABLES.....	xxiv	
ABBREVIATIONS	xxv	
Chapter		
I. PEROXYNITRITE: BIOCHEMICAL ORIGINS AND BIOLOGICAL EFFECTS		1
Protein Tyrosine Nitration.....		4
The Effect of Protein Nitration on Biological Molecules.....		6
II. DESIGN OF PEROXYNITRITE DECOMPOSITION CATALYSTS (PNDCs).....		10
Metalloporphyrins.....		10
Metalloporphyrins.....		10
Metalloporphyrins.....		15
Metallo-bis(hydroxyphenyl)-dipyrromethenes		16
III. RESEARCH OBJECTIVES AND SYNTHESIS		18
Part I. Synthesis of Functionalized Mn(III)-DPM Catalysts		19
Synthesis of Mn(III)- <i>meso</i> -(PEG-amide)-DPM 15		23
Characterization of Compounds 13 and 15		24
Part II. Synthesis of aza-DPM Ligand Systems.....		26
Part III. Future Direction: aza-DPMs as Oxidant-Activated PNDCs.....		29
IV. EVALUATION OF PNDCs ACTIVITY		32
Boronate Oxidation Assay		32
Results and Discussion		33
Prevention of Tyrosine Nitration Assay		42
Results and Discussion		44
Synthesis of Phe-Leu-OMe (33)		46

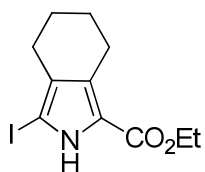
Synthesis of Boc-Tyr(OBn)-Gly-Gly-Phe-Leu-OMe (39)	46
Synthesis of LENK	47
Synthesis of Boc-Tyr(3-nitro)-Gly-Gly-OH (46)	48
Synthesis of Nitro-LENK	48
V. FUTURE DIRECTIONS: TARGETING PEROXYNITRITE IN T2DM.....	50
PPAR γ agonist/PNDC Conjugate Design.....	51
Synthesis of SR110/PPAR γ Conjugate.....	52
VI. CONCLUSION.....	54
VII. EXPERIMENTAL	56
General Method	56
Ethyl 4,5,6,7-tetrahydro-2 <i>H</i> -isoindole-1-carboxylate (1).....	57
Ethyl -3-iodo-4, 5, 6, 7-tetrahydro-2 <i>H</i> -isoindole carboxylate (2)	58
Ethyl 2- <i>tert</i> -butyl 1-3-iodo-4,5,6,7-tetrahydro-2 <i>H</i> -isoindole-1,2- dicarboxylate (4)	59
Ethyl 2- <i>tert</i> -butyl-1-3-(2-methoxyphenyl)-4,5,6,7-tetrahydro-2 <i>H</i> -isoindole- 1,2-dicarboxylate (6).....	60
Ethyl -3-bromo-4, 5, 6, 7-tetrahydro-2 <i>H</i> -isoindole carboxylate (3)	61
Ethyl 2- <i>tert</i> -butyl-1-3-bromo-4,5,6,7-tetrahydro-2 <i>H</i> -isoindole-1,2- dicarboxylate (5)	61
Ethyl 2- <i>tert</i> -butyl-1-3-(2-methoxyphenyl)-4,5,6,7-tetrahydro-2 <i>H</i> - isoindole-1,2-dicarboxylate (6).....	62
3-(2-Methoxyphenyl)-4,5,6,7-tetrahydro-2 <i>H</i> -isoindole-1- carboxylic acid (7)	63
3,3'-((4-Methoxyphenyl)methylene)-bis-(1-(2-methoxyphenyl)-4,5,6,7- tetrahydro-2 <i>H</i> -isoindole) (8).....	64
(<i>Z</i>)-3-(2-methoxyphenyl)-1-((4-methoxyphenyl)-(3-(2-methoxyphenyl)-4,5,6,7 tetrahydro-2 <i>H</i> -isoindol-1-yl)methylene)-4,5,6,7-tetrahydro- 1 <i>H</i> -isoindole (9).....	65
<i>meso</i> -(4-Hydroxyphenyl)-(O,N)-chelated-BODIPY 10	66
<i>meso</i> -4-(Methyl phenoxyacetate)-(O,N)-chelated-BODIPY 11	67
<i>meso</i> -4-(Phenoxyacetic acid)-(O,N)-chelated-BODIPY 12	68
<i>meso</i> -(PEG-amide)-(O,N)-chelated-BODIPY 13	69
<i>meso</i> -(PEG-amide)-(O,N)-DPM (14).....	71
Mn(III) <i>meso</i> -(PEG-amide)-(O,N)-DPM 15	72
Peptide Synthesis	74
Boc-Phe-Leu-OMe (32).....	74
Phe-Leu-OMe (33).....	75
Boc-Tyr(OBn)-Gly-OEt (35).....	75
Boc-Tyr(OBn)-Gly-OH (36).....	76
Boc-Tyr(OBn)-Gly-Gly-OEt (37).....	77

Boc-Tyr(OBn)-Gly-Gly-OH (38)	78
Boc-Tyr(OBn)-Gly-Gly-Phe-Leu-OMe (39).....	78
Boc-Tyr-Gly-Gly-Phe-Leu-OMe (40).....	79
Boc-Tyr-Gly-Gly-Phe-Leu-OH (41)	80
Tyr-Gly-Gly-Phe-Leu-OH (30)	80
Boc-Tyr(3-nitro)-OH (42)	81
Boc-Tyr(3-nitro)-Gly-OEt (43)	82
Boc-Tyr(3-nitro)-Gly-OH (44)	83
Boc-Tyr(3-nitro)-Gly-Gly-OEt (45).....	84
Boc-Tyr(3-nitro)-Gly-Gly-OH (46).....	85
Boc-Tyr(3-nitro)-Gly-Gly-Phe-Leu-OMe (47)	86
Boc-Tyr(3-nitro)-Gly-Gly-Phe-Leu-OH (48).....	87
Tyr(3-nitro)-Gly-Gly-Phe-Leu-OH (49)	88
Synthesis of the oxidant-activated systems	88
(<i>E</i>)-1-(2-Hydroxyphenyl)-3-(4-methoxyphenyl) prop-2-en-1-one (16).....	88
1-(2-Hydroxyphenyl)-3-(4-methoxyphenyl)-4-nitrobutan-1-one (19)	89
(<i>Z</i>)-2-(2-((5-(2-Hydroxyphenyl)-3-(4-methoxyphenyl)- <i>1H</i> -pyrrol-2-yl) imino)-3-(4-methoxyphenyl)-2 <i>H</i> -pyrrol-5-yl)phenol (22).....	90
Bis(methoxyphenyl)-aza-(<i>O,N</i>)-chelated BODIPY (26).....	90
(<i>E</i>)-3-(4-Bromophenyl)-1-(2-hydroxyphenyl)prop-2-en-1-one (17).....	91
3-(4-Bromophenyl)-1-(2-hydroxyphenyl)-4-nitrobutan-1-one (20).....	92
(<i>Z</i>)-2-(3-(4-Bromophenyl)-2-((3-(4-bromophenyl)-5-(2-hydroxyphenyl)- <i>1H</i> -pyrrol-2-yl)imino)-2 <i>H</i> -pyrrol-5-yl)phenol (23).....	92
(<i>E</i>)-1-(2-Hydroxyphenyl)-3-(4-iodophenyl)prop-2-en-1-one (18).....	93
1-(2-Hydroxyphenyl)-3-(4-iodophenyl)-4-nitrobutan-1-one (21).....	94
(<i>Z</i>)-2-(2-((5-(2-Hydroxyphenyl)-3-(4-iodophenyl)- <i>1H</i> -pyrrol-2-yl) imino)-3-(4-iodophenyl)-2 <i>H</i> -pyrrol-5-yl)phenol (24).....	94
Bis(iodophenyl)-aza-(<i>O,N</i>)-chelated BODIPY 25	95
PNDC Activity: Boronate Oxidation Assay.....	96
Percent Inhibition Sample Calculations.....	97
PNDC Activity: Prevention of Nitration Assay	99
REFERENCES	100

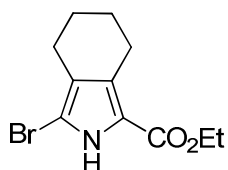
LIST OF COMPOUNDS



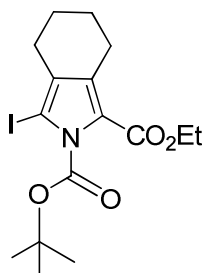
.....Compound 1



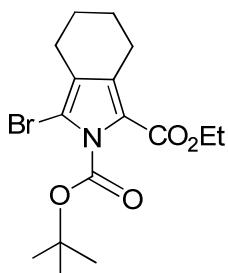
.....Compound 2



.....Compound 3

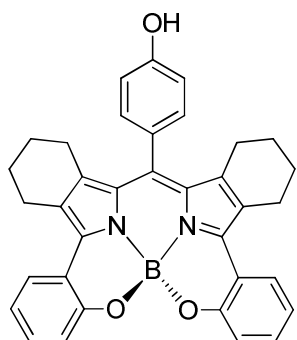


.....Compound 4

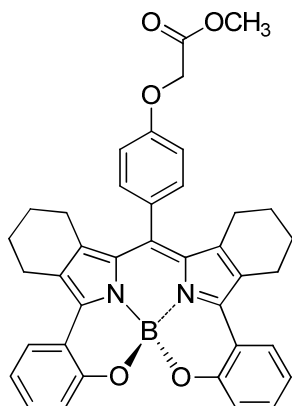


.....Compound 5

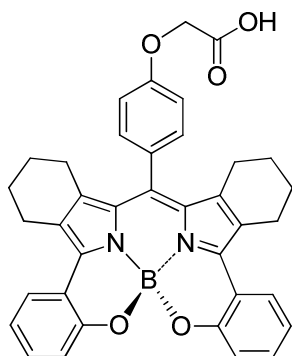
LIST OF COMPOUNDS



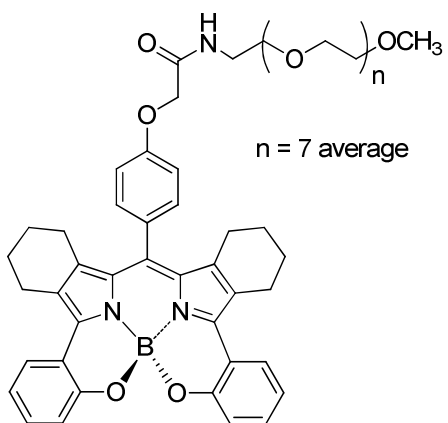
.....Compound 10



.....Compound 11

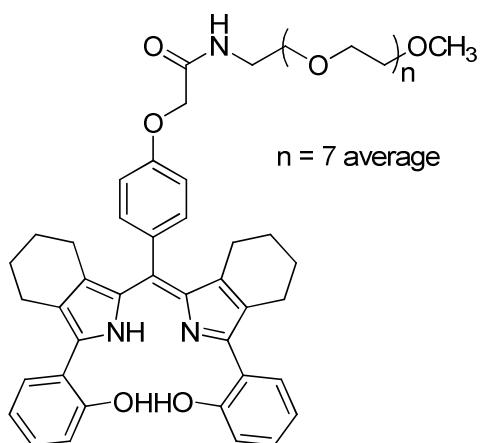


.....Compound 12

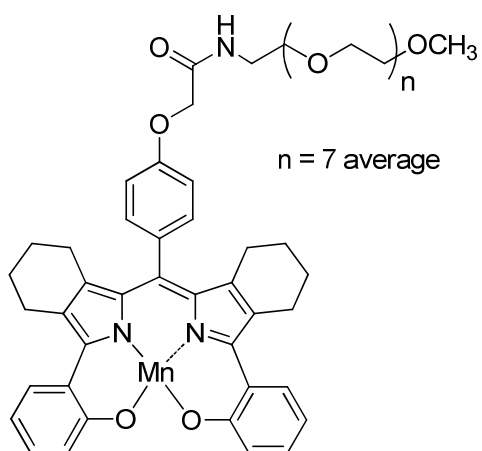


.....Compound 13

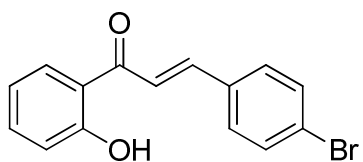
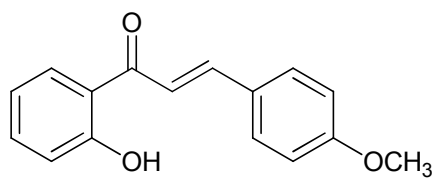
LIST OF COMPOUNDS



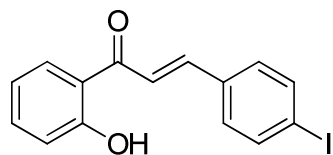
.....Compound 14



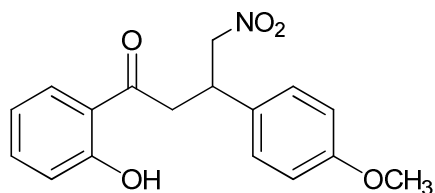
.....Compound 15



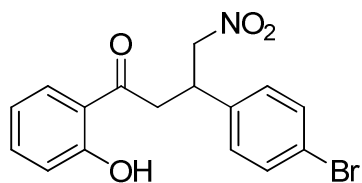
LIST OF COMPOUNDS



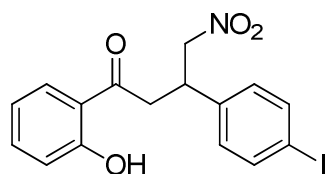
.....Compound **18**



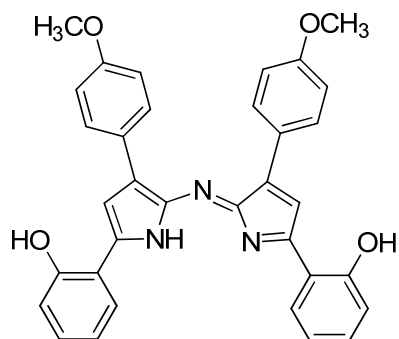
.....Compound **19**



.....Compound **20**

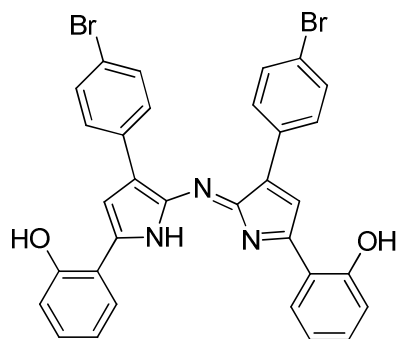


.....Compound **21**

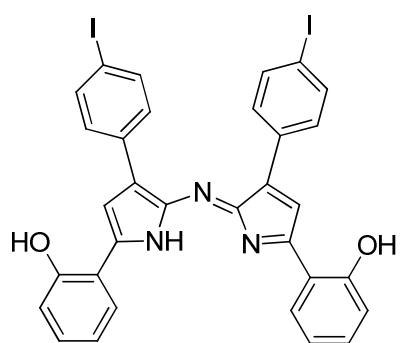


.....Compound **22**

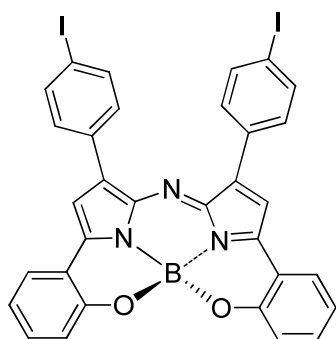
LIST OF COMPOUNDS



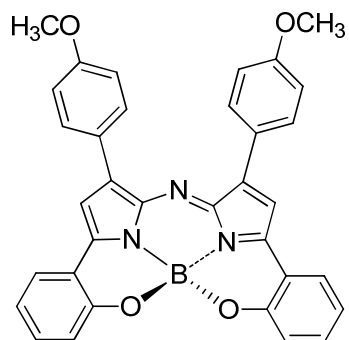
.....Compound 23



.....Compound 24

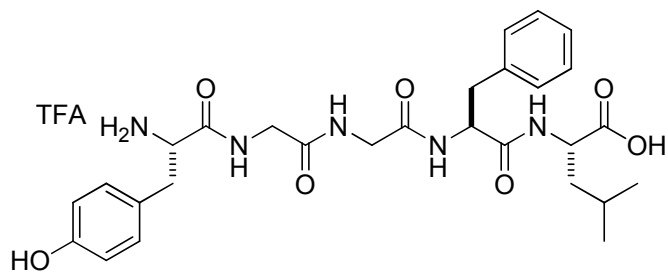
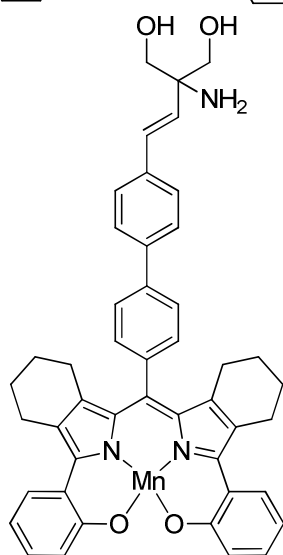
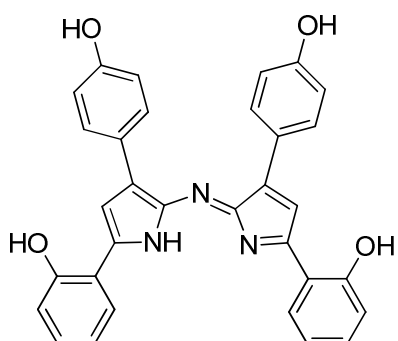
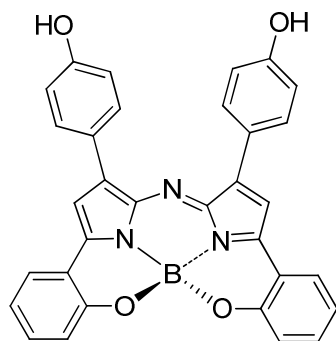


.....Compound 25

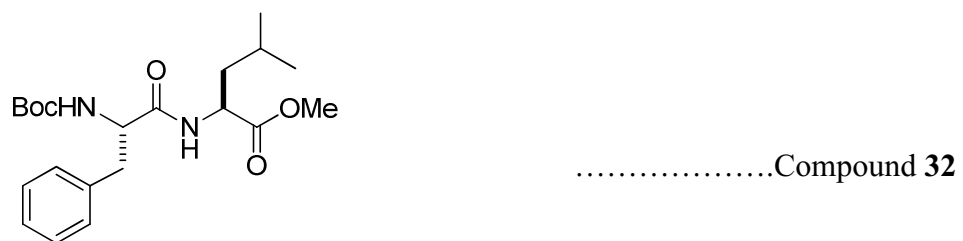
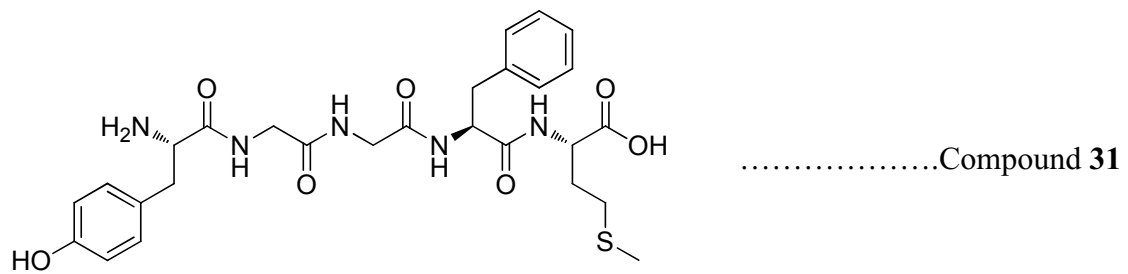


.....Compound 26

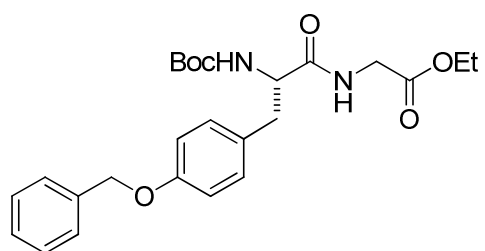
LIST OF COMPOUNDS



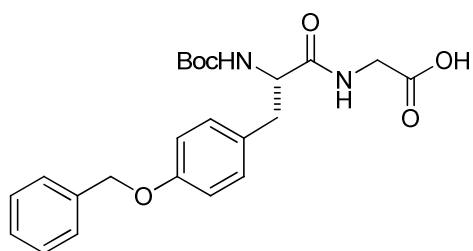
LIST OF COMPOUNDS



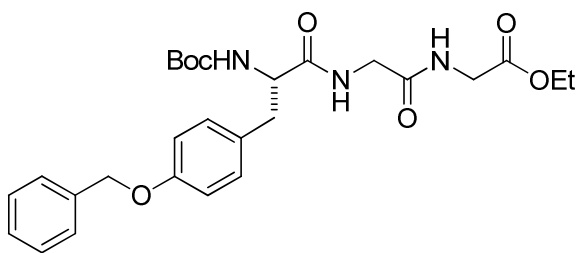
LIST OF COMPOUNDS



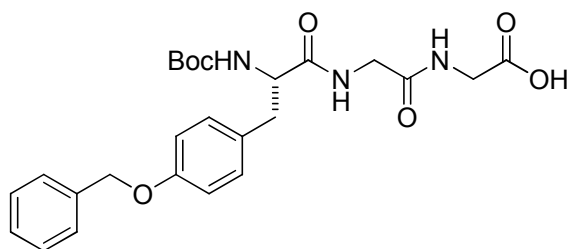
.....Compound 35



.....Compound 36

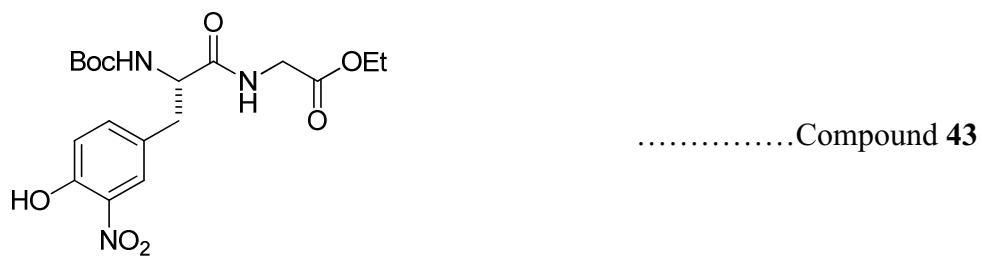
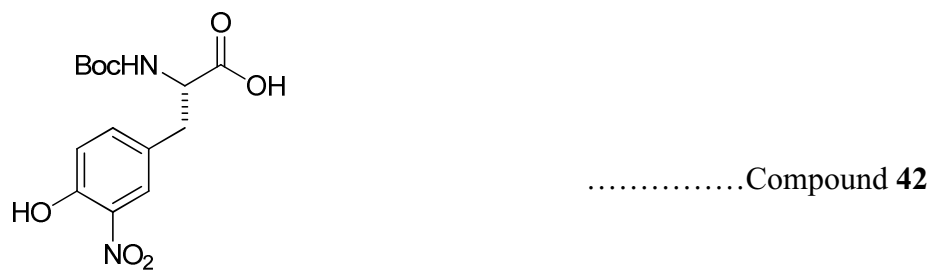
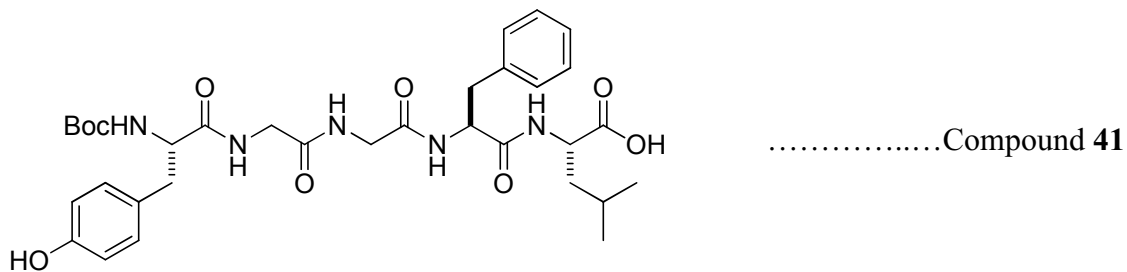
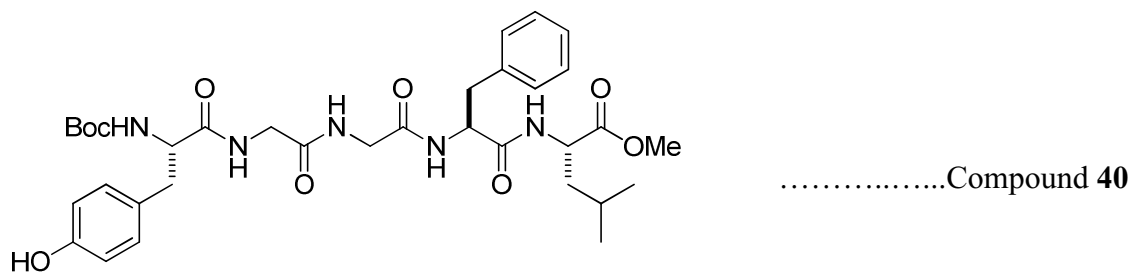
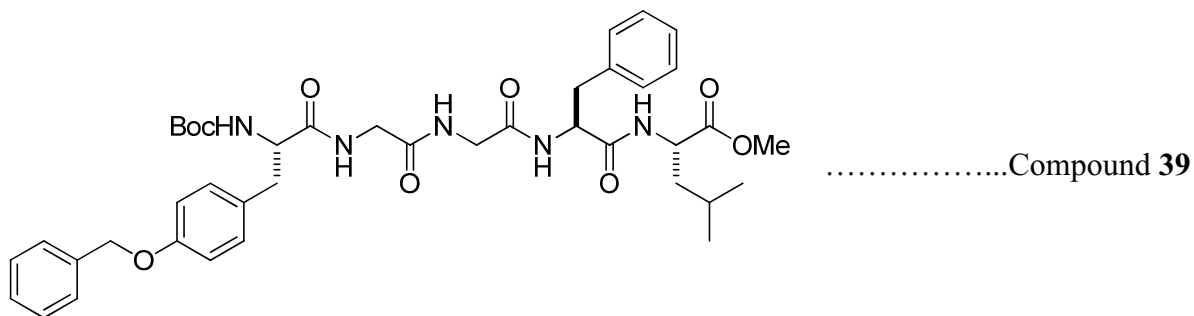


.....Compound 37

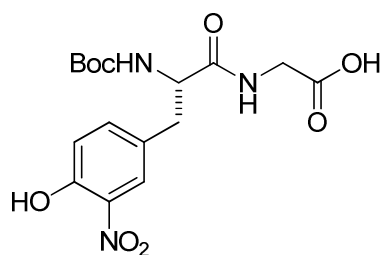


.....Compound 38

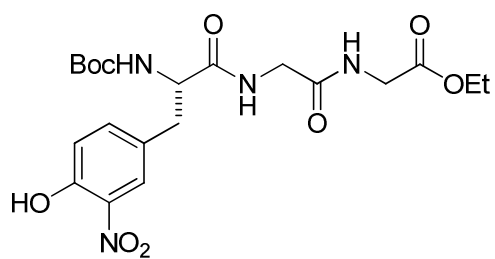
LIST OF COMPOUNDS



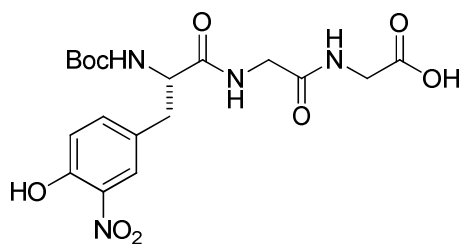
LIST OF COMPOUNDS



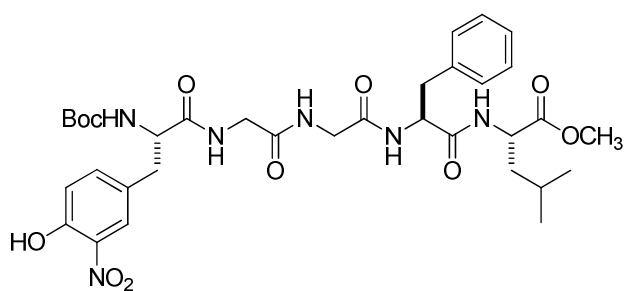
.....Compound 44



.....Compound 45

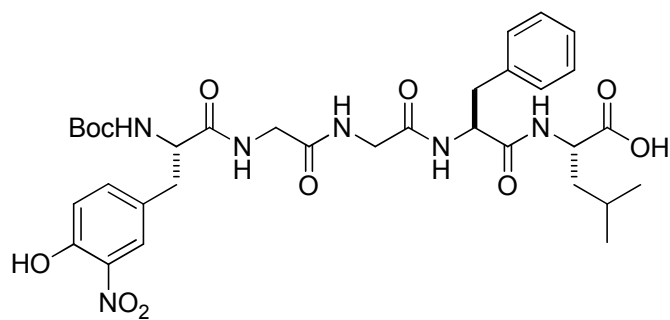


.....Compound 46

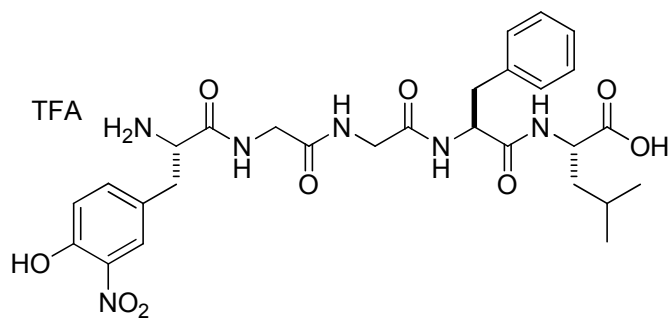


.....Compound 47

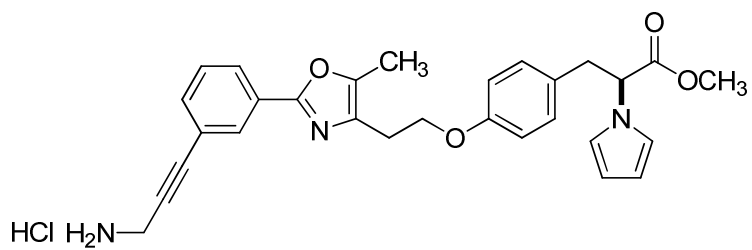
LIST OF COMPOUNDS



.....Compound **48**



.....Compound **49**



.....Compound **50**

LIST OF SCHEMES

Scheme

1. Biochemistry of Peroxynitrite (PN)	3
2. Mechanism of a Tyrosine Residue Nitration	5
3. PPAR γ Receptor Mode of Action	9
4. a) Metalloporphyrin, b) Metalloporphyrins, c) Metallo-bis(hydroxyphenyl)- dipyrromethenes.....	10
5. Detoxification of PN via Mn(III) porphyrin	12
6. Superoxide Dismutation by Mn(III) porphyrin, SODm.....	13
7. Catalytic Cycle of Mn(III) porphyrins with PN	16
8. PN Decomposition Activity of Mn(III)-DPMs.....	17
9. Synthesis of Ethyl 4,5,6,7-tetrahydro-2 <i>H</i> -isoindole-1-carboxylate (1).....	19
10. Barton-Zard Mechanism.....	20
11. Synthesis of Dipyrromethane Precursor 7	21
12. Synthesis of the Dipyrromethane Derivative 8	21
13. The Formation of Dipyrromethane 8 Mechanism.....	22
14. Conversion of the DPM Ligand to the Chelated-(<i>O,N</i>)-BODIPY Derivative 10	23
15. Synthesis of Mn(III)- <i>meso</i> -(PEG-amide)-DPM 15	23
16. General Synthesis of aza-DPM Ligand Analogues.....	27
17. Attempted Synthesis of a Linkable aza-BODIPY Analogue.....	28
18. Synthesis of bis(hydroxyphenyl)-aza-DPM Analogues.....	29
19. Oxidant Triggered Pro-catalyst.....	30

20. Oxidation of a Phenylboronic Acid to the Corresponding Phenol by PN.....	33
21. Nitration of LENK by PN.....	43
22. Synthesis of the Phe-Leu-OMe (33).....	46
23. Synthesis of Boc-Tyr(OBn)-Gly-Gly-Phe-Leu-OMe (39).....	47
24. Synthesis of the Natural Occurring Leu-enkaphalin 30	47
25. Synthesis of Boc-Tyr(3-nitro)-Gly-Gly-OH (46).....	48
26. Synthesis of Nitro-LENK 44	49
27. Synthesis of the PPAR γ / SR110 Conjugate.....	53

LIST OF FIGURES

Figure

1. General Structure of a Metalloporphrin Complex as a PNDC	11
2. Mn(III) tetracyclohexenylporphyrin chloride, SR6.....	14
3. Mn(III) bis-(<i>N</i> -methylpyridinium)-(4-methoxyphenyl) corrole.....	15
4. ¹ H NMR spectrum of Compound 13 in CDCl ₃ at 25 °C.....	25
5. LCMS analysis of SR110 and NM20 co-mixture.....	26
6. DPM and aza-DPM Structure Characteristics.....	27
7. PNDC Activity: Inhibition of the oxidation of 4-acetylphenylboronic acid.....	32
8. Mn(III)-tetrakis-(<i>meso-N</i> -methylpyridinium) porphyrin (MnTMPyP ⁵⁺) and Elbselen.....	34
9. General Structure of Surfactant with a PNDC Catalyst.....	36
10. The Complexes Tested for PNDC Activity.....	37
11. Brij-35 Micelle Structure.....	39
12. Sodium Dodecyl Sulfate (SDS) Micelle Structure.....	41
13. Leu-enkephalin 30 and Met-enkephalin 31 Chemical Structures.....	42
14. LCMS analysis of 1) PN + LENK; 2) PN + LENK + 1eq. SR110 and 3) PN + LENK + 1eq. SR6.....	44
15. Molecular Modeling Structure of PPAR γ Binding Domain.....	51
16. GI262570-FITC and PPAR γ Agonist Chemical Structures.....	52

LIST OF TABLES

Table

1. MnTMPyP ⁵⁺ and Ebselen Activity: Inhibition 4-acetylboronic acid Oxidation by PN.....	35
2. PNDC Inhibition of 4-acetylboronic acid Oxidation by PN using Brij-35 Surfactant.....	38
3. PNDC Inhibition of 4-acetylboronic acid Oxidation by PN using SDS Surfactant at pH 7.2	40
4. Tyrosine Nitration Prevention with varying SR135 Concentrations	44
5. UV-vis Data for <i>meso</i> -(PEG-amide)-(O,N)-chelated-BODIPY 13	70
6. UV-vis Data Mn(III) <i>meso</i> -(PEG-amide)-(O,N)-DPM (15).....	73
7. Example of SR135 Activity in 0.7% Brij-35 Buffer at pH 7.4.....	97

LIST OF ABBREVIATIONS

Tyr: Tyrosine

Leu: Leucine

Gly: Glycine

Phe: Phenylalanine

OBn: Benzyl ether protecting group

PNDC: Peroxynitrite Decomposition Catalyst

BF₃·OEt₂: Boron trifluoride diethyl etherate

DIPEA: N,N-(diisopropyl)ethylamine

EtOAc: Ethyl Acetate

TLC: Thin Layer Chromatography

LCMS: Liquid Chromatography-Mass Spectroscopy

BBr₃: Boron Tribromide

FeCl₃·6H₂O: Ferric (III) chloride hexahydrate

MeOH: Methanol

TEA: Triethylamine

HCl: Hydrochloric acid

TFA: Trifluoroacetic acid

BODIPY: Boron dipyrromethene

KOH: Potassium hydroxide

B(OCH₃)₃: Trimethyl borate

DPM: Dipyrromethene

NADPH Oxidase: Nicotinamide adenine dinucleotide phosphate oxidase

NBS: *N*-Bromosuccinimide

NIS: *N*-Iodosuccinimide

4-DMAP: 4-Dimethylaminopyridine

MnTMPyP⁵⁺: Mn(III)-tetrakis-(*meso-N*-methylpyridinium) porphyrin

p-chloranil: 2,3,5,6-Tetrabenzonquinone

EDC·HCl: 1-(3-Dimethylaminopropyl)-3-ethylcarbodiimide hydrochloride

Boc: Di-*tert*-butyl dicarbonate

CHAPTER I

PEROXYNITRITE: BIOCHEMICAL ORIGINS AND BIOLOGICAL EFFECTS

Over the past two decades, scientists world-wide have been focused on the development of novel synthetic molecules for preventing and treating various diseases associated with nitroxidative stress. Nitroxidative stress is caused by the overproduction of reactive nitrogen species (RNS) and reactive oxygen species (ROS). The potentially damaging molecules from these categories include superoxide radical anion ($O_2^{\cdot-}$), nitric oxide ($\cdot NO$), hydrogen peroxide (H_2O_2), the hydroxyl radical ($\cdot OH$) and, most importantly, peroxynitrite ($OONO^-$, PN).¹⁻³ When overproduced, these highly reactive oxygen-derived species are known to be central contributors to the development of chronic inflammatory diseases, cancer, aging, and neurodegenerative conditions, such as Alzheimer's and Parkinson's diseases.¹ However, minimal concentrations of ROS are crucial to the cell biological functions in that, they are signaling molecules that regulate cell proliferation, apoptosis and gene expression.¹⁻³ For my thesis research, we have focused on the biological significance of PN and its derived species. Rafael Radi defines PN as a powerful short-lived ($t_{1/2} \sim 10ms$ *in vivo*) species produced from the diffusion-controlled reaction ($k \sim 1.0 \times 10^{10} M^{-1} s^{-1}$) of $\cdot NO$ and $O_2^{\cdot-}$.²⁻³

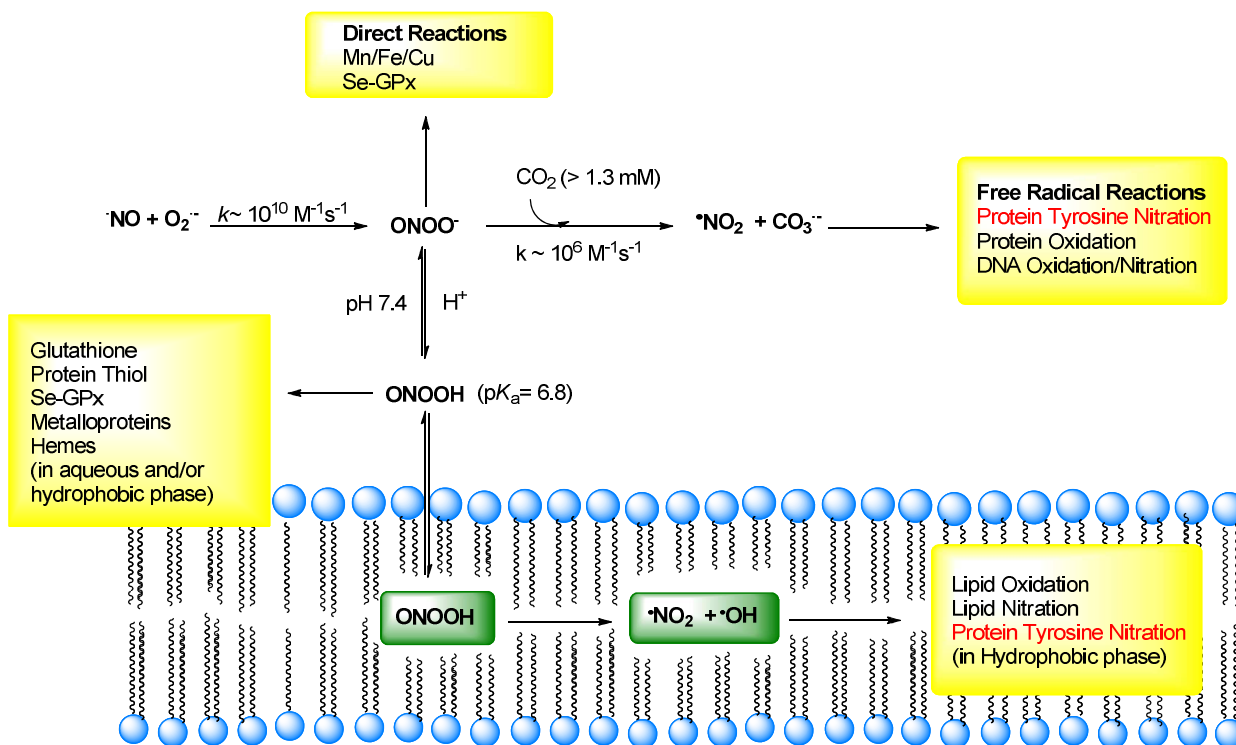
On the cellular level, the mitochondrion is the key loci for PN production, due to the tendency for $O_2^{\cdot-}$ to be produced as a side product during cellular respiration. $O_2^{\cdot-}$ is the one electron reduction product of molecular oxygen (O_2) and the key species from which most other important ROS are derived. The major sources of $O_2^{\cdot-}$ production originate from Complexes I and III (NADH dehydrogenase and cytochrome bc_1 complex, respectively) of the electron transport chain (ETC).

$\cdot\text{NO}$ is a key component in the development of nitroxidative stress. It is produced from the oxidation of L-arginine.^{5,6} This reaction is catalyzed by a family of nitric oxide synthase enzymes (NOS), which includes the three isoforms: inflammatory stimuli-inducible NOS (iNOS), and the constitutive forms neuronal and endothelial NOS (nNOS and eNOS, respectively).^{5,4} The three NOS isoforms are expressed in different tissues in the body and are also known to exhibit distinct functions.⁵ nNOS and eNOS are constitutively expressed to produce basal level of $\cdot\text{NO}$. nNOS is produced mainly in the nervous system and skeletal muscle tissues and functions in cell communication/signaling. Meanwhile, eNOS is expressed in endothelial tissues of blood vessels to regulate vasodilation and smooth muscle tone. On the other hand, iNOS is expressed in immune cells to produce higher concentrations of $\cdot\text{NO}$ in response to an inflammatory stimuli. Under normal physiological conditions, $\cdot\text{NO}$ (*in vivo* basal levels $\sim 200\text{-}1000$ nM) acts as signaling molecule and as a neurotransmitter.⁷ In the 1990s, $\cdot\text{NO}$ was shown to be the endothelial-derived relaxation factor (EDRF), an essential mediator of vasodilation. Interestingly, $\cdot\text{NO}$ is neutral and essentially non-polar. Thus, it is capable of diffusing easily through cell membranes.

PN is formed by a rapid reaction of $\text{O}_2^{\cdot-}$ with $\cdot\text{NO}$ and is considered the primary driver of nitroxidative stress. At physiological pH (*in vivo*, pH = 7.4), PN exists in equilibrium with its protonated form, peroxynitrous acid (ONOOH; $\text{pK}_a = 6.8$), as shown on equation 2.



Through either the acid or conjugate base form, PN can react directly or indirectly with biomolecules through one- and two-electron oxidation reactions, leading to cellular damage and toxicity.^{2,7}



Scheme 1: Biochemistry of peroxynitrite (PN)²

At the cellular level, the highly reactive PN has two main direct oxidation pathways with biomolecules (scheme 1).^{2, 3, 6} First, PN can interact directly with redox-active transition metal centers (manganese, iron, and copper), thiols and selenium enzymes (glutathione peroxidase; Se-GPx). Secondly, and most importantly, PN can react directly with carbon dioxide (CO₂). With millimolar concentrations of CO₂ present in cells, the reaction of PN and CO₂ governs most of the PN chemistry *in vivo*. The direct reaction of PN with CO₂ leads to the formation of nitrosoperoxocarbonate (ONOOCO₂⁻), a thermodynamically unstable adduct. Upon formation, this adduct immediately homolyzes into nitrogen dioxide radical (•NO₂) and carbonate radical anion (CO₃^{•-}). The formation of these highly reactive secondary free radicals forms the basis for the “indirect reactions of PN.” Through these secondary free radical species PN is able to nitrate and oxidize proteins and DNA via single-electron mechanisms.

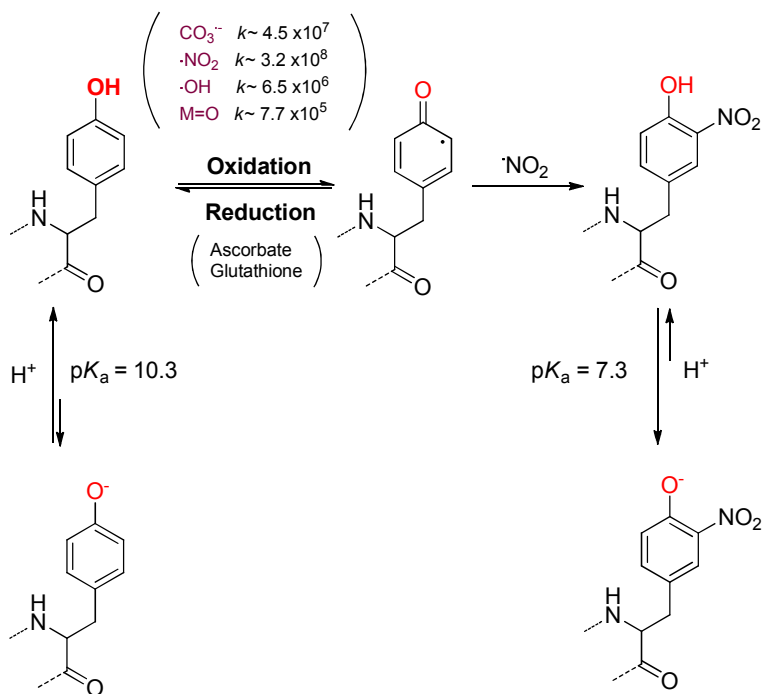
As mentioned above, at physiological pH a substantial amount of PN exists in its protonated form, ONOOH. Since the protonated form of PN is neutral and small, it readily diffuses into the lipid compartment of cell membranes.⁵⁶ In this hydrophobic environment, ONOOH can homolyze to produce NO_2^- and $\cdot\text{OH}$ radicals (~30% yield), while the other 70% isomerizes to nitrate (NO_3^-). NO_2^- and $\cdot\text{OH}$ oxidants can also lead to lipid peroxidation and protein and lipid nitration within the cell membrane by this pathway.⁵

In summary, PN can undergo direct nucleophilic attack on biomolecules, predominately with CO_2 *in vivo* producing $\cdot\text{NO}_2$ and CO_3^- . The protonated PN derivative (ONOOH) can also homolyze to produce NO_2^- and $\cdot\text{OH}$ radicals. The formation of these secondary free radicals leads to the modification of various biological molecules. These modifications include: 1. Nitration and oxidation of tyrosine residues of numerous proteins, following the inactivation of cellular antioxidant enzymes/non-enzymatic molecules and/or activation of pro-inflammatory agents. 2. Oxidation of nucleic acids. 3. Peroxidation and nitration of lipids. The destruction of these macromolecules can result in cell toxicity and ultimately cell death.

Protein Tyrosine Nitration

Numerous human pathologies are associated with nitroxidative stress, which is mediated by increased levels of PN.³ As mentioned above, one key component of cellular damage on the molecular level is the nitration of tyrosine residues. While PN has also been shown to lead to nitration and/or oxidation of other amino acid residues such as cysteine and methionine, the nitration of tyrosine is considered to be a molecular fingerprint for PN overproduction *in vivo*.^{2,13} Numerous studies have now been reported correlating the overproduction of PN to protein tyrosine nitration which often results in the loss or gain of

function of proteins involved. These structural and functional changes which occur within proteins upon tyrosine nitration very often lead to protein dysfunction, toxicity and cell death.^{2,8}



Scheme 2: Mechanism of a tyrosine residue nitration⁸

Protein tyrosine nitration is a posttranslational modification that results from the imbalance of oxidant formation and antioxidant defense systems.^{3,8} In general, PN-mediated tyrosine nitration is a result of the formation of secondary free radicals $\cdot\text{NO}_2$, $\cdot\text{OH}$ or $\text{CO}_3^{\cdot -}$ radicals, through the decomposition of PN *in vivo*. Protein tyrosine nitration is very selective and largely depends on the “protein structure, nitration mechanism, and the environment where the protein is located.”⁸ It is also largely pH-dependent. The nitration mechanism affecting tyrosine residues is a two-step process (Scheme 2: this scheme was modified from mechanisms of protein tyrosine nitration presented in Accounts of Chemical Research-Radi paper).⁸ First, the hydrogen atom is abstracted from the phenol functional group by various

oxidants (derived from PN) which include $\text{CO}_3^{\cdot-}$, $\cdot\text{NO}_2$, $\cdot\text{OH}$, and high valent metal oxo species ($\text{M}=\text{O}$) that form from Fe/Mn heme proteins (through oxidation by PN or other ROS). This oxidation reaction results in the formation of the tyrosyl radical ($\text{Tyr}\cdot$). It is important to mention that in the presence of endogenous reductants, the tyrosyl radical can be reduced back to tyrosine. The second step is a radical-radical coupling reaction between the $\text{Tyr}\cdot$ and $\cdot\text{NO}_2$ which yields 3-nitrotyrosine.

The phenol pK_a , redox potential, hydrophobicity and the protein volume are several physiochemical factors that are altered from the modification of the tyrosine residue.⁸ In aqueous media, it was observed that the phenolic-OH group of tyrosine has a pK_a in the range of 10.0-10.3. However, the addition of the nitro- NO_2 group on the C-3 of the phenol ring significantly reduces the pK_a to 7.2-7.5. This pK_a value is also affected by polarity of the medium and surrounding amino acids that are adjacent to that specific nitrotyrosine residue.⁸

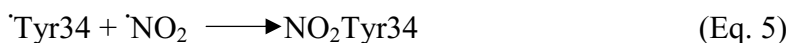
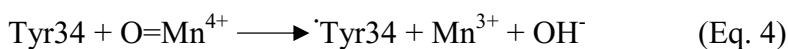
The Effect of Protein Nitration on Biological Molecules

Protein nitration causes profound effects on the structure and function of the protein. Some proteins are activated (*gain-of-function*) or inactivated (*loss-of-function*) upon nitration. There are countless essential cellular biomolecules that are known to get nitrated and inactivated including manganese superoxide dismutase (MnSOD), peroxisome proliferator-activated receptors (PPARs), and enkephalins.^{7-8,14}

MnSOD is an essential antioxidant metalloenzyme that is located in the mitochondrial matrix. This enzyme catalyzes the dismutation or disproportionation (rate $k = 2.4 \times 10^8 \text{ M}^{-1}\text{s}^{-1}$) of $\text{O}_2^{\cdot-}$ to H_2O_2 and O_2 , thus preventing the formation of PN by removal of one of its precursors. This protects the mitochondria from nitroxidative stress by keeping $\text{O}_2^{\cdot-}$ at a steady-state concentration in the picomolar-nanomolar range.⁵ Human MnSOD is a

homotetramer with the molecular weight of 88kD. Unfortunately, under chronic inflammatory conditions, MnSOD activity is annihilated due to the nitration of Tyr34.^{2, 10}

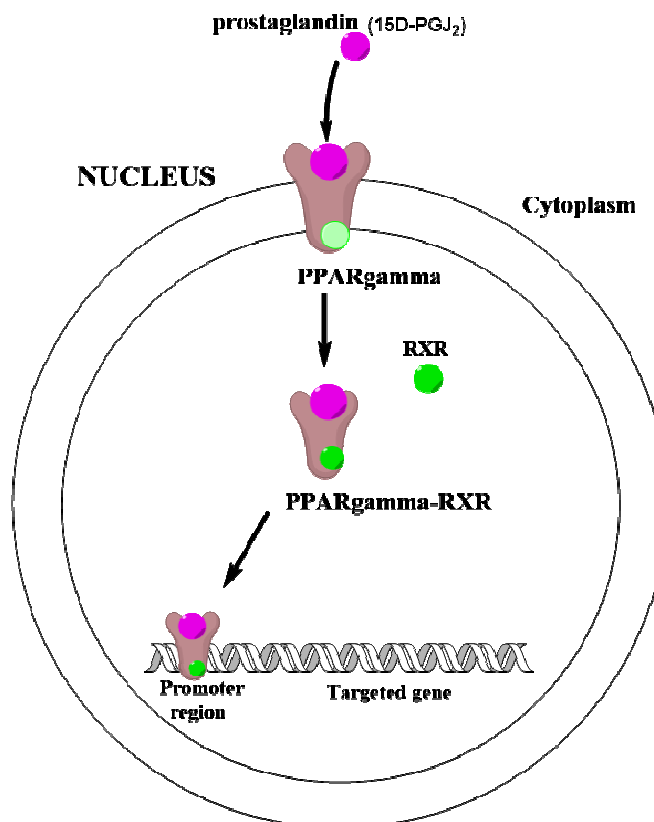
According to Radi, “MnSOD undergoes a *self-catalyzed* or *self-directed* oxidation/nitration reaction” in the presence of PN.⁸ Radi proposed a three step mechanism to this phenomenon, which is shown below (equation 3-5). The first step of this process, PN oxidized Mn^{3+} to $O=Mn^{4+}$ oxo, generating $\cdot NO_2$.



Either one of these species ($\cdot NO_2$ and $O=Mn^{4+}$) can abstract the hydrogen atom of Tyr-34. However, the high valent metal oxo ($O=Mn^{4+}$) has a slight higher second order constant of $k = 7.7 \times 10^5 \text{ M}^{-1}\text{s}^{-1}$ compared to $\cdot NO_2$ (rate $k = 3.2 \times 10^5 \text{ M}^{-1}\text{s}^{-1}$). Thus, $O=Mn^{4+}$ oxo catalyzes the nitration of Tyr34 forming the one-electron oxidant, $\cdot \text{Tyr34}$ radical. This is the “*self-catalyzed*” step. As a result, $O=Mn^{4+}$ oxo is reduced to Mn^{3+} . The reaction proceeds with the radical-radical termination as $\cdot \text{Tyr34}$ couples with $\cdot NO_2$ form the 3-nitroTyr34 product.⁵

Tyr34 of MnSOD is a very important amino acid residue. It is located in active site of the MnSOD enzyme. Thus, nitration of this single amino acid amino acid can alter MnSOD structure and function. Computational and X-ray crystallography results show that 3-nitrotyrosine blocks the active site of MnSOD enzyme. The physicochemical properties of the bulky $-NO_2$ group causes steric hindrance and prevents O_2^- from entering the active site. As mentioned earlier, the pKa the tyrosine is also lowered from ~ 10 to ~ 7 which is close to the physiological pH of 7.4. Thus, a substantial fraction of the phenol is deprotonated and anionic. This phenomenon can lead to electrostatic repulsion of O_2^- , thus inhibiting the critical function of MnSOD.¹⁰

PPAR γ , a nuclear receptor and transcription factor, is another essential biological molecule that is known to get nitrated and inactivated in the presence of PN.¹⁹⁻²¹ PPAR is composed of three subtypes: alpha (α), beta (β), and gamma (γ).¹⁹ *In vivo*, their function is to regulate gene expression and cellular metabolism (carbohydrate and lipid homeostasis).²⁰⁻²¹ Both PPAR α and PPAR β regulate lipid utilization. PPAR γ regulates lipid storage and synthesis in the liver and adipose tissues and also has a direct effect on insulin sensitivity in the muscle cells.¹⁹⁻²⁰ *In vivo*, in order for the PPAR γ nuclear receptor to regulate gene expression, it must be activated by an endogenous PPAR γ ligand (one example of many possibilities is the cyclopentanone prostaglandin; 15D-PGJ₂) (scheme 3).¹⁹ PPAR ligands can be synthetic such as anti-inflammatory, insulin-sensitizing or antidiabetic drugs (Thiazolidinedione; TZD).²⁶ The activation of PPAR γ allows the receptor to bind to a retinoid X receptor (RXR) to form a heterodimer. The PPAR γ -RXR heterodimer exist in both active and inactive form. When active, the heterodimer binds to a specific PPAR response element (PPRE) in the promoter region of the DNA sequence for genes that encode proteins that regulate lipid and glucose homeostasis.^{19-22, 26} Unfortunately, the overproduction of PN alters PPAR γ nuclear receptor function. PPAR γ can be nitrated, thus destroying PPAR γ cellular function. However, PN can activate other endogenous molecules (imparting a gain of function) such as cytochrome c, fibrinogen, protein kinase C ϵ , glutathione-s-transferase 1, and the nuclear factor kappa-light-chain-enhancer of activated B-cell (NF- κ B).¹⁹



Scheme 3. PPAR γ receptor mode of action

Contrary to PPAR γ , under oxidative stress NF- κ B activity is increased. NF- κ B is a nuclear transcriptional factor that stimulates the expression of numerous proinflammatory genes that encode for the production of inflammatory cytokines (tumor necrosis factor α , interleukin 1 β , interleukin-6, interferon- γ), intracellular adhesion molecule 1 (ICAM1), iNOS, and NADPH oxidase.¹⁹ The overexpression of iNOS and NADPH oxidase up-regulates the formation of \cdot NO and $O_2^{\cdot-}$, respectively. This leads to the continued production of PN, which would increase cell toxicity and eventually death.

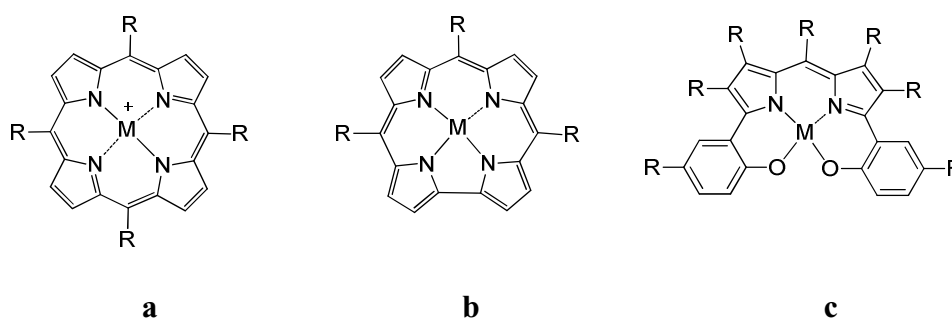
CHAPTER II

DESIGN OF PEROXYNITRITE DECOMPOSITION CATALYSTS (PNDCs)

The attenuation of PN-mediated cytotoxicity in various diseases (e.g. diabetes mellitus, cardiovascular disease, and neuropathic pain) has been the motive behind the synthesis of several different classes of PNDCs as potential pharmaceutical agents. Redox active transition metal complexes have a long history for being used as PNDCs. Here are several important criteria used in the design of known PNDCs: ¹³

1. The PNDC should react rapidly with PN before PN can oxidize other biomolecules.
2. The PNDC should be catalytically active and have good pharmaceutical properties.
3. The products formed from the decomposition of PN reaction should not be toxic or have the oxidative potential to harm other biological molecules.

There are three different classes of metal complexes that have emerged as active PNDCs: metalloporphyrins, metallocorroles, and metallo-bis(hydroxyphenyl)dipyrromethenes (DPMs).^{5,14}



Scheme 4. a) metalloporphyrin, b) metallocorroles, c) metallo-bis(hydroxyphenyl)-dipyrromethenes

Metalloporphyrins

Metalloporphyrins were the first group of compounds discovered to have PNDC activity. Porphyrins are planar dianionic ligand systems which form monocationic complexes with

trivalent transition metals (Mn^{3+} or Fe^{3+}). Many of the important metalloporphyrin catalysts described in the literature also incorporate highly electron withdrawing groups (e.g. *N*-methylpyridinium) in the *meso*-positions. These groups are important for controlling the redox potential of the metal center and for imparting water solubility to the complex. The most well-known examples of PNDCs from this class are shown in Figure 1.

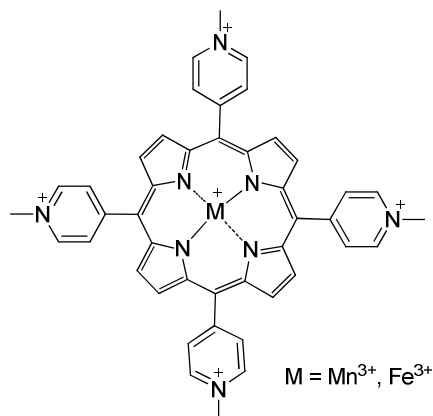
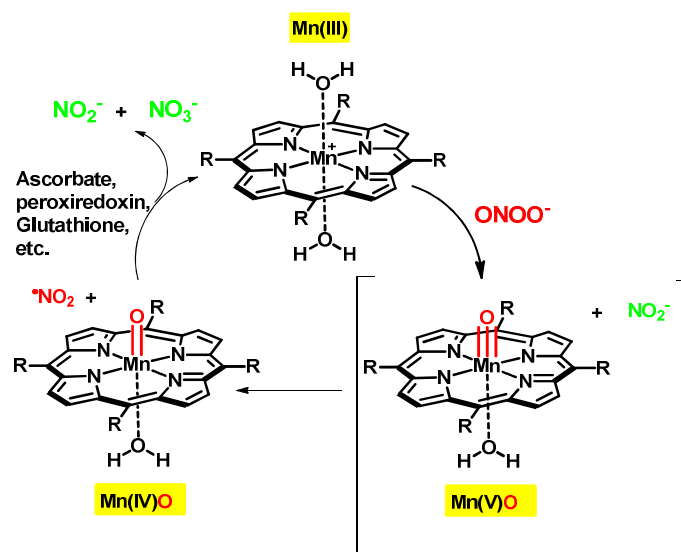


Figure 1. General structure of a metalloporphyrin complex as a PNDC

The interest in metalloporphyrins may be due to the fact that, porphyrins exist in almost all living organisms.²³ Metalloporphyrins can act as prosthetic groups embedded in variety of proteins that play a key role in numerous biological processes. These biomolecules include hemoglobin, myoglobin, cytochromes, and peroxidases.²³⁻²⁴ Currently, metalloporphyrins that employ Mn(III) and Fe(III) metal centers are the most well-studied compounds. These compounds are exceptional catalysts due to their ability to dismute O_2^- and decompose of PN both *in vivo* and *in vitro*. Currently, there are a number of groups attempting to develop this class as potential therapeutic agents.²

Mn(III) porphyrins are known to decompose PN via a single-electron mechanism (Scheme 5). The catalytic cycle initiates when, PN rapidly oxidizes the Mn(III) to generate Mn(V)O intermediate and NO_2^- .¹⁵ Even though Mn(V)O may be formed initially, it is so

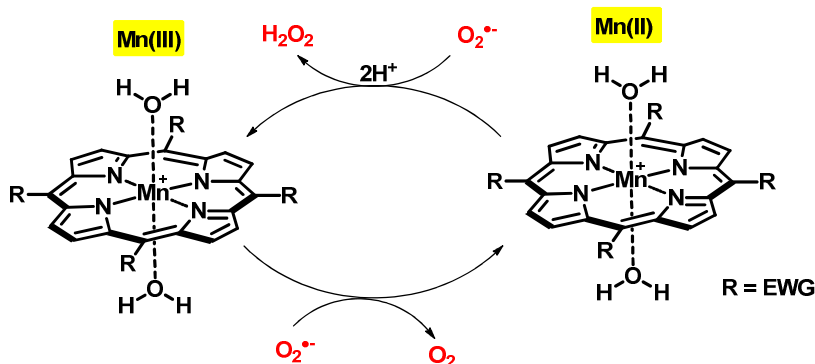
reactive that it instantly oxidizes NO_2^- to $\cdot\text{NO}_2$ within the solvent cage. Mn(V)O is therefore reduced to Mn(IV)O . *In vivo*, the presence of endogenous antioxidants are critical. Once Mn(IV)O is formed co-reductants are required to reduce Mn(IV)O back to Mn(III) since it reverts slowly on its own. As mentioned earlier, $\cdot\text{NO}_2$ is a toxic radical that can oxidize and/or nitrate essential biological molecules. Therefore, it must be quenched by endogenous antioxidants into the less toxic species NO_2^- in order to complete the reductase cycle.¹⁴



Scheme 5. Detoxification of PN via Mn(III) porphyrin

Initially, Mn(III) porphyrins were developed as SOD mimics (SODm). As mentioned in chapter 1, an SOD enzyme catalyzes the disproportionation of $\text{O}_2^{\cdot-}$ to O_2 and H_2O_2 in order to protect the cell from oxidative stress. Therefore, if MnSOD is inhibited, an SOD mimic could be utilized to decrease $\text{O}_2^{\cdot-}$ levels in an attempt to decrease PN formation. A catalytic cycle of Mn porphyrin involves two steps in which the redox-active Mn center cycles between Mn(III) and Mn(II). The first step is referred as the rate-determining step, corresponding to the reduction of Mn(III) porphyrin by $\text{O}_2^{\cdot-}$ to yield Mn(II), in return $\text{O}_2^{\cdot-}$ is oxidized to O_2 . The second step is the oxidation of Mn(II) porphyrin by $\text{O}_2^{\cdot-}$ to yield H_2O_2

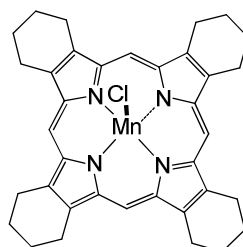
and reestablishing the Mn(III) porphyrin oxidation state, thus completing the catalytic cycle (Scheme 6).²⁴



Scheme 6. Superoxide dismutation by Mn(III) porphyrin, SODm²⁵

Mn(III)-tetrakis-(*meso*-*N*-methylpyridium)porphyrin (Mn(III)-4-TMPyP⁵⁺) is an example of a metalloporphyrin with both potent PNDC and SODm activity (Figure 1). As mentioned earlier, the presence of an electron withdrawing substituent such as the *N*-methylpyridinium groups in the *meso*-position significantly increases SOD mimic activity. The *meso*-position of the electron-withdrawing groups reduce the electron density at the metal center, permitting the reduction of Mn(III) by O₂^{•-}.²⁴⁻²⁵ Mn(III)-4-TMPyP⁵⁺ may exhibit a high degree of SODm and PNDC activity, but there are some limitations that might prohibit Mn(III)-4-TMPyP⁵⁺ from being an exceptional therapeutic agent. Several disadvantages that might limit Mn(III)-4-TMPyP⁵⁺ activity *in vivo* are based on its composition. It has been reported that this complex lacks the “ability to adopt to a near-planar structure” which may hinder the O₂^{•-} from reaching the active site (Mn-site).²⁴ More importantly, the *N*-methylpyridinium groups of Mn(III)-4-TMPyP⁵⁺ significantly increase the hydrophilic nature of the complex. This limits its ability to penetrate and partition through cell membranes and makes them poor drug candidates. To this end, our research group has

designed and synthesized a new class of PNDCs in the efforts to improve the membrane solubility. The new series of the Mn(III) porphyrin systems incorporated the β -fused cyclohexenyl shielding groups to enhance membrane solubility.²⁵ One specific example of these new Mn(III) tetracyclohexenylporphyrin (TCHP) analogues is shown on Figure 2.



SR6

Figure 2. Mn(III) tetracyclohexenylporphyrin chloride, SR6

Mn(III)TCHP chloride (SR6) is a monocationic metalloporphyrin system (in solution) that has been shown to be an orally active PNDC.²⁵ In comparison to MnTMPyP⁵⁺, it was hypothesized and shown that the lipophilic cyclohexenyl groups of Mn(III)TCHP provide shielding for the charged metal centers which enables the complex to effectively pass through cell membranes. The reduction potential of SR6 has been determined to be in the range of -0.2 to -0.4V which is not ideal for a SODm. For an SODm to exhibit optimal SOD activity, the reduction potential should be in the range of +0.3V, similar to the SOD enzymes.²⁴ Thus, SR6 is not an effective SODm. However, since PN is such a powerful oxidant, SR6 can still be oxidized by PN which makes SR6 a very selective catalyst for the decomposition of PN.

Fe(III) porphyrins have also been extensively studied and are known to decompose PN in a catalytic fashion analogous to Mn(III) porphyrins. Amazingly, Fe(III) porphyrins can isomerize PN to NO_3^- . Ideally, this may be the most enzyme-like method to alleviate excess levels PN levels *in vivo* because the isomerization product (NO_3^-) is unreactive and does not

require addition antioxidants to complete the catalytic cycle. While Fe(III) porphyrin PNDC rate constants (range $k = 10^5$ to $10^6 \text{ M}^{-1}\text{s}^{-1}$) might be slightly lower than Mn(III) porphyrins (range $k = 10^6$ to $10^7 \text{ M}^{-1}\text{s}^{-1}$), Fe(III) porphyrins are still in a very useful range for the decomposition of PN.¹³ However, it has been suggested that the redox cycling of Fe(III) to Fe(II) can be very toxic *in vivo*. The loss of Fe(II) metal from the porphyrin complex or the reduced Fe(II) chelated to the porphyrin ligand can give rise to Fenton chemistry in the presence of H_2O_2 . The reduced Fe(II) can readily react with H_2O_2 to yield a highly oxidizing and most damaging free radical, the $\cdot\text{OH}$ species. Thus, the scientific community has been more interested in Mn(III) porphyrin derivatives to avoid Fenton chemistry *in vivo*.¹⁸

Metallocorroles

Metallocorroles are similar to metalloporphyrins except that their corrole ligands are missing one *meso*-carbon.¹⁴⁻¹⁷ Thus, corroles are ring-contracted analogues of porphyrins. Many research groups have studied and reported metallocorroles to be orally active PNDCs. Both Mn(III) and Fe(III) corroles system have been discovered to have the catalytic ability to decompose PN in the absence of reducing agents. One specific example is the Mn(III) complex of bis-(*N*-methylpyridinium)-(4-methoxyphenyl)corrole (Figure 3).

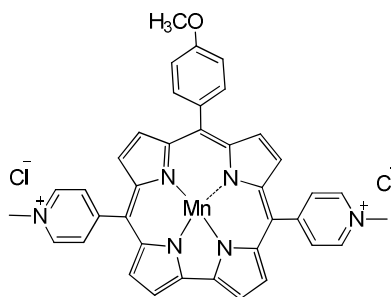
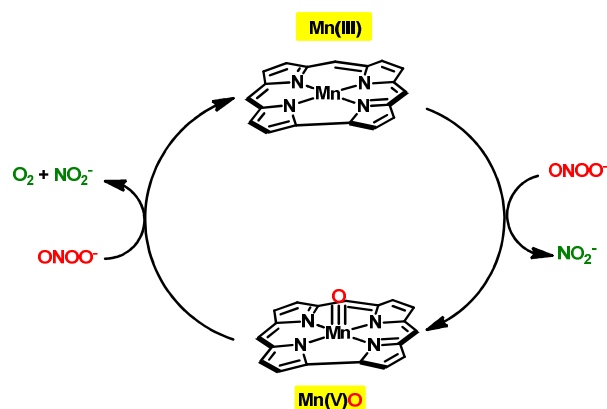


Figure 3. Mn(III) bis-(*N*-methylpyridinium)-(4-methoxyphenyl) corrole

The corrole systems are structurally capable of stabilizing transitional metals centers with higher oxidation states. In addition, Gross proposed a two-electron catalytic cycle for the reaction between PN and Mn(III) corroles as shown on Scheme 7, where the Mn(III) complex is oxidized to Mn(V)O by PN.⁵⁸ However, since this is a two-electron process PN is reduced to the less toxic NO_2^- . The Mn(V)O can then oxidize another molecule of PN to generate NO_2^- and O_2 .



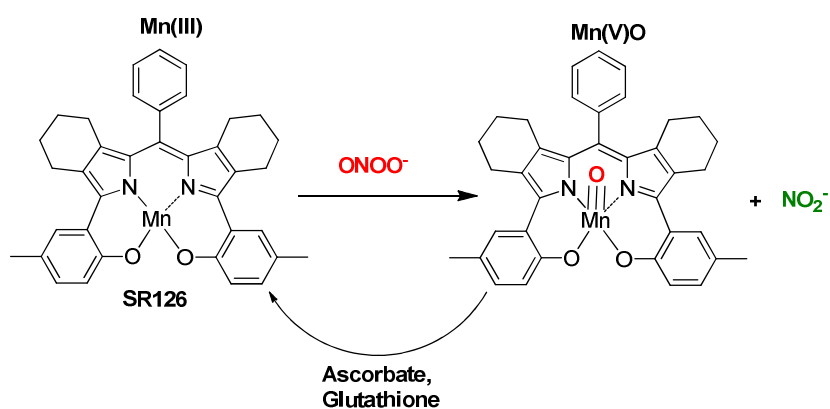
Scheme 7. Catalytic cycle of Mn(III) corroles with PN⁵⁸

Mechanistically, metallocorroles would be excellent therapeutic agents for the detoxification of PN *in vivo*. Unfortunately, the synthesis of functionalized corroles can be challenging. The macrocyclization yields are often quite low and purifications can be tedious. We felt that these factors may hinder structure-activity relationship studies (SAR) required for studying the performance of the catalysts both *in vivo* and *in vitro*.

Metallo-bis(hydroxyphenyl)-dipyrromethenes

The discovery of metallocorrole systems as orally active PNDCs with an improved (2-electron) catalytic cycle over that of the metalloporphyrins prompted our research group to think about new, simpler ways to effect a two-electron PNDC mechanism. Efforts to identify two-electron catalysts that can be readily prepared for SAR studies led to a new class of

compounds based upon Mn(III) complexes of bis(hydroxyphenyl)dipyrromethenes (DPMs).¹⁴ Mn(III)-DPM complexes have a chelate system that simulates the Mn(III)-corrole's trianionic chelate environment and have now been shown to decompose PN via a two-electron mechanism.¹⁴ In a catalytic cycle similar to Mn(III)-corroles, Mn(III)-DPM complexes are oxidized by PN, thus capturing the oxidative potential in the form of Mn(V)O (Scheme 8). This effectively destroys PN by converting it to NO_2^- . The reduction of Mn(V)O species can be accomplished by the assistance of endogenous reducing agents (e.g. glutathione, ascorbate). However, we now have evidence that Mn(III)-DPMs are catalytic on their own.¹⁴



Scheme 8. PN decomposition activity of Mn(III)-DPMs¹⁴

As a major advantage over corrole systems, DPM ligands can be readily synthesized with high percentage yield through modular methods which allow the incorporation of a wide-range of functional groups.¹⁴ This makes them ideal for SAR studies and for varying physicochemical properties to study *in vivo* performance. Therefore, we chose to further investigate Mn(III)-DPM systems and their closely related Mn(III)-aza-DPM analogues for their catalytic ability to decompose PN.

CHAPTER III

RESEARCH OBJECTIVES AND SYNTHESIS

The nitration of biomolecules by PN is known to be the primary biomarker of nitroxidative stress which can lead to the development variety of disease conditions. One therapeutic approach is to search for new probes that are PN-selective and can alter PN concentrations both *in vitro* and *in vivo*. This has been the focus of our research group and others. As mentioned in chapter II, there are two therapeutic approaches currently used to reduce PN levels *in vivo*. These strategies include the inhibition of ROS/RNS intermediates (i.e. $O_2^{\cdot -}$ via SODm) that react to produce PN and decomposing PN after it is formed. In addition, the use of redox active transition metal such as Mn(III) and Fe(III) have been employed to redirect PN oxidative potential, thus altering PN activity. In recent years, our research group has been involved in the development different classes of PNDCs. We have designed and shown that Mn(III)-DPMs are effective and selective PNDCs.¹⁴ Mn(III)-DPMs are orally bioavailable and active in models of nutrient overload/insulin resistance and in models of inflammatory and neuropathic pain.^{14, 30, 32} In addition, the DPM ligand systems are synthetically more accessible for medicinal chemistry purposes over corrole analogues.

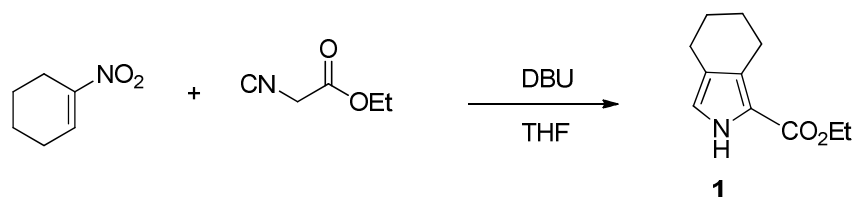
The current Mn(III)-DPMs were designed to be lipid soluble with enhanced drug-like properties. Even though Mn(III)-DPM analogues are orally active and membrane penetrating, they are some-what insoluble. Therefore, the bioavailability of the Mn(III)-DPM class of PNDCs needs to be improved.

My research project was divided into two parts, mainly centered on synthesizing more soluble Mn(III) complexes of *aza*- and non-*aza*-DPM derivatives to improve the bioavailability of our PNDCs compounds. The first part of the project was to design and

synthesize a functionalized Mn(III)-DPM with a conjugation site. A conjugation site permits us to tether a water-solubilizing functional group in order to enhance the water-solubility properties of our original Mn(III)-DPM catalysts. The second approach was to extend this study and examine Mn(III) bis(hydroxyphenyl-*aza*-dipyrromethenes (*aza*-DPM) catalysts, which structurally contains two sites of conjugation. A final more advanced goal was to also develop “oxidant triggered” *aza*-DPM pro-catalysts as PNDCs, which are generated *in vivo* in response to endogenous toxic free iron. These systems would be designed to scavenge free iron *in vivo* and thereby generating a PNDC in the process. Thus, this approach would eliminate the requirement of dosing an exogenous transition metal.

Part I. Synthesis of a Functionalized Mn(III)-DPM Catalysts

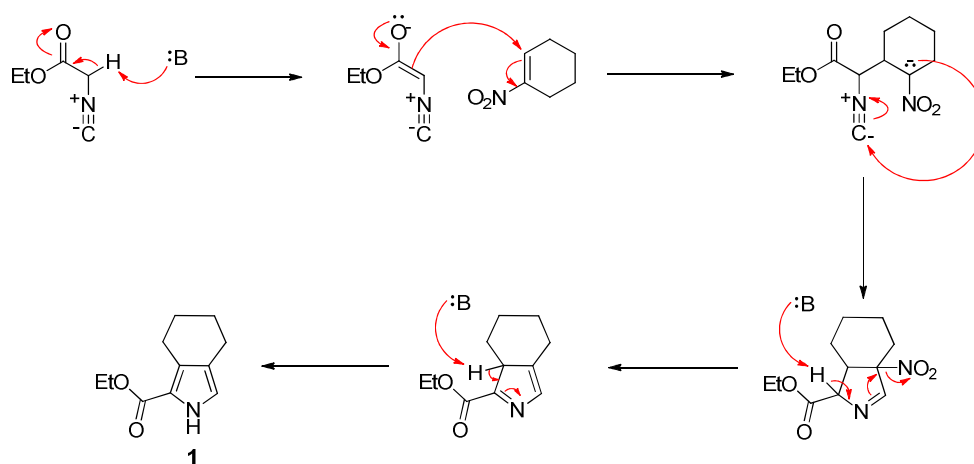
The synthesis of a DPM derivative with a conjugation site began with the preparation of tetrahydroisindole derivative **1**.²⁷⁻²⁸ Tetrahydroisindole **1** was synthesized via the condensation of 1-nitrocyclohexene with ethyl isocyanoacetate under basic conditions shown in Scheme 9. This is a well-known reaction first reported in 1990 by Derek Barton and Samir Zard, which became commonly known as the Barton-Zard Reaction.²⁷⁻²⁸



Scheme 9. Synthesis of Ethyl-4,5,6,7-tetrahydro-2*H*-isindole-1-carboxylate (**1**)

The Barton-Zard reaction undergoes a five step mechanism. The first step is the enolization of the carbonyl of ethyl isocyanoacetate. A Michael-addition between the ethyl isocyanoacetate enolate and 1-nitrocyclohexene affords the nitronate anion which cyclizes by a nucleophilic attack on the isocyanide’s carbenoid carbon. This is followed by base

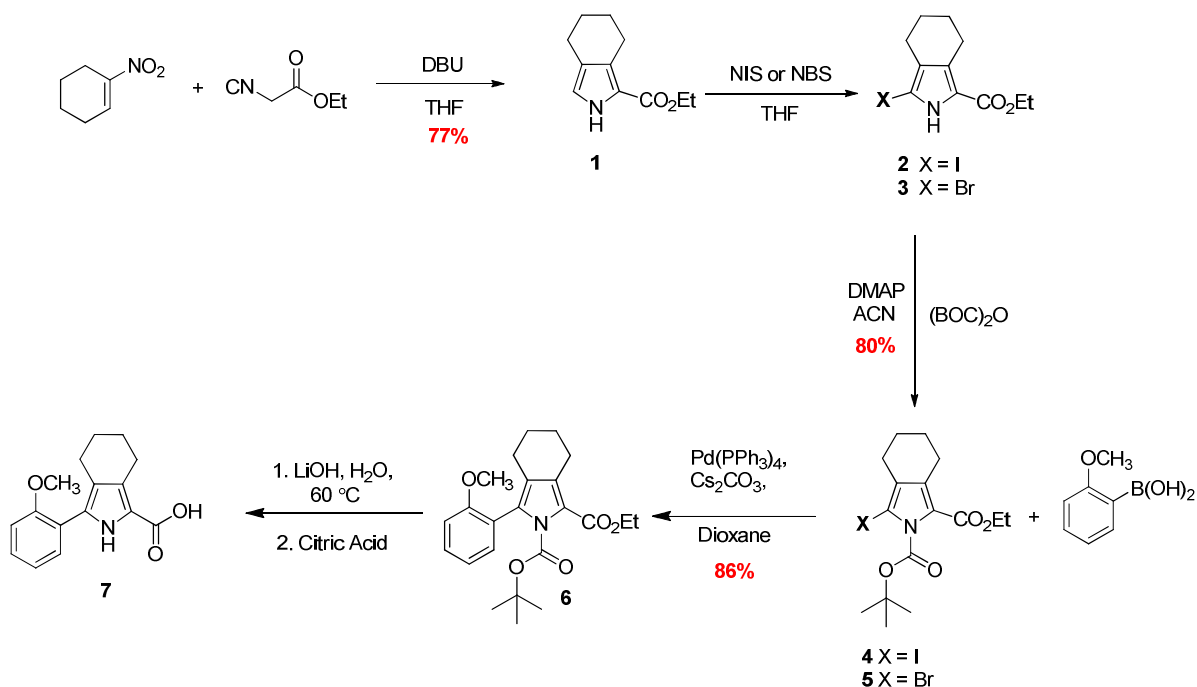
catalyzed elimination of the nitro group followed by tautomerization and aromatization to afford the desired pyrrole **1** (Scheme 10).



Scheme 10. Barton-Zard mechanism

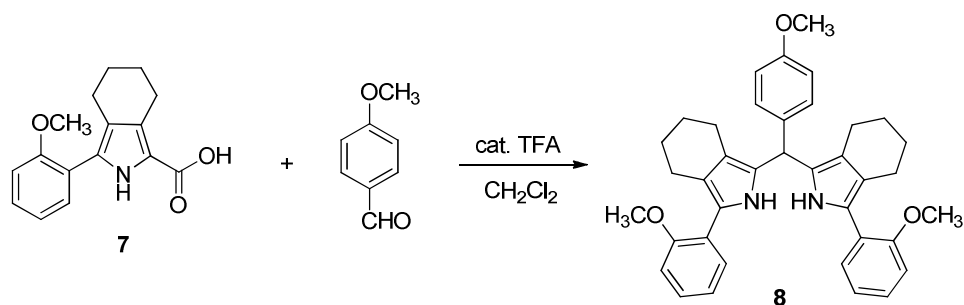
Tetrahydroisindole **1** was then converted to the iodo- or bromo-derivative **2** or **3**, using, NIS or NBS, respectively. The pyrrole nitrogen was protected using Boc-anhydride with 4-DMAP in acetonitrile to afford a boc-protected pyrrole **4** or **5** (Scheme 11). Our group discovered that the Boc-protection is a very crucial and necessary step for a successful Suzuki coupling reaction. Thus, the Boc-protected bromo- or iodo-pyrrole compounds were coupled to 2-methylphenylboronic acid using $\text{Pd}(\text{PPh}_3)_4$ as the catalyst and sodium carbonate as the base to afford the highly functionalized pyrrole **6**. For this palladium-catalyzed Suzuki reaction, we wanted to explore different halide derivatives to optimize coupling with the corresponding boronic acid. In theory, the relative reactivity of halides are indicated as follows: $\text{I} > \text{Br} > \text{Cl}$.^{16, 37} However, in our case, the overall coupling efficiency of the bromo-pyrrole **5** was better than that of the iodo-pyrrole **4**.

Under basic conditions the Boc-protecting group was removed and the ethyl ester was saponified to afford a crystalline carboxylic acid **7**, a key intermediate for the dipyrromethane formation reaction.



Scheme 11. Synthesis of dipyrromethane precursor **7**

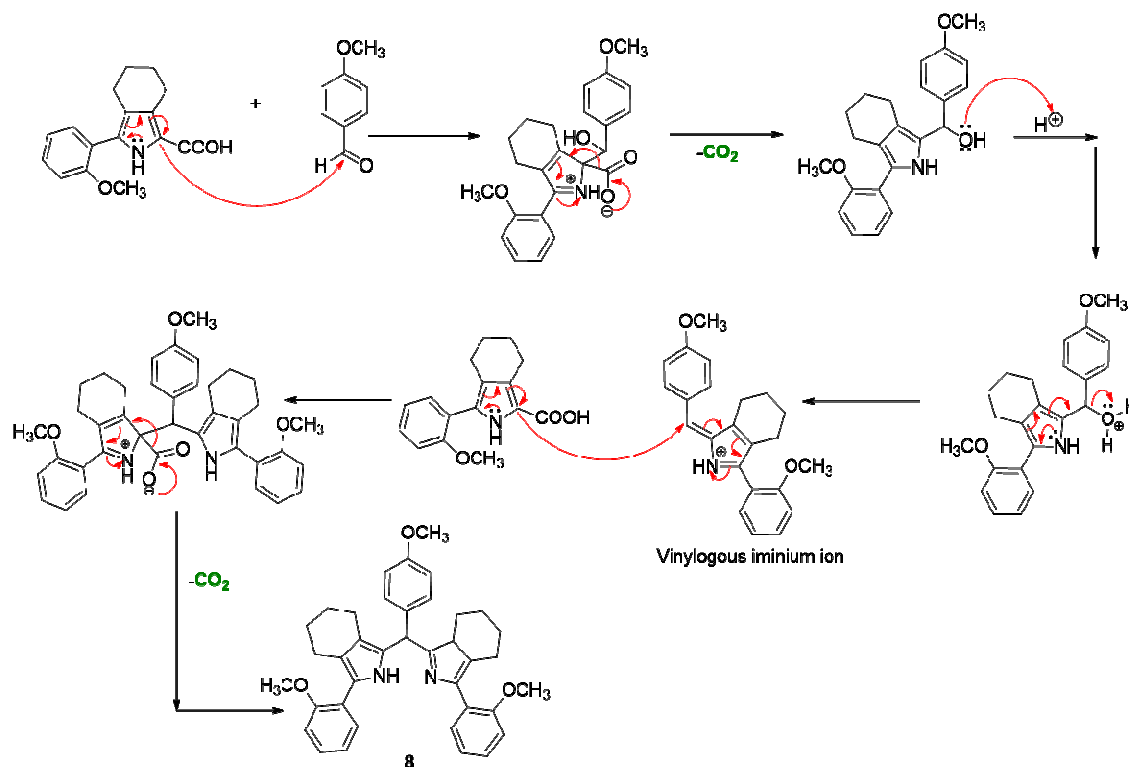
The synthesis of the dipyrromethane derivative **8** was accomplished using standard Lindsey conditions.²⁹ Therefore, compound **8** was obtained by condensation reaction of 2 equivalents of crystallized pyrrolic acid **7** with 4-methoxybenzaldehyde using TFA as catalyst (Scheme 12).



Scheme 12. Synthesis of the dipyrromethane derivative **8**

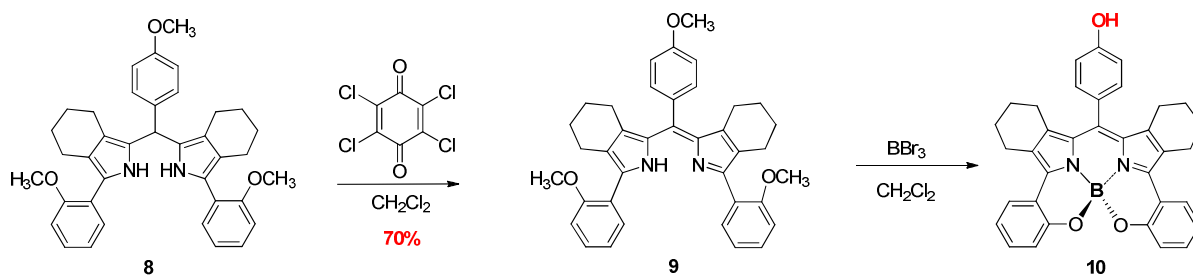
The formation of dipyrromethane occurs through the following mechanistic steps: First, the 5'-position of pyrrolic acid undergoes an electrophilic substitution with the carbonyl group of the 4-methoxybenzaldehyde.³¹ The compound rearranges and decarboxylates *in situ*,

following an acid-catalyzed dehydration of the alcohol (hydroxyl group) to yield the vinylogous iminium ion. An electrophilic substitution of the second pyrrolic acid, with subsequent a decarboxylation afforded the dipyrromethane ligand **8** (Scheme 13).



Scheme 13. The formation of dipyrromethane **8** mechanism

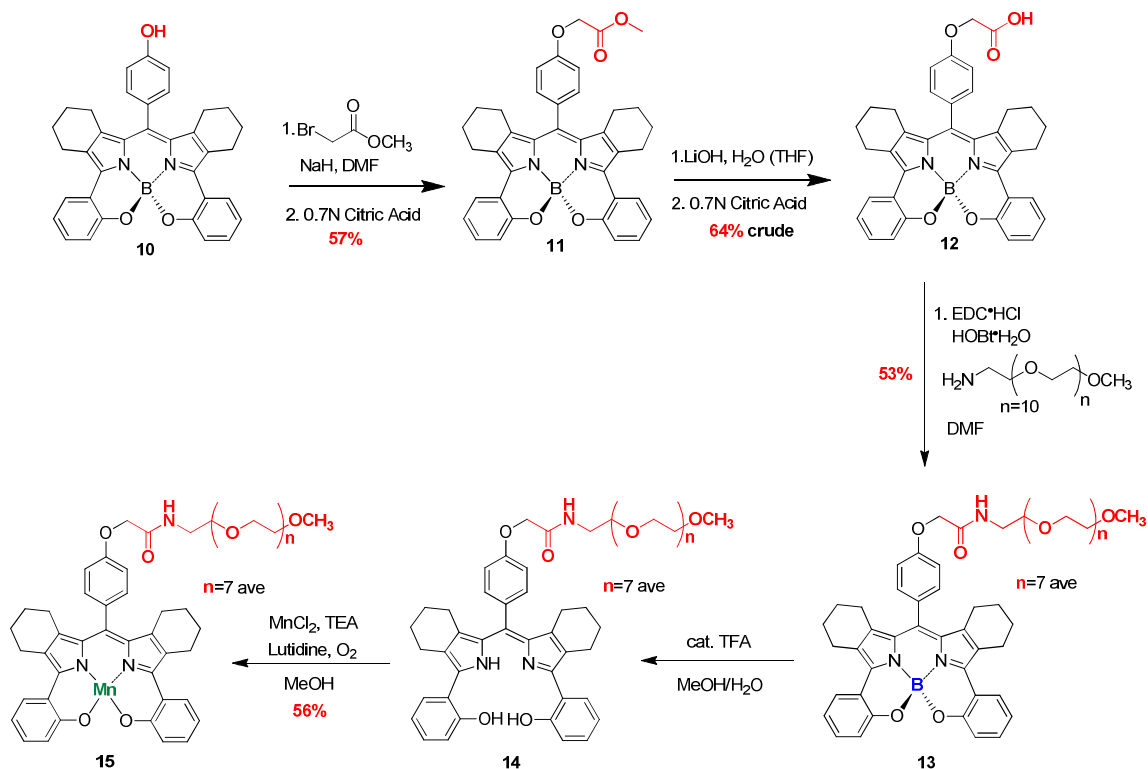
The oxidation of dipyrromethane **8** to the corresponding dipyrromethene **9** was accomplished by the treatment with *p*-chloranil to afford 70% yield after purification (Scheme 14).²⁹ To prepare the *meso*-site for conjugation and to deprotect the phenols, the dipyrromethene ligand **9** was converted to the chelated BODIPY derivative with the treatment of excess boron tribromide (BBr₃). In this reaction, the BBr₃ is used to cleave all three methyl ethers and two phenol groups are protected by the boron atom *in situ* through the formation of the chelated BODIPY. The free phenol (in red) at the *meso*-position was our site of conjugation used for further chemistry (Scheme 14).



Scheme 14. Conversion of the DPM ligand to the chelated-(*O, N*)-BODIPY derivative **10**

Synthesis of Mn(III)-*meso*-(PEG-amide)-DPM 15

As illustrated in Scheme 15, the *meso*-(4-hydroxyphenyl)-(*O, N*)-BODIPY **10** was converted to the alkylated BODIPY **11** via an $\text{S}_{\text{N}}2$ reaction. In this Williamson ether synthesis the phenol is deprotonated with sodium hydride to give the phenolate anion, which acts a nucleophile and attacks the α -carbon of methyl bromoacetate to form the desired complex **11** in 57% yield after purification.



Scheme 15. Synthesis of Mn(III)-*meso*-(PEG-amide)-DPM **15**

Under basic conditions, the methyl ester of complex **11** was hydrolyzed to afford the carboxylic acid-(*O*, *N*)-chelated-BODIPY **12** in 64% crude yield. Compound **12** is a key intermediate for bioconjugation studies. For the synthesis of the functionalized pegylated Mn(III)-DPM complex (NM20) **15**, complex **12** was coupled with poly(ethyleneglycol) methyl ether amine (PEG-amine) (reported average molecular weight ~500) under standard EDC conditions to afford the pegylated BODIPY derivative **13** (NM20B). Complex **13** was hydrolyzed with catalytic amount of TFA in MeOH/water and the free dipyrromethene ligand **14** was isolated for the next step. A direct conversion of compound **14** to NM20 **15** was accomplished by stirring the pegylated DPM ligand with Mn(II)Cl₂, TEA and lutidine (a transfer ligand) opened to air (to effect the oxidation of Mn(II) to Mn(III) *in situ*).

Characterization of Compounds 13 and 15

The newly synthesized pegylated BODIPY NM20B **13** and pegylated Mn(III)-DPM NM20 **15** were characterized by standard methods. NM20B, **13** was analyzed by ¹³C and ¹H NMR to evaluate the structure of this new compound prior to synthesizing the paramagnetic Mn(III) complex. The ¹H NMR spectrum for NM20B, **13** is shown in Figure 4. The most aliphatic protons on the cyclohexenyl groups afford peaks upfield around 1.5 ppm and the protons (on the cyclohexenyl groups) adjacent to the pyrrole are further downfield (2.5-3.0 ppm). The two protons in the methylene group adjacent to the oxygen atom are chemically equivalent and are seen as a singlet at 4.6 ppm. The large broadened peak around 3.65 ppm corresponds to the hydrogen atoms in the PEG-amine functional group. Since the protons are all in nearly identical chemical shift environments, they all appear and are observed under one large broadened peak. The integration of the peak at 3.65 ppm is also consistent to the hydrogens of the PEG-amine group. The aromatic peaks are further

downfield (around 6.5-8.0 ppm). In addition of being a precursor to making the Mn(III) complex, this pegylated BODIPY could potentially be used as a laser dye, sensor or an optical probe for biological imaging.^{38, 39} The absorbance/emission wavelength maxima (621/651 nm) were observed for compound **13**. The emission wavelength of **13** is in the far red region of the electromagnetic spectrum, which is a desirable property for a fluorescent dyes which are used for biological imaging.^{32, 38-39}

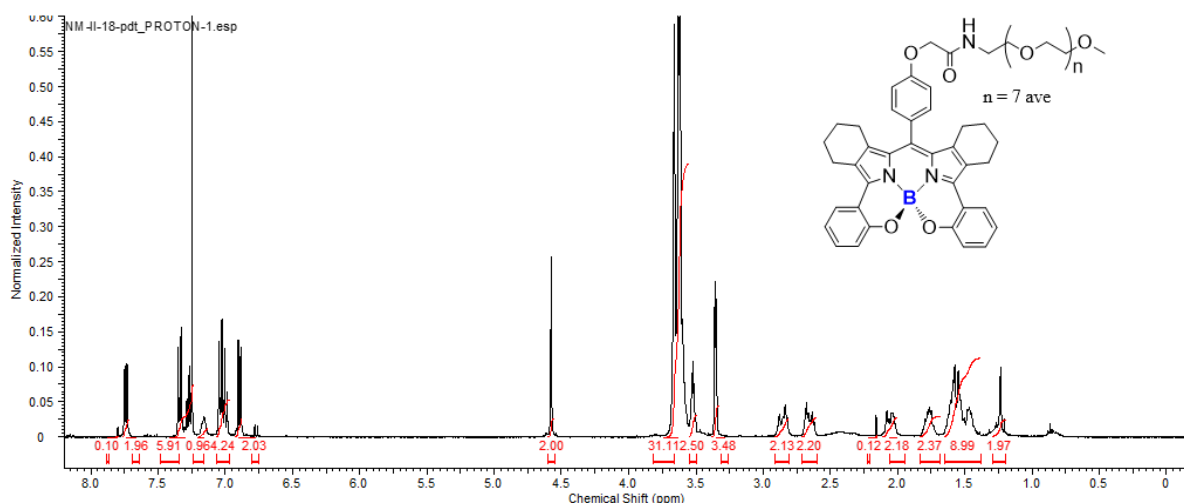


Figure 4. ¹H NMR spectrum of compound **13** in CDCl₃ at 25 °C

The first goal of thesis research was to use our original developed synthetic methods to achieve a functionalized catalyst for the purpose of improving their bioavailability while maintaining suitable lipophilicity. In this study, the newly functionalized Mn(III)-DPM was compared to the originally designed Mn(III)-DPM prototype, SR110. A co-mixture of both complexes was analyzed via HPLC. HPLC is a powerful analytical technique with the ability to separate, identify, and quantitate any mixture of compounds.³³ In addition, it is an excellent instrument to measure the lipophilicity of these components. This characteristic is determined based on the retention time of the individual components. Using reversed-phase

chromatography, longer the retention times on the column indicate more lipophilic analytes. This is illustrated by the chromatogram on Figure 5, SR110 is eluted off the column at 5.40 minutes, while the pegylated Mn(III)-DPM elution time was right at the solvent front (2.33 min.). Since a polydispersed PEG was used, we see an envelope of little peaks which are different pegylated Mn(III) derivatives with an average number of ethylene glycol units = 7 for the major constituent. The LCMS analysis indicates that we might have improved hydrophilicity of the originally designed Mn(III)-DPM catalyst.

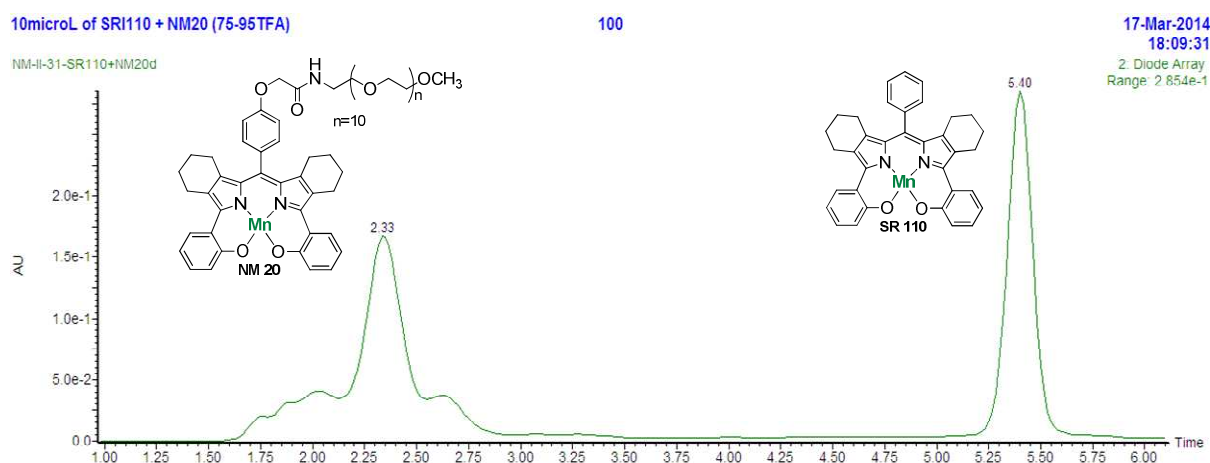


Figure 5. LCMS analysis of SR110 and NM20 co-mixture

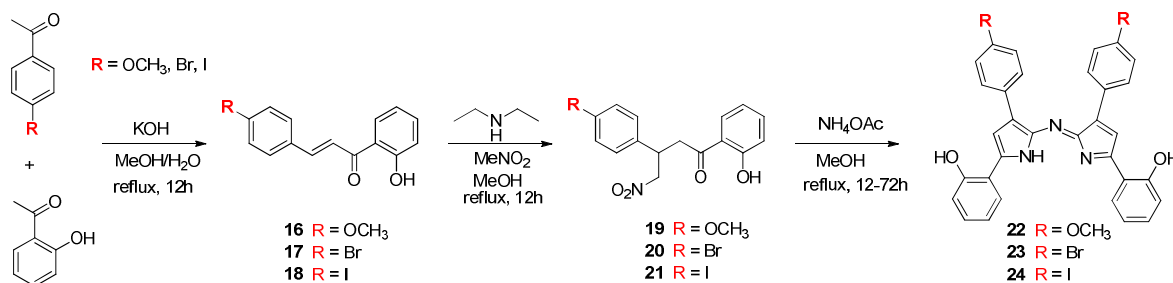
Part II. Synthesis of aza-DPM Ligand Systems

In our efforts to extend our design and synthesis for more water soluble analogues, *aza*-DPM ligands were prepared using the standard synthesis conditions shown on Scheme 16.^{32, 34, 38-39} As shown in Scheme 16, the general synthesis of an *aza*-DPM ligand began with a mixed aldol reaction of a benzaldehyde derivative and acetophenone to afford diaryl α , β -unsaturated ketones **16**, **17**, or **18**. In the next step, nitromethane was reacted with

compound **16**, **17**, or **18** under basic conditions to afford the Michael adduct **19**, **20**, or **21**.

Compound **19**, **20**, or **21** was then subjected to a condensation reaction with excess ammonium acetate to give the aza-DPM ligand **22**, **23**, or **24** through a complex process.³⁴

38-39



Scheme 16. General synthesis of aza-DPM ligand analogues

One reason these aza-DPM ligand systems were chosen was due to their ease of synthesis. It only requires four-steps to synthesize a BODIPY-chelated aza-DPM derivative.

The differences between these ligand systems and resulting complexes are highlighted in Figure 6.

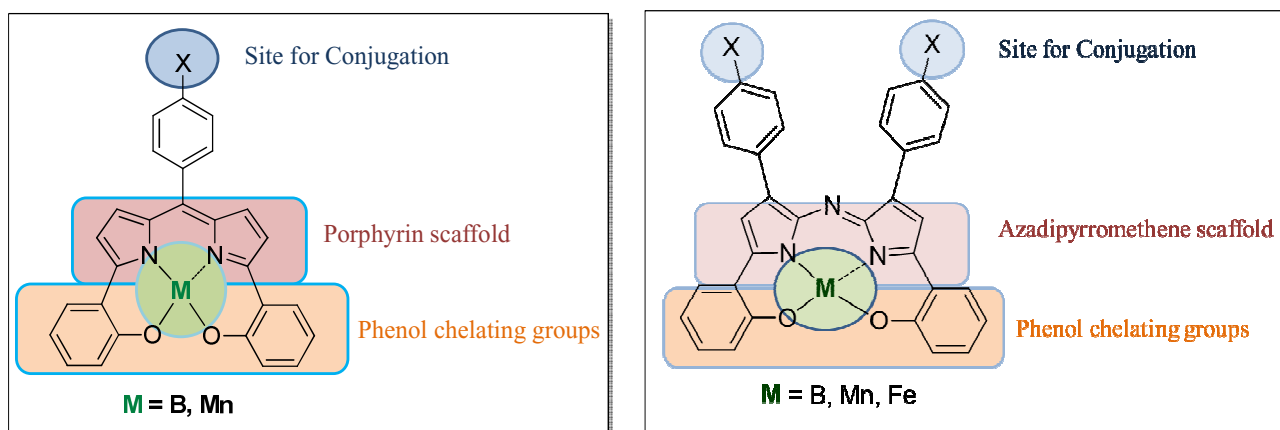
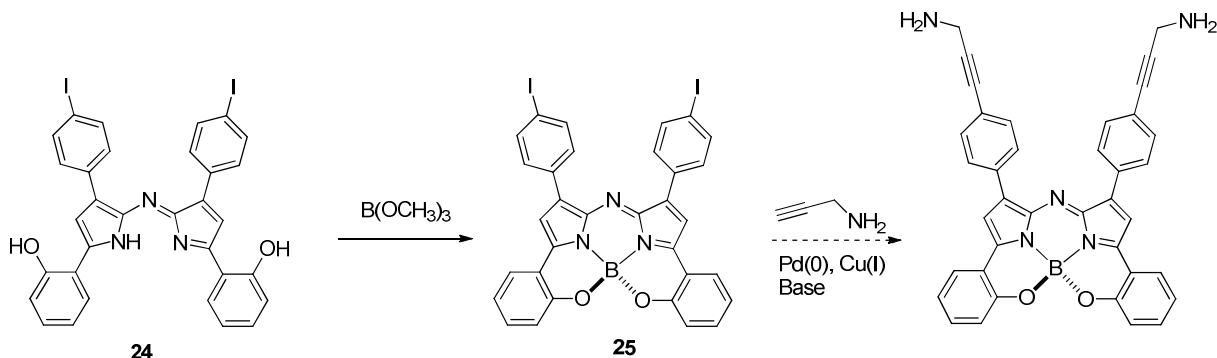


Figure 6. DPM and aza-DPM structure characteristics

Structurally, these systems are relatively similar except for the *aza*-DMP systems there is a nitrogen instead of a carbon at *meso*-position.^{32, 38} Most *aza*-DMP analogues are known to

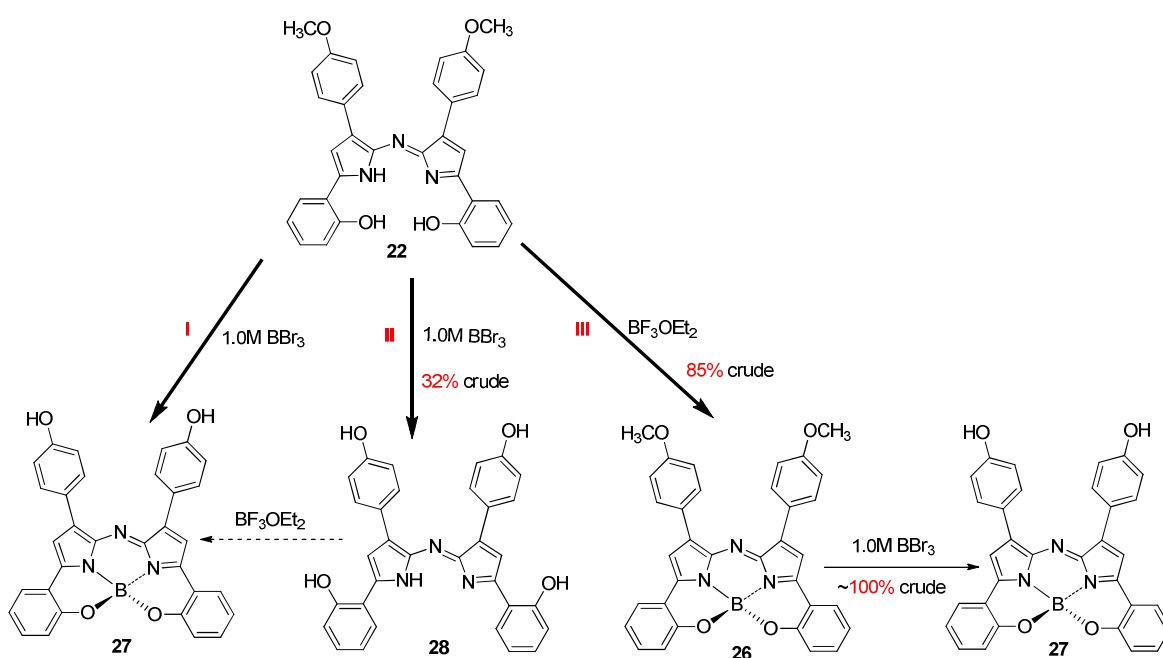
have tetraphenyl substitution giving them an extra site of conjugation X (Figure 6). This site for conjugation (X) is useful for attaching solubilizing groups or other active organic molecules. In order to substitute these types of functional groups, we proposed to use the Sonogashira cross-coupling reaction.⁶¹ To this end, the bis(iodophenyl)-*aza*-DPM **24** was converted to the aza-(*O,N*)-BODIPY complex **25**. In order to prepare the propargyl amine functionalized BODIPY complex (Scheme 17), the Sonogashira coupling of propargyl amine with the di-iodo-compound **25** was attempted. Unfortunately, while small amounts of desired product was formed, the yields were very low and, the product mixture was very insoluble which made it difficult to isolate and purify.



Scheme 17. Attempted synthesis of a linkable aza-BODIPY analogue

At this point, we shifted our synthetic work to the bis(methoxyphenyl)-bis(hydroxyphenyl)-*aza*-DPM systems (Scheme 18). In method I, the bis(methoxyphenyl)-*aza*-DPM **22** was treated with excess BBr_3 to deprotect the methyl ethers and form the aza-(*O,N*)-chelated-BODIPY **27** in one-pot reaction. Unfortunately, the bis(hydroxyphenyl)-*aza*-BODIPY **27** did not form, which is very unusual since this reaction works well in the related non-*aza*-BODIPY systems. In the second method, treatment of **22** with excess BBr_3 in CH_2Cl_2 solution afforded tetra(hydroxyphenyl)-*aza*-DPM ligand **28** in 32% yield after a

methanol (acidic) workup. In an attempt to prepare the chelated aza-BODIPY, compound **28** was reacted with $\text{BF}_3 \cdot \text{OEt}_2$ under basic conditions. Unfortunately, this reaction was also unsuccessful. As an alternative, we attempted to make the desired bis(hydroxyphenyl)-aza-BODIPY **28** in two steps as shown by using $\text{BF}_3 \cdot \text{OEt}_2$ on the free ligand **22** to form **26**. This time, removing the methyl ethers with excess BBr_3 in methylene chloride solution after aza-BODIPY formation was successful affording the final product **27**.

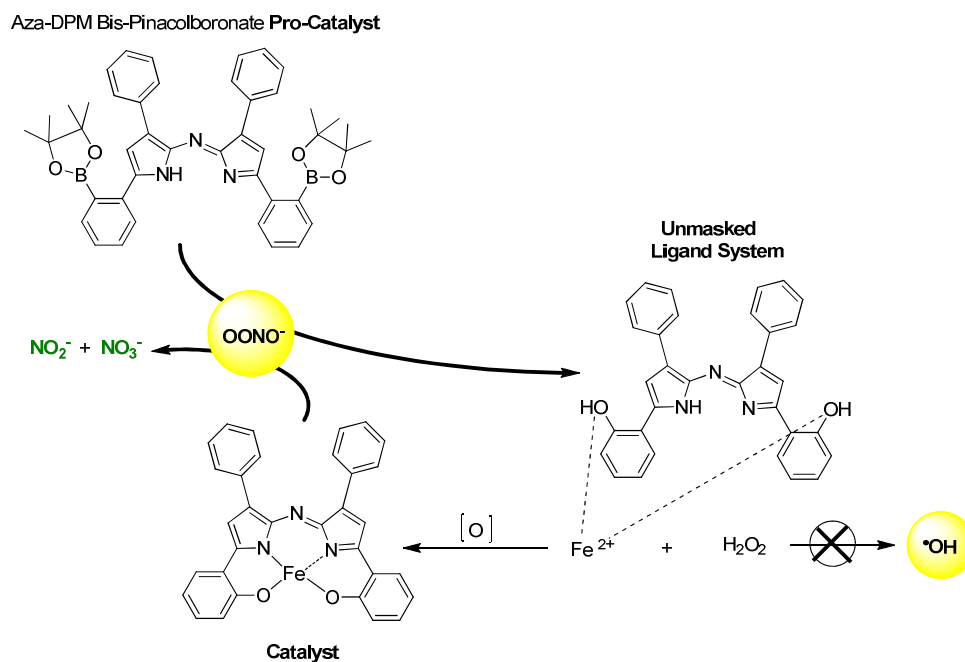


Scheme 18. Synthesis of bis(hydroxyphenyl)-aza-DPM analogues

Part III: Future Direction: aza-DPMs as Oxidant-Activated PNDCs

The idea behind the synthesis of aza-dipyrromethenes systems is their relevance to our “oxidant triggered and activated peroxyxynitrite decomposition catalysts” project. The major obstacle to the development of metallopharmaceuticals appears to be the concern of the FDA, the pharma companies, and the research community regarding potential metal

dissociation from the metallopharmaceutical. If this were to occur, there may be cell toxicity from the generated free metal *in vivo*. With this concern in mind, we worked on developing a new approach which takes advantage of oxidative stress as a triggering mechanism for the activation of a non-metallic pro-catalyst (Scheme 19). Thus, in response to the developing pathology, the pro-catalyst (bis-pinacolboronate analogue) is oxidatively unmasked by the reaction of PN or H_2O_2 to yield the corresponding bis(hydroxyphenyl)-aza-DPM. These unmasked ligand systems would then scavenge endogenous toxic free iron and convert these ligands into an iron-based PNDC. Thus, under physiological conditions, the activated Fe(III)-aza-DPM catalyst can destroy additional PN species *in vivo* and reduce PN to the less toxic NO_2^- .¹⁶ Thus, the conditions of oxidative stress are attenuated by a two-fold mechanism of action: 1. the scavenging of $\bullet\text{OH}$ generating iron, and 2. the *in situ* generation of a Fe(III)-based PNDC without the need for dosing an exogenous metal complex.



Scheme 19. Oxidant triggered pro-catalyst

To this end, the Fe(III)-based aza-DPM complex (catalyst in Scheme 19) was synthesized as a standard and analyzed using our boronate oxidation assay. In preliminary studies, the Fe(III)-aza-DPM complex was able to inhibit the PN-mediated oxidation reaction of 4-acetylboronic acid but the percent inhibition values were low and irreproducible. We believe that this is due to the insolubility of the Fe(III)-complex in the assay media. To solve this problem, future studies by the group will involve new substituted *aza*-DPM systems with enhanced water solubility properties similar to those described for the non-*aza*-DPM systems earlier in this thesis. Future studies involving oxidant-triggered pro-catalysts will probe their efficiency in scavenging iron, the stability of the resulting complexes, and their ability to catalyze the decomposition of PN under a variety of biologically relevant conditions.

CHAPTER IV

EVALUATION OF PNDC ACTIVITY

Boronate Oxidation Assay

As mentioned in Chapter 1, PN has a very short half-life of 10 milliseconds and therefore it cannot be directly observed *in vivo*. PN has been studied both *in vivo* and *in vitro* by analysis of the reactions of its decomposition products ($\cdot\text{NO}_2$, $\text{CO}_3^{\cdot-}$, $\cdot\text{OH}$) and/or modification of biological molecules.^{2,6,8,40} Several analytical techniques currently used to study the presence ROS/RNS include: chemiluminescent immunoassay, electron paramagnetic resonance (EPR) spin trapping, and stopped flow kinetic analysis of various reactions of these species.^{40, 45-47} Although these techniques are effective in studying ROS/RNS, they are highly specialized techniques. Our group wanted a simpler, cost effective protocol in order to evaluate PNDC activity toward PN. Thus, the boronate oxidation assay was therefore developed. This assay has now become a simple and efficient *in vitro* method for the direct measurement of our synthesized complexes (e.g. Mn(III)-DPMs and Mn(III)-porphyrins) ability to inhibit the oxidation of 4-acetylboronic acid by PN (Figure 7).^{14, 30}

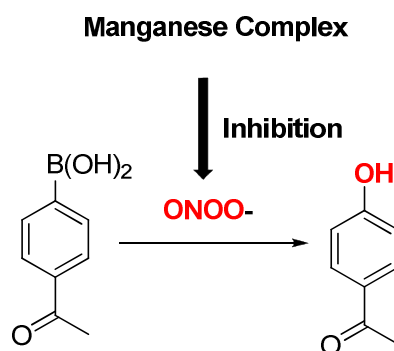
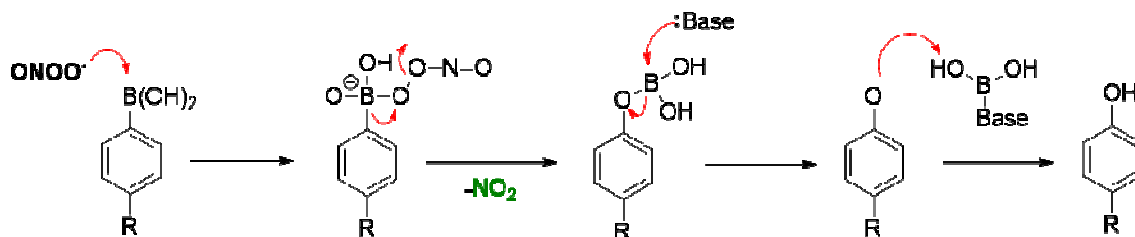


Figure 7. PNDC activity: inhibition of the oxidation of 4-acetylphenylboronic acid

Boronic acids are well-known to undergo rapid direct oxidation by PN, H_2O_2 and HOCl .⁴⁰⁻⁴¹ In this reaction, the PN (ONOO^-) behaves as a nucleophile and attacks the empty p-orbital of the sp^2 hybridized boron atom. A peroxyborate intermediate is produced which undergoes rearrangement and hydrolysis to yield corresponding phenolic product (Scheme 20).



Scheme 20. Oxidation of a phenylboronic acid to the corresponding phenol by PN

In this assay, the PNDC complexes compete with 4-acetylphenyl boronic acid by reacting directly with PN. If the rate of interception of PN by the PNDC is in the range of the rate of reaction of the boronate with PN, then the complexes would be able to inhibit the oxidation. The second-order rate constant for the conversion of 4-acetylphenyl boronic acid to 4-acetylphenol by PN ($k = 1.0 \times 10^6 \text{ M}^{-1}\text{s}^{-1}$ at pH = 7.4) was measured via stopped-flow kinetic methods.⁴⁰⁻⁴¹

Results and Discussion

The primary use of the boronate oxidation assay is to determine if our complexes are active towards the decomposition of PN by direct reaction with a rate that is faster than PN can decompose on its own in aqueous media. The PNDCs activity can be measured by the percent inhibition (Equation 6), where OX_{cat} = 4-acetylphenol oxidation product in the presence of catalyst and $\text{OX}_{\text{control}}$ = 4-acetylphenol oxidation product in the absence of catalyst:^{14, 30}

$$\% \text{ Inhibition} = \left(1 - \frac{OX_{\text{cat}}}{OX_{\text{control}}} \right) \times 100 \quad (\text{Eq. 6})$$

Also, given a measured second-order rate constant, the estimated second-order rate constants for the oxidation of Mn(III) to Mn(V)O for all of our catalysts can be determined by the following formula (equation 7):^{14, 30}

$$k = \left(\frac{\%I}{100 - \%I} \right) \times (1.6 \times 10^6) \quad (\text{Eq. 7})$$

Previously work published by our group determined the percent inhibition values of various PNDCs.^{14, 26} All of the complexes were found to be active and effective in the decomposition of PN. The Mn(III)-DPM compounds (SR110, SR126, SR135) were tested and showed a percent inhibition in the range of 25-30% with their estimated k values ranged from of 10^5 - $10^6 \text{ M}^{-1}\text{s}^{-1}$. These results indicated that these catalysts were exceptional in preventing the oxidation of 4-acetylboronic acid by PN. In order to validate our results and the assay, MnTMPyP⁵⁺ and Ebselen were both analyzed as controls. MnTMPyP⁵⁺ and Ebselen (Figure 8) are known to react with PN and are considered therapeutic molecules that detoxify PN *in vivo*.^{5, 14, 26}

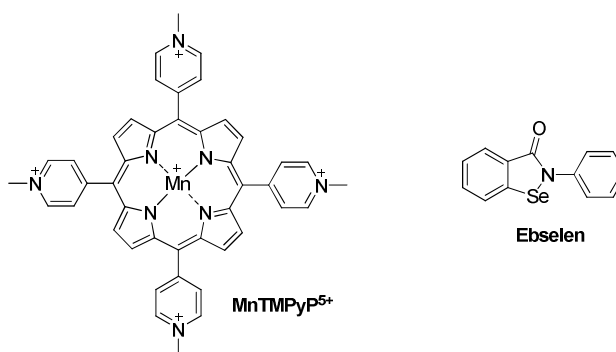


Figure 8. Mn(III)-tetrakis-(*meso*-N-methylpyridinium) porphyrin and Ebselen

Catalyst	Log P	% Inhibition at 25 °C	Second-Order Rate Constant k ($M^{-1}s^{-1}$) at 25 °C
MnTMPyP ⁵⁺	-4.54 ± 0.16	62.4 ± 0.68	^b 2.6 x10 ⁶ ^a 1.8 x10 ⁶
Ebselen	-----	51.7 ± 1.14	^b 1.7 x10 ⁶ ^a 2.0 x10 ⁶

(a) Second-order rate constant measured via stopped-flow spectroscopy (b) Experimental calculated apparent second-order rate constant based upon % Inhibition. ²⁵

Table 1. MnTMPyP⁵⁺ and Ebselen activity: inhibition 4-acetylboronic acid oxidation by PN²⁵

Based on the data in table 1, the polycationic MnTMPyP⁵⁺ and Ebselen can inhibit the 4-acetylboronic acid oxidation reaction by approximately 62% and 52%, respectively. The apparent second order rate constants for these compounds (as determined by the assay) are relatively close to the reported literature value (determined by stopped-flow methods). This information validates that the boronate oxidation assay is a reliable method for determining the activity of PNDCs *in vitro*.

As mention in Chapter III, the prototype Mn(III)-DPMs used in these studies were originally designed to be lipophilic (membrane soluble) to promote oral activity and cell penetration. As a result, these prototypes are somewhat insoluble in aqueous media. Thus, the compounds require surfactants to get them into solution for assay studies. Surfactants are amphiphilic surface-active agents containing both hydrophilic “polar head” group and a hydrophobic “nonpolar tail” (Figure 10).⁵⁷ In an aqueous environment, the hydrophobic groups aggregate to form spherical micelles and other aggregated architectures.⁵⁰ These architectures can only exist at or above the critical micelle concentration (CMC). The CMC is defined as the monomer surfactant concentration above which micelles are formed or appear.^{49-50, 57} The hydrophilic nature of the outer shell of a micelle mainly depends on the chemical nature of surfactant. Surfactants are usually categorized as anionic, nonionic, cationic and amphoteric. Based on the composition of surfactants and the lipophilic nature of

our PNDC complexes, a PNDC would be found in the core/interior portion of the micelle (Figure 9).

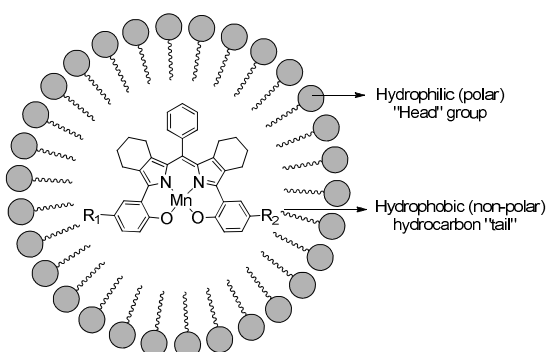


Figure 9. General structure of surfactant with a PNDC catalyst

In order to improve the solubility and catalytic activity of our PNDCs, two surfactants, Brij-35 and sodium dodecyl Sulfate (SDS) were investigated. The purpose of this study was mainly to compare and contrast these two surfactants and ultimately determine the best one for this assay. Importantly, our goal was to identify a surfactant that gave reproducible results for structure-activity relationship (SAR) studies.

SDS ($\text{CH}_3(\text{CH}_2)_{11}\text{OSO}_3\text{Na}$) is non-toxic anionic surface-acting agent commonly used in household and personal care products. Structurally, SDS contains a 12-carbon alkyl chain that is attached to a sulfate ion “polar head” group.⁴² In biochemical research, SDS is used as a detergent that disrupts cells or protein structures. Prior to the current studies with Brij-35, SDS was the main surfactant used to analyze PNDC activity in our group. Brij-35 is a neutral (nonionic) surfactant containing a hydrophilic polyoxyethylene glycol (23) lauryl ether ($\text{C}_{12}\text{EO}_{23}$) chain.⁴⁹ The ether oxygens in the polyethylene glycol chain interact with the water molecules while the alkyl chain can solubilize the lipophilic PNDC complexes. Brij-35 is also used as a detergent in various biological methods usually to solubilize membrane proteins.⁴⁹⁻⁵⁰

In this study, four different solutions of 100 mM phosphate buffer at pH = 7.4 (containing either 0.07% or 0.7% concentrations of Brij-35 or SDS) and 100mM DTPA were prepared. It is important to note that both concentrations (0.07% and 0.70%) are well above the CMC for both surfactants (CMC for SDS = 0.23% w/v or 7-10mM and Brij-35 = 0.11% w/v or 0.09mM in pure water).^{55, 59} All PNDC compounds (Figure 10) analyzed for the PNDC activity were active (to some extent), however the percent inhibition for individual PNDCs varied between surfactants and also when different concentrations of surfactant were used.

The data in table 2 compares the inhibition of 4-acetylphenyl boronic acid oxidation and the estimated rate constant of complexes **15**, **29**, SR110, SR135, SR175, SR6, and MnTMPyP⁵⁺ as the concentration of Brij-35 is varied. These studies were done using either 0.07% or 0.70% surfactant.

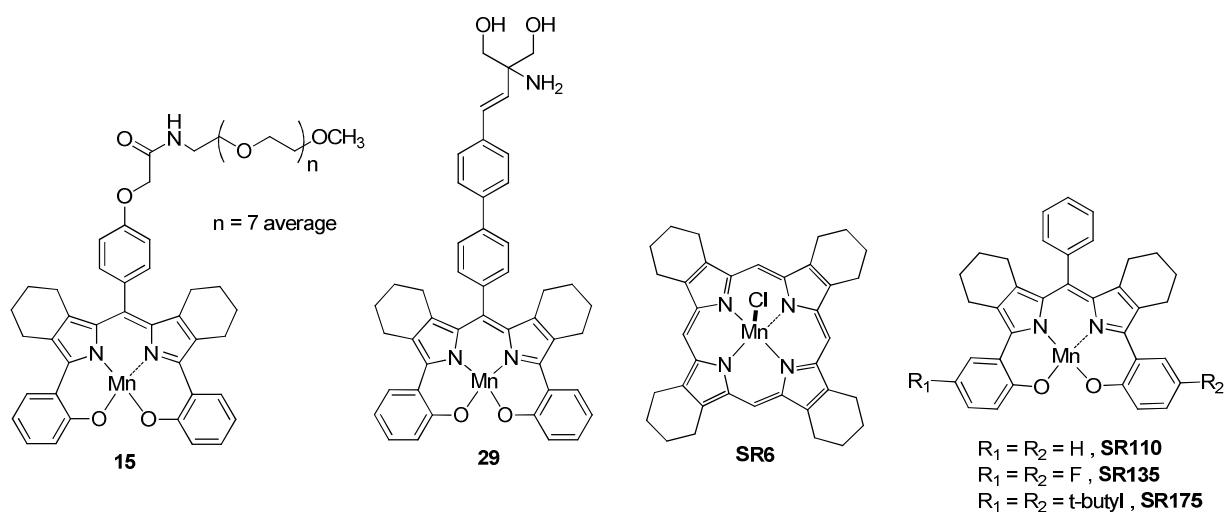


Figure 10. The complexes tested for PNDC activity

	0.07% Brij-35	0.70% Brij
Catalyst	% Inhibition (25 °C)	% Inhibition (25 °C)
15	28.8 ± 5.2	59.4 ± 2.6
29	-	30.6 ± 5.0
SR110	18.5 ± 6.1	60.2 ± 1.2
SR135	11.4 ± 2.0	31.4 ± 4.5
SR175	22.5 ± 2.2	32.9 ± 2.1
SR6	39.8 ± 2.3	32.4 ± 4.8
MnTMPyP ⁵⁺	67.3 ± 2.4	69.8 ± 3.6

Table 2. PNDC inhibition of 4-acetylboronic acid oxidation by PN using Brij-35 surfactant

Our data shows that by varying the concentration of Brij-35 surfactant the percent inhibition values vary for individual complexes. For example, SR110 inhibits the 4-acetylboronic acid oxidation reaction by 60% in 100mM phosphate buffer (containing 0.70% Brij-35), yet only 18% inhibition in 100mM phosphate buffer (containing 0.07% Brij-35). Based on the data presented, we hypothesized that at higher concentrations of surfactant (0.70% Brij-35) there are more micelles to solubilize the lipophilic complex. With more micelles present, the distance required for PN to travel and encounter a micelle with a PNDC complex is shortened. In solutions containing the 0.07% Brij-35, SR110 shows less activity because there are less micelles in solution, thus decreasing the probability that PN will encounter a micelle containing a PNDC.

Furthermore, the data shows that by conjugating the PEG-amine functional group to SR110 to form Mn(III)-*meso*-(PEG-amide)-DPM **15** gives clearly enhances solubility. This

feature might explain the small difference in percent inhibitions between SR110 and Mn(III)-*meso*-(PEG-amide)-DPM **15**. As shown in Figure 11, it was hypothesized that in the buffer solution containing 0.70% Brij-35 both Mn(III)-*meso*-(PEG-amide) and SR110 would be sequestered in the interior of the micelle, yet situated differently. The PEG-amide group of Mn(III)-*meso*-(PEG amide)-DMP **15** is believed to be interacting with the PEG layer (in the periphery) of the Brij-35 micelle. Thus, allowing this PNDC **15** to be more accessible to PN in bulk solution therefore providing higher PNDC activity. Lastly, when SR110 and complex **15** are compared in the buffer solution containing 0.07% Brij-35, the percent inhibition may or may not be significantly different.

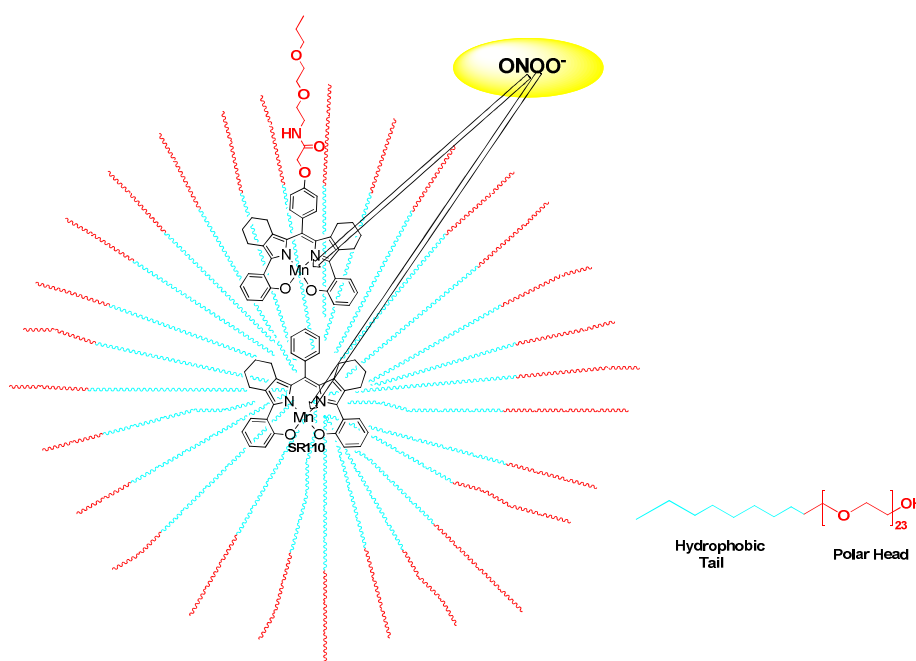


Figure 11. Brij-35 micelle structure

These results support our initial hypothesis that the PNDCs activity would be higher in solutions containing higher surfactant concentrations (0.70% Brij-35), which is demonstrated by the increased in percent inhibitions compared to percent inhibitions obtained from solution with low surfactant concentration (0.07% Brij-35). We concluded that

the differences in percent inhibition may directly be influenced by the amount of micelles present in solution. Since the micelles assist with the solubilization of the lipophilic complex, more micelles increase the probability of a PNDC to encounter PN in the aqueous media. In addition, the physicochemical properties of PNDCs may also affect the PNDC activity. This phenomena can be observed between SR110 and Mn(III)-*meso*-(PEG-amide) **15** in solutions that contained lower surfactant concentrations (0.07% Brij-35). Since these solutions contain less micelles, the hydrophilic component of the Mn(III)-*meso*-(PEG-amide) permits the complex to be slightly more soluble by situating itself differently in the aqueous media. This hydrophilic property allows Mn(III)-*meso*-(PEG-amine) **15** to be more accessible to PN in comparison to SR110. All of the compounds were also analyzed in solutions containing SDS surfactant. These results are reported in table 3.

	0.07% SDS	0.70% SDS
Catalyst	% Inhibition (25 °C)	% Inhibition (25 °C)
15	30 ± 2.5	27.1 ± 2.5
SR110	2.1 ± 1.8	25.7 ± 5.3
SR135	0	13-30
SR6	7.5 ± 2.4	11-30
MnTMPyP ⁵⁺	---	62.4 ± 0.68

Table 3. PNDC inhibition of 4-acetylboronic acid oxidation by PN using SDS surfactant at pH 7.2

Finally, our data shows that the percent inhibitions for the individual compounds are lower when SDS was used. It was hypothesized that the lower values resulted from an electrostatic repulsion between the negative charged head groups at the periphery of the SDS

surface and the negatively charged PN ion. This characteristic would make it harder for PN to penetrate the micelle and encounter the Mn site of the PNDC, which is sequestered inside the micelle (Figure 12).

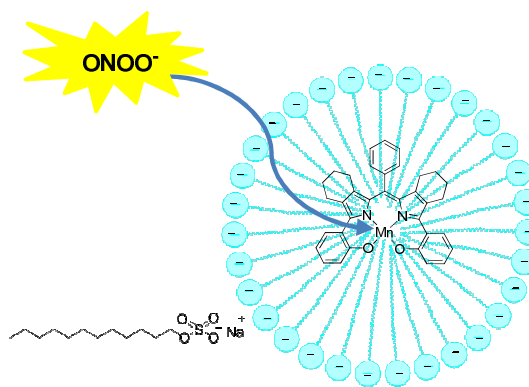


Figure 12. Sodium dodecyl sulfate (SDS) micelle structure

The percent inhibition obtained for MnTMPyP^{5+} in buffer solution containing SDS are consistent with the percentage inhibition of MnTMPyP^{5+} obtained in buffer solution brij-35 surfactant. These results are consistent because MnTMPyP^{5+} has a highly negative partition coefficient ($\log P$). Partition coefficient measures the distribution and/or solubility of an organic molecule in a polar (water) and non-polar (octanol) solvents. Generally, the $\log P$ values less than 1 are hydrophilic and $\log P$ values greater than 1 are lipophilic. Since, MnTMPyP^{5+} has $\log P$ of -4.54 ± 0.16 , in this assay MnTMPyP^{5+} would be localized in the aqueous phase exclusively and not in the interior of the micelle (hence no micelle effect).²⁵ Thus, it is more accessible to PN, enhance higher PNDC activity in both surfactants compared to other PNDCs.

Prevention of Tyrosine Nitration Assay

PN is a highly reactive oxidant that can modify numerous biological molecules and disrupt cellular processes. The principal biological reaction of PN is the nitration of tyrosine

residues of proteins to yield 3-nitrotyrosine. As an example of this, our research group has determined that PN can inactivate methionine enkephalin (met-enkephalin) principally through tyrosine nitration (sulfide oxidation was also observed).⁴³ Enkephalins are endogenous neuropeptides, synthesized in the mammalian spinal cord, and bind to opioid receptors to suppress pain sensitivity.^{22, 43-44} Two types of enkephalins are leu-enkephalin **30** and met-enkephalin **31** (Figure 13).

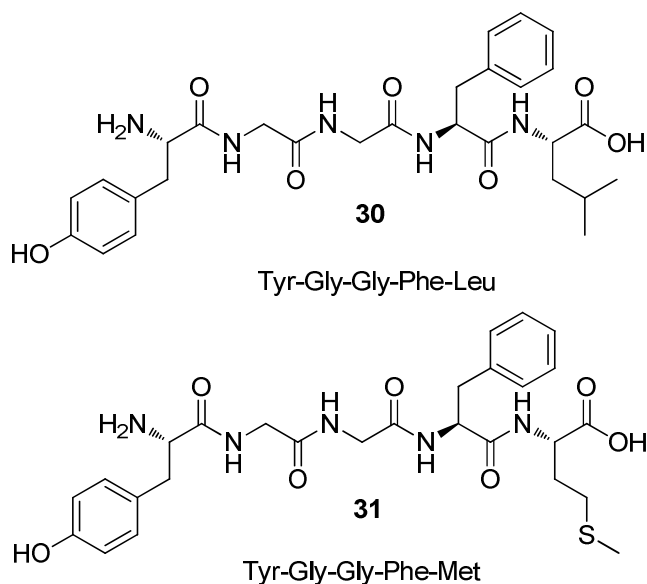


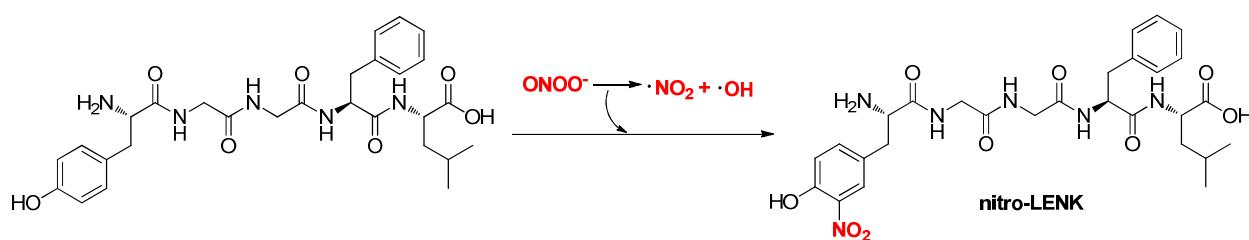
Figure 13. Leu-enkephalin **30** and Met-enkephalin **31** chemical structures

Most opioid peptides have a conserved amino acid sequence in the N-terminus, which consists of four amino acids: Try-Gly-Gly-Phe.⁴³⁻⁴⁴ This amino acid sequence plays an essential role in the general activation of opioid receptors. Furthermore, these neuropeptides differ from each other at their C-terminus. Leu-enkephalin has a Leucine (Leu) and met-enkephalin has a methionine (Met) amino acid. This difference allows the pentapeptide to be very selective and only target a specific opioid receptor.⁴³

Initially, the effects of PN on Met-enkephalin (Met-Enk) were studied. Met-Enk was treated with 5 equivalent of PN *in vitro* at pH = 7.2 (100 mM phosphate buffer) and the

products were analyzed via LCMS. The HPLC chromatogram showed four products, which corresponded to the unreacted Met-Enk, the 3-nitrotyrosine product, and a diastereomeric nitro sulfoxide mixture. This study revealed that PN interacts with Met-Enk by nitrating the tyrosine residue and oxidizing the methylsulfide of methionine to the sulfoxide. Furthermore, the carrageenan-induced hyperalgesia assay was performed to examine palliative effectiveness of Mek-Enk and nitrated/oxidized PN product (3-nitro-sulfoxide Met-Enkephalin, NSO-MENK) in rats.²⁵ The NSO-MENK showed no analgesic effect. Our group concluded that the NSO-MENK had no interaction with the opioid receptor (this was also shown by μ -receptor binding studies). Thus, Mek-Enk and the opioid receptor activities are inhibited when the peptide is modified by PN.³⁰ This may be relevant in chronic pain states, where PN is overproduced.

These studies lead to the design of the prevention of tyrosine nitration assay. This assay examines the ability of our PNDC to protect essential endogenous tyrosine-containing molecules from PN. Leu-enkephalin (LENK) was chosen as the probe for this assay due to its simplicity given that it can only get modified at the tyrosine residue (Scheme 21).



Scheme 21. Nitration of LENK by PN

In order to determine the PNDCs catalytic ability to prevent tyrosine nitration by PN, LENK was treated with 1 eq. of PN *in vitro*. These experiments were done in a 100mM phosphate buffer at pH = 7.4, in the presence or absence of catalyst (SR110, SR135, or SR6). The amount of nitration was followed by LCMS.

Experimentally, when 1 equivalent of LENK was treated with 1 equivalent of PN approximately 33% of the LENK tyrosine residue was nitrated (Figure 14). In contrast, when 1.0 equivalent LENK was treated with 1 equivalent of PN in the presence of 1.0 equivalent of the Mn(III)-DPM SR110, a 60% inhibition of tyrosine nitration was observed. Interestingly, the Mn(III) porphyrin SR6 showed an increase in nitration over the control under the same conditions. These experiments confirmed the catalytic nature of two different classes of PNDCs. As one of the Mn(III)-DPMs, SR110 rapidly reacts with PN in a two-electron fashion, converting PN to NO_2^- , and thus significantly preventing tyrosine nitration. Whereas SR6, a one electron catalyst, converts PN to $\cdot\text{NO}_2$ radical. Due to the rapid decomposition of PN by SR6, more $\cdot\text{NO}_2$ is generated than is normally produced when PN decomposes on its own (i.e. in the PN+LENK control reaction). This feature leads to more nitration *in vitro*.

Results and Discussion

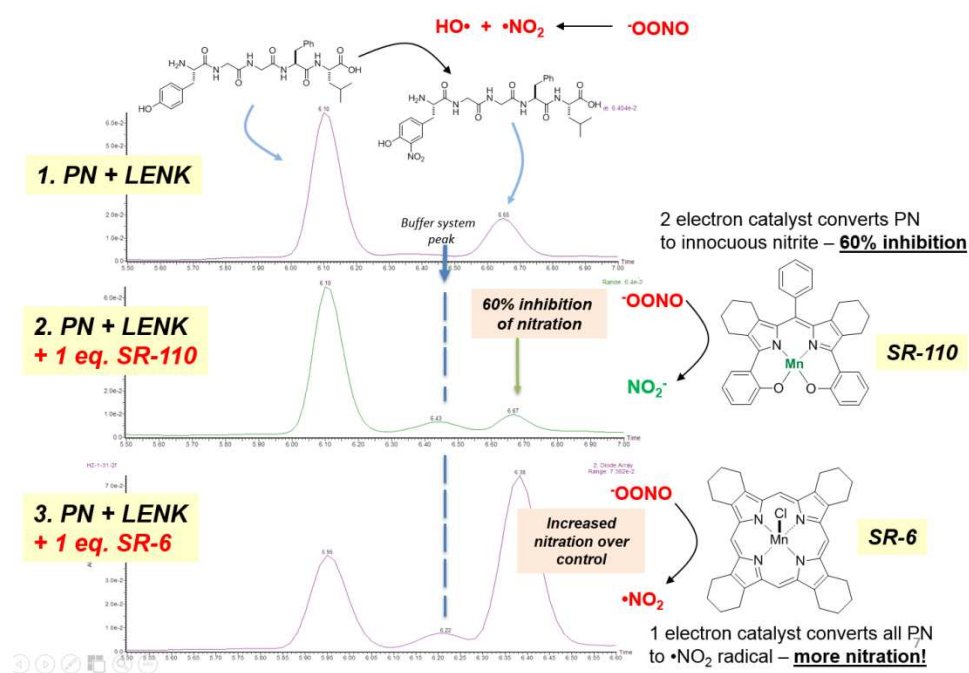


Figure 14. LCMS analysis of 1) PN + LENK; 2) PN + LENK + 1 eq. SR110 and 3) PN + LENK + 1 eq. SR6

As mentioned earlier, the purpose of this assay is to determine the effectiveness of Mn(III)-DPMs in preventing the tyrosine nitration of LENK by PN. SR135 was used to further optimize this assay. In this study, a solution of 1 μ mol of LENK in 3 mL of 100mM phosphate buffer at pH = 7.4 (containing 0.70% Brij-35 surfactant and 100mM DTPA) was prepared. To the mixture was added 1.0, 0.2, or 0.1 equivalent μ mol of catalyst (SR135). To this rapidly stirring mixture 2 μ mol of PN was added. The percent inhibition values of SR135 are reported in table 4. Remarkably, with the treatment of 2 μ mol PN, SR135 afforded: 45% inhibition with 1.0 equivalent of catalyst, 31% inhibition with 0.2 equivalent of catalyst, and 13% inhibition with 0.1 equivalent of catalyst. In summary, these results (in table 4) suggests that the Mn(III)-DPM complexes (e.g. SR135) are acting in a catalytic matter. SR110 is not only able to destroy PN but it is effective in preventing the tyrosine nitration of the endogenous LENK *in vitro*.

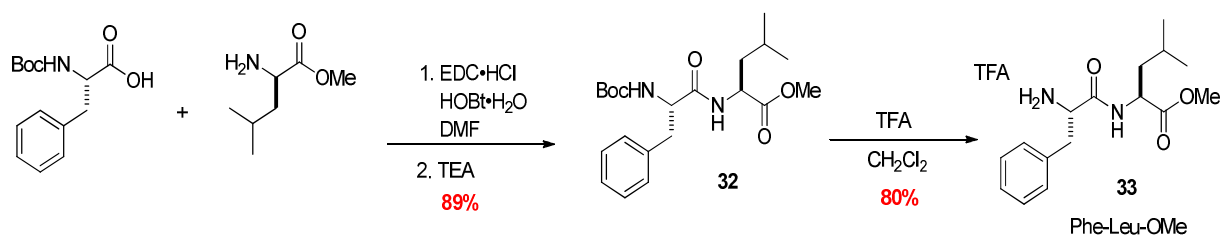
Equivalent (mmol)	SR135 concentration (mM) (in 3 mL buffer solution)	% Inhibition
1.0	0.334	44.6 \pm 3.8
0.2	0.067	31.0 \pm 2.0
0.1	0.033	13.2 \pm 8.3

Table 4. Tyrosine nitration prevention with varying SR135 concentrations

For the prevention of nitration assay, LENK and nitroLENK were both prepared via solution phase synthesis. The nitroLENK metabolite was synthesized to determine the retention time/elution time of the nitroLENK in the HPLC.

Synthesis of Phe- Leu-OMe (33)

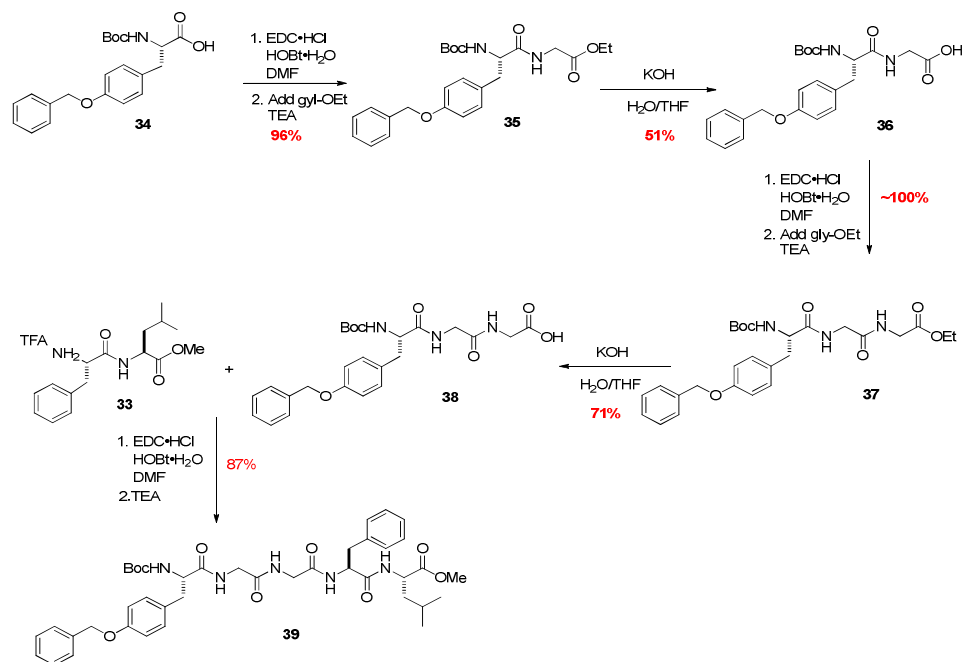
As illustrated on Scheme 23, the dipeptide **32** was synthesized by the EDC-mediated coupling reaction of Leu-OMe with Boc-Phe. The deprotection of the Boc group of the resulting Boc-Phe-Leu-OMe **32** was achieved with TFA in CH₂Cl₂ to yield the TFA salt of Phe-Leu-OMe peptide **33**.



Scheme 22. Synthesis of the Phe-Leu-OMe (**33**)

Synthesis of Boc-Tyr(OBn)-Gly-Gly-Phe-Leu-OMe (39)

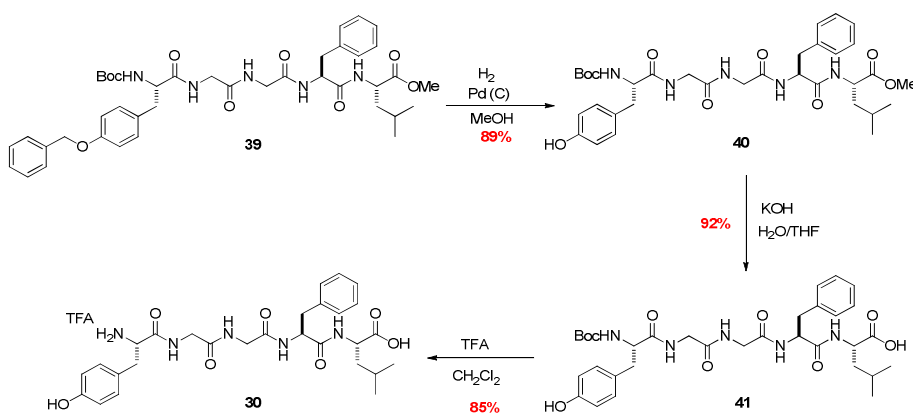
The preparation of LENK began with an EDC coupling reaction of Boc-Tyr(OBn) **34** and Gly-OEt to afford the corresponding benzyl protected dipeptide **35** in 96% yield. Under basic conditions, the ethyl ester of **35** was hydrolyzed to free acid **36**. This material was then coupled with Gly-OEt under standard EDC conditions to give **37**. Tripeptide **37** was then saponified to afford the free acid **38** in 71% yield. The synthesis of **39** required an EDC coupling reaction of **38** and **33** which provided the pentapeptide **39** in 87% yield after purification.



Scheme 23. Synthesis of Boc-Tyr(OBn)-Gly-Gly-Phe-Leu-OMe (39)

Synthesis of LENK

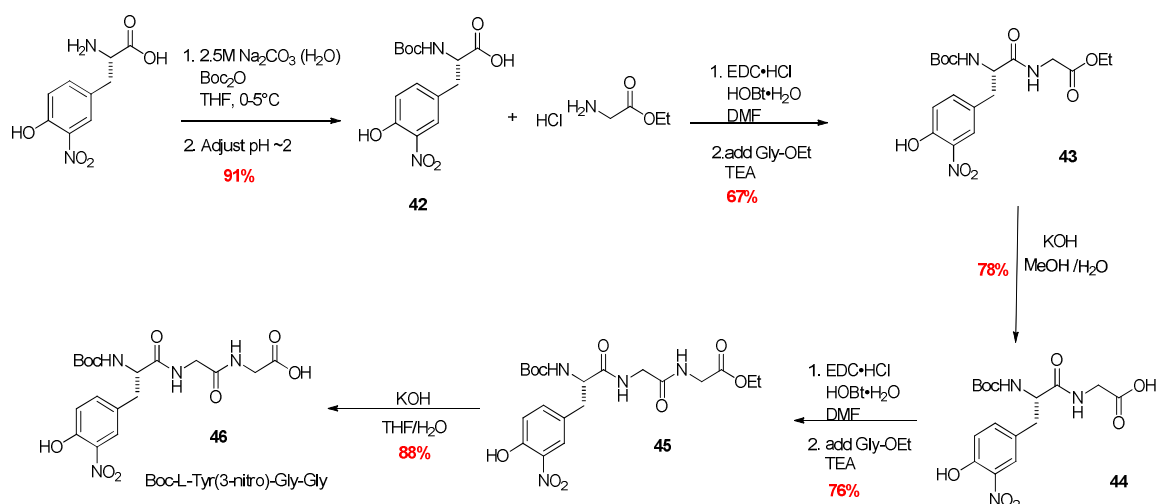
As outlined in Scheme 24, the benzyl protecting group of 39 was removed by hydrogenolysis, which afforded compound 40 with a free tyrosine side chain. This reaction was followed by the hydrolysis of the methyl ester of 40 under basic condition to afford 41 in 92% yield. Finally, the Boc protecting group was removed using TFA in CH₂Cl₂ solution to afford the fully deprotected pentapeptide 30.



Scheme 24. Synthesis of the natural occurring leu-enkephalin 30

Synthesis of Boc-Tyr(3-nitro)-Gly-Gly-OH (46)

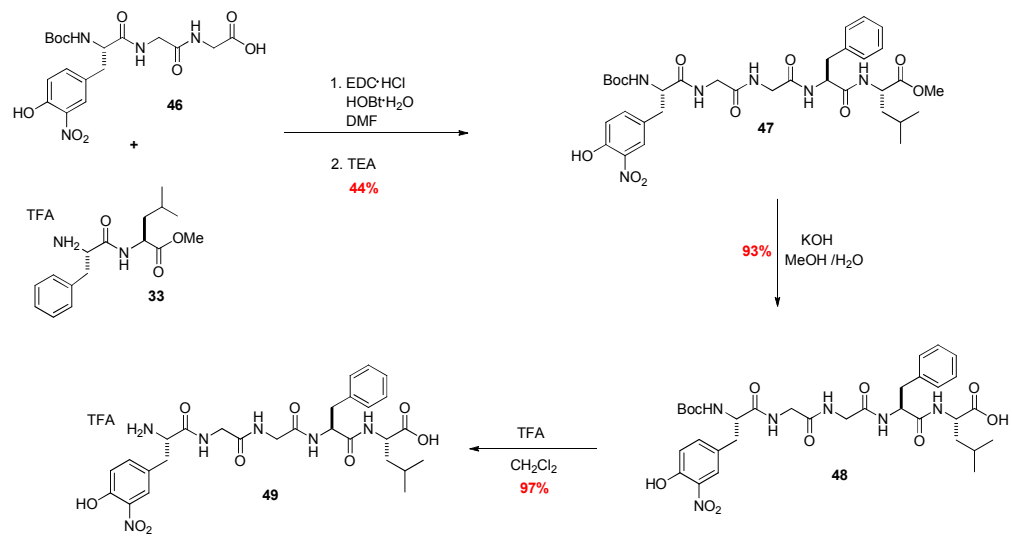
The amine group of 3-nitro-Tyr was protected as the Boc-derivative by treatment of Boc-anhydride under basic conditions. This reaction was followed by an EDC coupling of Boc-3-nitro-Tyr **42** with Gly-OEt·HCl to yield the dipeptide **43**. Hydrolysis of the dipeptide under basic condition gave free acid **44** in 78% crude yield. Compound **44** was coupled again with Gly-OEt to afford Boc-Tyr(3-nitro)-Gly-Gly-OEt **45**. Compound **45** was then saponified to the free acid **46** using KOH in THF/H₂O solution (Scheme 25).



Scheme 25. Synthesis of Boc-Tyr(3-nitro)-Gly-Gly-OH (**46**)

Synthesis of nitro-LENK

To prepare the nitrated LENK derivative **49**, the newly synthesized peptides **33** and **46** were coupled using EDC standard conditions. Compound **47** was then saponified with KOH in MeOH solution to afford **48** in 93% yield. Then, the Boc-group was removed using TFA in CH₂Cl₂ to afford the desired nitro-LENK **49** as a yellow solid in 97% yield (Scheme 26). All intermediate steps were analyzed by LCMS to ensure the completion of each reaction.



Scheme 26. Synthesis of nitro-LENK **49**

CHAPTER V

FUTURE DIRECTIONS: TARGETING PEROXYNITRITE IN T2DM

According to the World Health Organization (WHO), it is estimated that 347 million people are living with diabetes worldwide and of these diagnosed cases 90 to 95 percent are type II diabetes (T2DM).⁵¹ Unhealthy diet, smoking, and/or physical inactivity can lead to obesity. Obesity and insulin resistance are known to be a primary cause of T2DM. T2DM is a chronic inflammatory disease caused by elevated levels of triglyceraldehyde/free fatty acids, blood sugar (hyperglycemia), and pro-inflammatory cytokines (e.g. NF-kappaB). These conditions lead to a chronic inflammatory status and elevated production of PN.^{5, 21, 51-52, 58, 60} As described in Chapter I, PN is known to induce nitration and oxidation of critical biomolecules important to cellular homeostasis. Currently, many proteins have been shown to be nitrated and modified in skeletal muscles, pancreatic β -cells, and adipose tissues as a result of elevated PN levels. Although it is still somewhat controversial, PN appears to be a major component of pancreatic β -cell destruction and pathogenesis of insulin resistance in animals and humans.⁵²⁻⁵³ Thus, the development of new agents that can decompose PN should be a viable approach for treating T2DM.

In fact, under chronic nutrient overload conditions that simulate β -cell dysfunction, the Kwon group has shown SR135 (Mn(III)-DPM PNDC prototype) inhibits lipid droplet formation, restored insulin content and normalized the architecture of the pancreatic islets of high fat diet-fed mice. With these results in hand, to further extend the activity of our complexes for applications to diabetes, we chose to develop a methodology for the synthesis of Mn(III)-DPMs which incorporate site(s) for conjugating a biomolecule such as the PPAR agonist. As stated in Chapter 1, PPAR receptors (particularly the PPAR γ isoform) regulate

lipid and glucose metabolism and insulin sensitivity (in muscle cells).²² Therefore, the PPAR γ subtype has been an attractive target for the treatment of T2DM. A series of synthetic PPAR γ agonists (rosiglitazone, GI262570, pioglitazone) have been shown to be effective in reducing plasma glucose and free fatty acid levels *in vivo*.⁵⁴ However, PPAR γ is known to be nitrated and inactivated by PN under the chronic inflammation of metabolic syndrome. Thus, we hypothesized that a combination/conjugation of our functionalized PNDC and a PPAR γ agonist maybe an interesting therapeutic approach not only to protect the PPAR γ receptor from nitration and inactivation but effectively restore insulin sensitivity. Thus, we hypothesized that a co-dose of PNDC/PPAR γ may have a synergistic action. This could ultimately reduce the effective dose of the PPAR γ agonist.

PPAR γ agonist/PNDC Conjugate Design

In 2001, researchers from GSK reported a study on the synthesis of tyrosine-based PPAR γ agonists with a reduced molecular weight.¹⁹ The X-ray crystallography and molecular modeling of the PPAR γ ligand-binding domain with bound their GI262570 agonist were studied. These studies indicated that the carbon meta to oxazole of bound GI262570 was exposed to solvent (Figure 15).²⁰

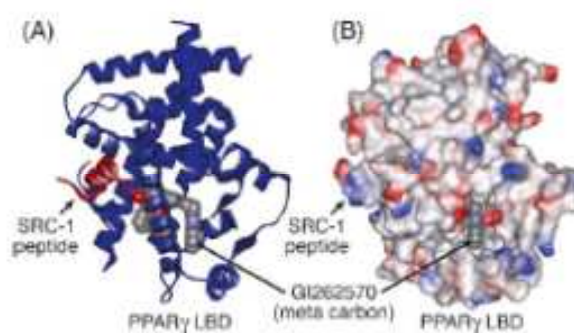


Figure 15. Molecular modeling structure of PPAR γ binding domain²⁰

This information was used to design a fluorescent probe (fluorescein isothiocyanate, FITC)-GI262570 conjugate system to further investigate the PPAR γ binding domain by fluorescence polarization studies. Since GI262570-FITC had a good binding affinity ($K_i = 61$ nM) to PPAR γ , we believe our proposed conjugate system (SR110/PPAR γ agonist) may be a viable design due to structural similarities (Figure 16).¹⁹ The benzophenone group (highlighted in red) of GI262570-FITC is replaced with pyrrole in our design of a PNDC-PPAR γ agonist conjugate based upon GSK SAR studies.

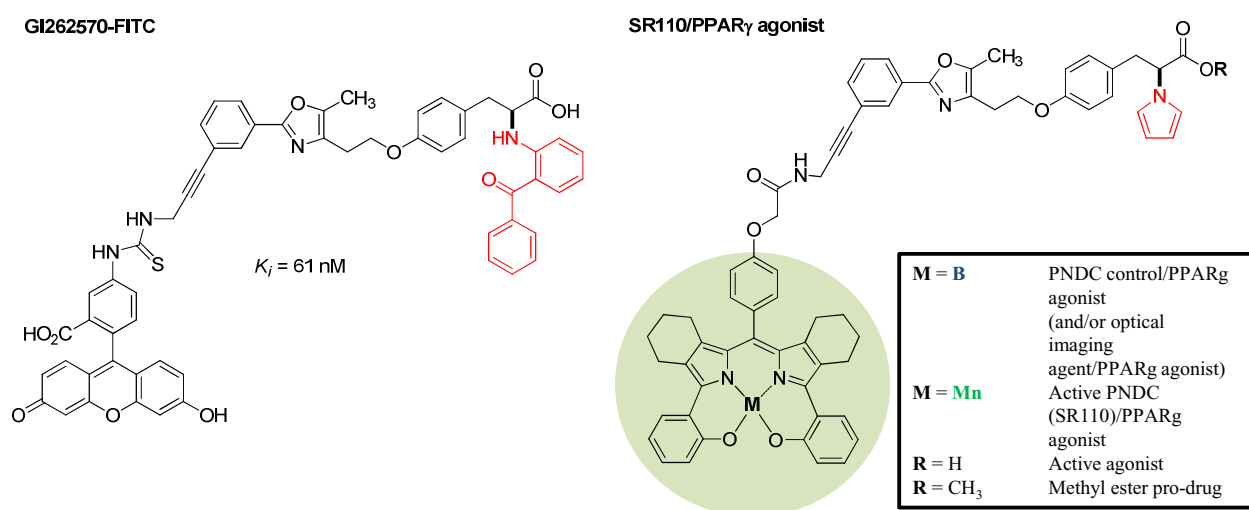
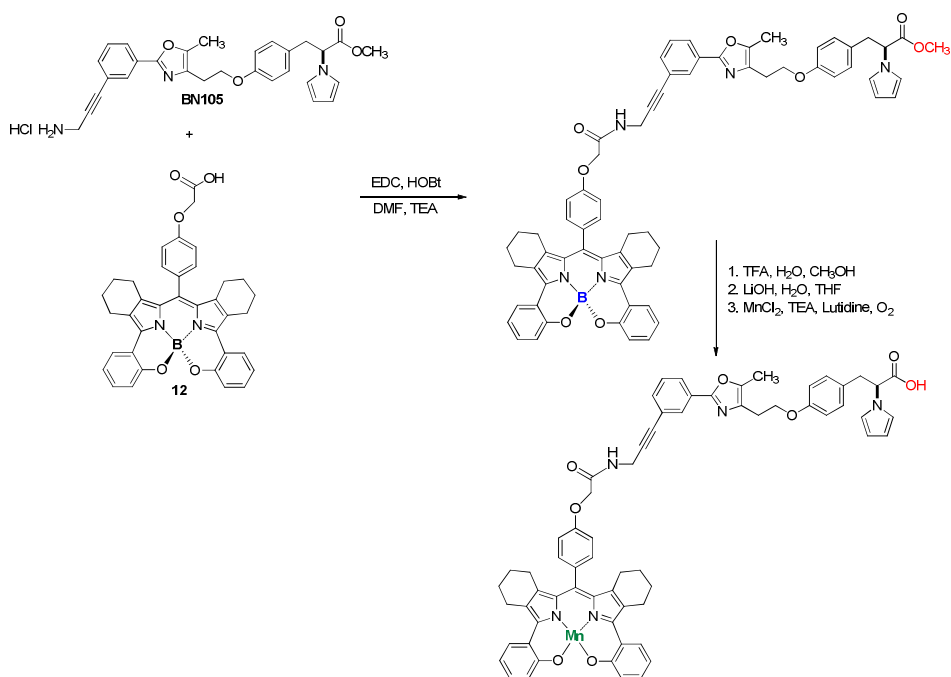


Figure 16. GI262570-FITC and PNDC-PPAR γ agonist chemical structures

Synthesis of SR110/PPAR γ Conjugate

The development of synthetic chemistry for preparing the chelated-(*O*, *N*)-BODIPY **12** containing a phenoxyacetic acid group for conjugation has been an important goal for this research. As illustrated in Scheme 27, compound **12** can be linked to the propargyl-amine derivative BN105 **50** using EDC coupling standard conditions to afford a chelated-(*O*, *N*)-BODIPY-PPAR γ agonist conjugate. The following reactions would include: the hydrolysis of the methyl ester to the active PPARagonist acid and substituting boron atom with the Mn

transition metal to afford the desired PPAR γ agonist/PNDC product. This chemistry is currently under development in the group to further extend the studies in this thesis.



Scheme 27. Synthesis of the PPAR γ / SR110 conjugate

A future goal will be further study the anti-diabetic effects of these compounds in nutrient overload/ insulin resistance models in collaboration with the Kwon group at SIUE school of pharmacy. In addition, we would like to investigate the synergistic effects of individual compounds (SR110 + BN105) as a co-mixture compared to the SR110-PPAR γ agonist conjugate to determine if the conjugate system has a greater synergistic effect over the individual compounds (co-mixture).

CHAPTER VI

CONCLUSION

The overproduction of PN is responsible for the oxidation and nitration of a number of important biomolecules. This highly reactive oxidant species is well-known to play a central role in the development of various pathologies associated with chronic inflammation such as diabetes, Alzheimer's disease and neuropathic pain.^{2, 5, 7, 21, 30} Therefore, agents that can intercept and decompose PN may offer a new mechanism for treating these pathophysiological conditions. Redox-active transition metal complexes such as Mn(III)-DPMs are suitable candidates for attenuating PN both *in vivo* and *in vitro*. These complexes have been shown to redirect oxidative potential of PN through a two-electron mechanism reducing PN to less toxic NO_2^- , and therefore may show great promise as therapeutics and pharmacological agents.

The original Mn(III)-DPM prototypes were designed to be lipophilic to promote oral activity. In fact, these complexes have been shown to be orally active in animal models of nutrient overload/insulin resistance and in models of inflammatory and neuropathic pain.¹⁴ However, these catalysts are somewhat insoluble in water and we believed that their bioavailability could be improved by increasing their water solubility while maintaining suitable lipophilicity. In this study, effective synthetic methods were developed for preparing a functionalized Mn(III)-DPM with a site of conjugation for the coupling of water-solubilizing groups (i.e. PEG) and bioactive organic molecules (i.e. PPAR γ agonist). The crosslinking of phenoxyacetic acid on the DPM backbone with a primary amine like PEG-amine under standard EDC coupling conditions to prepare Mn(III) *meso*-(PEG-amide)-DPM **15** were investigated. In addition, preliminary synthetic studies for the development oxidant-

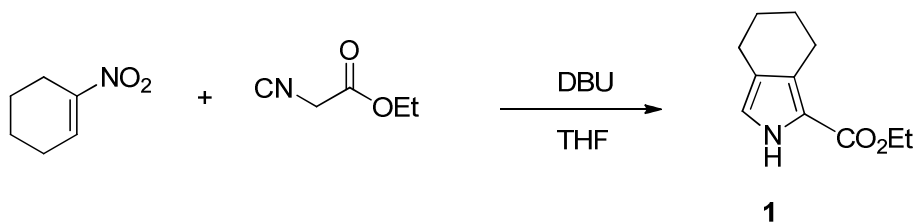
triggered *aza*-DPM pro-catalyst systems were also explored. Finally, the boronate oxidation and prevention-of-nitration assays have been further improved. Various surfactants were analyzed and amongst the chosen surfactants, Brij-35 gave us the most reproducible results. Studies with Brij-35 were found to be quite useful in characterizing how the functionalized PNDCs may interact with membranes *in vivo*.

CHAPTER VII

EXPERIMENTAL

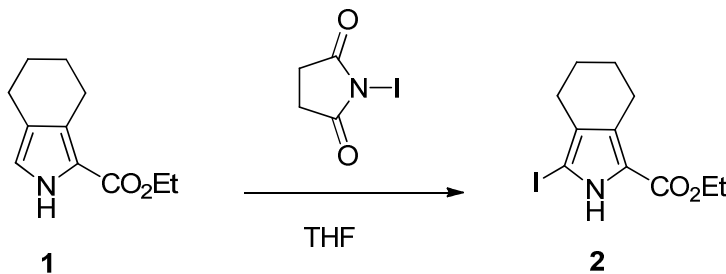
General Methods

Analytical thin layer chromatography (TLC) was performed on Analtech 0.25 mm silica gel GF plates. Visualization was accomplished with exposure to UV light or by developing in an iodine chamber. Solvents for extraction were HPLC or ACS grade. Chromatography was performed by the protocol of Still with Dynamic Adsorbents silica gel 60 (200-400 mesh) with the specified solvent system. The ^1H NMR and ^{13}C NMR spectra were recorded on a JEOL ECS 400. ^1H NMR spectra were reported in ppm from tetramethylsilane on the δ scale. Data are reported as follows: Chemical shift, multiplicity (s = singlet, d = doublet, t = triplet, q = quartet, m = multiplet, b = broadened, obs = obscured), coupling constants (Hz), and assignments or relative integration. ^{13}C NMR spectra were reported in ppm from the central deuterated solvent peak. Data are reported as follows: chemical shift, multiplicity. Grouped shifts are provided where an ambiguity has not been resolved. LCMS were run on a Waters Alliance-SQ 3100 system using Agilent Eclipse (XBD-C18, 4.6 x 150 mm, 5- Micron) column and the indicated gradient solvent system.

Ethyl 4,5,6,7-tetrahydro-2*H*-isoindole-1-carboxylate (**1**)

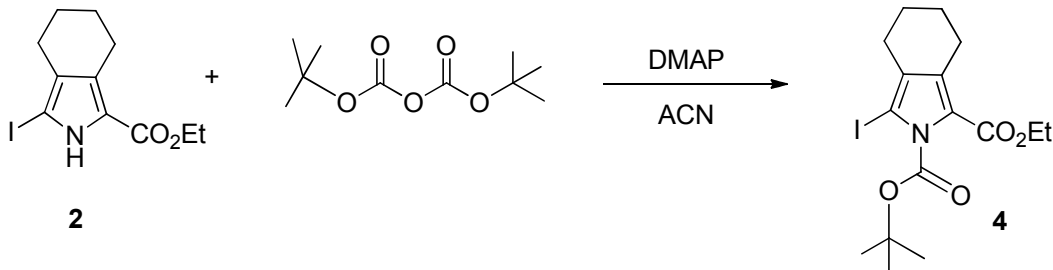
A solution of 1-nitrocyclohexene (8.87 mL, 78.7 mmol) in THF (100 mL) was placed in a flask in a cool water bath. Carefully, ethyl isocyanoacetate (8.75 mL, 78.7 mmol, 1 equiv) was added. DBU (12.0 mL, 78.7 mmol, 1 equiv) was then added dropwise via an addition funnel and the reaction mixture was stirred at room temperature under argon for 18 hr. The reaction mixture was treated with CH₂Cl₂ (300 mL) and washed with water (2 x 200 mL) and brine (200 mL). The organic layers were separated, dried over anhydrous Na₂SO₄, filtered and concentrated. The brown residue was purified by flash column chromatography (silica gel/CH₂Cl₂/MeOH 10:1 to 5:1) to afford 11.7 g of compound **1** (77% yield) as bright yellow crystals: ¹H NMR (CDCl₃) δ 8.91 (bs, 1 H), 6.64 (d, *J* = 3.21 Hz, 1 H), 4.28 (q, *J* = 7.03 Hz, 2 H), 2.80 (t, *J* = 5.95 Hz, 2 H), 2.53 (t, *J* = 5.70 Hz, 2 H), 1.77-1.68 (complex m, 4 H), 1.33 (t, *J* = 7.35 Hz, 3 H). ¹³C NMR (CDCl₃): δ 161.8, 128.2, 122.2, 118.8, 117.8, 59.9, 23.5, 23.4, 23.2, 22.0, 14.7. LCMS (50-95% acetonitrile in 0.05% TFA over 10 minutes) retention time = 5.93 minutes, C₁₁H₁₅NO₂, [M + H]⁺ = 194.

Ethyl -3-iodo-4, 5, 6, 7-tetrahydro-2H-isoindole carboxylate (2)



A solution of **1** (1.00 g, 5.17 mmol) in THF (60 mL) was treated with NIS (1.16 g, 5.17 mmol, 1.0 equiv). The reaction mixture was stirred at room temperature for 1.5 h and followed by LCMS. At this time there was still starting material present. Additional *N*-iodosuccinimide (0.120 g, 0.53 mmol, 0.10 equiv) was added. After 15 minutes, the reaction mixture was diluted with CH₂Cl₂ (100 mL) and washed with water (2 x 100 mL) and brine (75 mL). The organic layers were separated, dried (Na₂SO₄), filtered, and concentrated to give 1.42 g of **2** (86% crude yield) as red brown solid. This material was used in the next step without further purification: ¹H NMR (CDCl₃) δ 9.10 (bs, 1 H), 4.30 (q, *J*=7.17 Hz, 2 H), 2.75 (distorted t, *J*=5.70 Hz, 2 H), 2.33 (distorted t, *J*=5.50 Hz, 2 H), 1.75-1.68 (complex m, 4 H), 1.33 (t, *J*=7.10 Hz, 3 H) ¹³C NMR (CDCl₃): δ 160.77, 129.55, 128.11, 122.58, 71.10, 60.21, 23.53, 23.26, 23.22, 23.18, 14.64. LCMS (50-95% acetonitrile in 0.05%TFA over 10 minutes) retention time =7.37 min, C₁₁H₁₄INO₂, [M + H]⁺ = 320. TLC (silica plate) R_f = 0.55 (4:1 Hexane/ Ethyl Acetate).

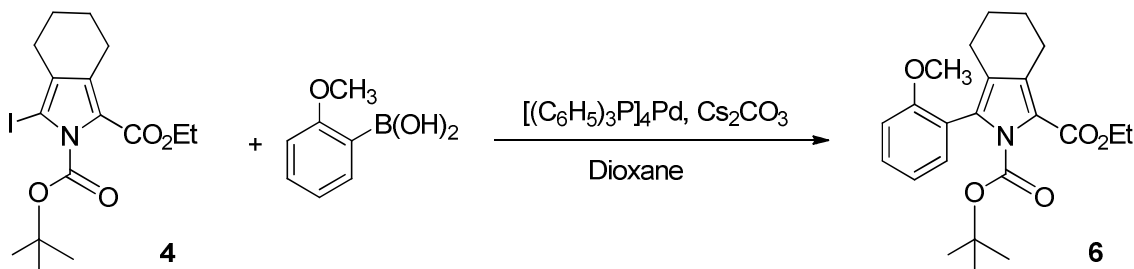
Ethyl 2-*tert*-butyl-1-3-iodo-4,5,6,7-tetrahydro-2*H*-isoindole-1,2-dicarboxylate (**4**)



A solution of **2** (5.00 g, 15.7 mmol) in acetonitrile (150 mL) was treated with DMAP (0.285 g, 2.33 mmol, 0.149 equiv) and di-*tert*-butyldicarbonate (4.45 g, 20.4 mmol, 1.30 equiv). The mixture was stirred at room temperature under argon atmosphere for 26 h. The reaction mixture was then partitioned with diethyl ether (100 mL) and 1N aqueous NaHSO₄ (200 mL). The organic layer was separated and washed with water (200 mL), saturated NaHCO₃ (200 mL) and brine (100 mL), respectively. The organic layer was then dried (Na₂SO₄), filtered, and concentrated. The crude product was purified by flash column chromatography (silica gel/Hexanes/Ethyl Acetate 20:1) to afford 3.95 g of pure **4** (60% yield) as a yellow solid. ¹H NMR (CDCl₃): δ 4.27 (q, *J* = 7.03 Hz, 2 H), 2.69 (distorted t, *J* = 5.70 Hz, 2 H), 2.33 (distorted t, *J* = 5.75 Hz, 2 H), 1.71-1.65 (complex m, 4 H), 1.60 (s, 9 H), 1.31 (t, *J* = 7.35 Hz, 3 H). ¹³C NMR (CDCl₃): δ 160.2, 149.3, 132.4, 129.5, 124.0, 122.2, 85.6, 60.5, 27.7, 24.4, 23.4, 23.2, 23.0, 14.6. LCMS (75-95% acetonitrile in 0.05% TFA over 10 minutes) retention time = 6.72 min, [M + H]⁺ = C₁₆H₂₂INO₄ = 319.

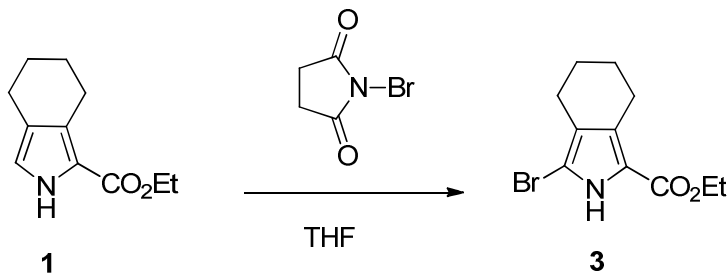
Ethyl 2-*tert*-butyl-1-3-(2-methoxyphenyl)-4,5,6,7-tetrahydro-2*H*-isoindole-1,2-dicarboxylate

(6)



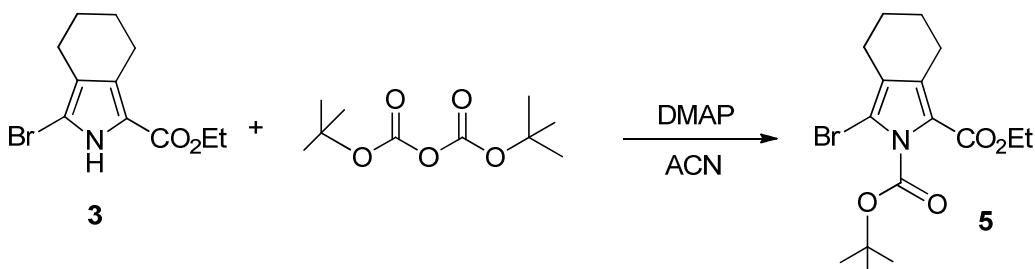
A mixture of the iodopyrrole **4** (0.500 g, 1.19 mmol), 2-methoxyphenylboronic acid (0.219 g, 1.44 mmol, 1.21 equiv), tetrakis(triphenylphosphine)palladium(0) (0.035 g, 0.030 mmol) and cesium carbonate (1.17 g, 3.58 mmol, 3.0 equiv) were added to a round bottom flask, fitted with a vacuum adaptor and a temperature control thermocouple. The flask was subjected to 3 vacuum/argon cycles and degassed 1,4-dioxane (50 mL) was added via syringe. The reaction mixture was heated to 80 °C for 2h and monitored by LCMS. At this time additional 2-methoxyphenylboronic acid (0.181 g, 1.19 mmol, 1 equiv) and $[(C_6H_5)_3P]_4Pd$ cat. (0.035 g, 0.030 mmol) were added and the reaction mixture was stirred at 80 °C overnight. The reaction mixture was cooled and partitioned with EtOAc (100 mL) and water (200 mL). The layers were separated and EtOAc layer was washed with water (200 mL). The organic layer was dried (Na_2SO_4), filtered through a plug of silica gel or Celite using EtOAc as eluent, and concentrated to afford 1.12 g of the crude mixture of **6** and other by-products as a yellow viscous oil. LCMS (75-95% acetonitrile in 0.05% TFA over 10 minutes) retention time = 5.93 min, $C_{23}H_{29}NO_5$ $[M + H]^+ = 400$. This material was not purified further but retained as a product standard while the Suzuki reaction sequence was developed using the bromide analogue described in the next set of experiments.

Ethyl 3-bromo-4, 5, 6, 7-tetrahydro-2H-isoindole carboxylate (3)



A solution of **1** (5.00 g, 25.9 mmol) in THF (110 mL) was treated with NBS (4.61 g, 25.9 mmol, 1 equiv) and the reaction mixture was stirred at room temperature for 2h. The mixture was diluted with EtOAc (200 mL), washed with water (200mL) and brine (100mL). The organic layer was separated, dried over anhydrous Na₂SO₄, filtered, and concentrated to afford 7.24 g of **3** as a bright yellow solid (~100% yield). This product was essentially pure and used in the next step without further purification. ¹H NMR (CDCl₃): δ 9.33 (bs, 1 H), 4.29 (q, *J* = 7.03 Hz, 2 H), 2.77-2.74 (m, 2 H), 2.38-2.35 (m, 2 H), 1.73-1.68 (m, 4 H), 1.33 (t, *J* = 7.03 Hz, 3 H). ¹³C NMR (CDCl₃): δ 161.2, 129.7, 122.0, 118.9, 102.7, 60.3, 23.3, 23.1, 22.9, 21.7, 14.6. LCMS (50-95% acetonitrile in 0.05% TFA over 10 minutes) retention time = 7.08 C₁₁H₁₄BrNO₂ = [M + H]⁺ = 272.

Ethyl 2-tert-butyl-1-3-bromo-4,5,6,7-tetrahydro-2H-isoindole-1,2-dicarboxylate (5)

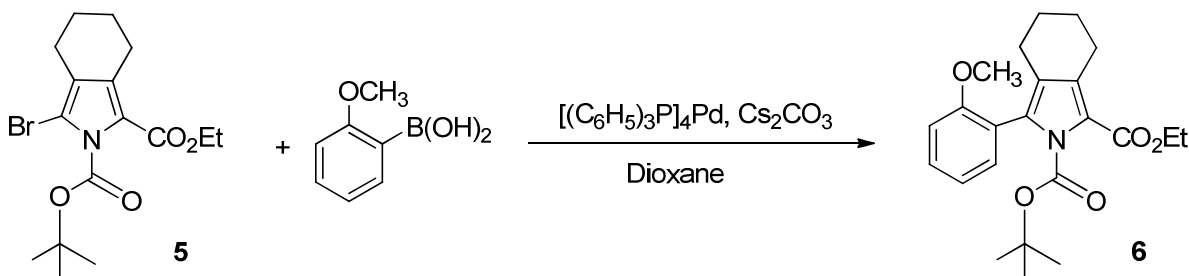


A solution of bromopyrrole **3** (6.34 g, 24.1 mmol) in acetonitrile (250 mL) was treated with DMAP (0.439 g, 3.59 mmol, 0.149 equiv) and di-tert-butyl dicarbonate (6.84 g, 31.4 mmol, 1.3equiv). The reaction mixture was stirred at room temperature for 24h. LCMS at this time

confirmed that the reaction was complete. The reaction mixture was partitioned with EtOAc (200 mL) and 1.0 N NaHSO₄ (40 mL). The layers were separated and the organic phase was washed with 1.0 N NaHSO₄ (200 mL), water (200 mL) and brine (300 mL). The organic layer was separated, dried (Na₂SO₄), filtered, and concentrated. The residue was purified by flash column chromatography (silica gel/ CH₂Cl₂) to give 7.19g of **5** (80% yield) as a bright yellow solid: ¹H NMR (CDCl₃): δ 4.26 (q, *J* = 7.03 Hz, 2 H), 2.72-2.69 (m, 2 H), 2.36-2.33 (m, 2 H), 1.70-1.66 (m, 4 H), 1.58 (s, 9 H), 1.30 (t, *J* = 7.10 Hz, 3 H). ¹³C NMR (CDCl₃): δ 160.3, 148.7, 132.0, 123.1, 120.9, 104.9, 85.6, 60.5, 27.6, 23.4, 23.0, 22.7, 22.0, 14.6. LCMS (75-95% acetonitrile in 0.05% TFA over 10 minutes) retention time = 6.65mins, C₁₆H₂₂^{78.9}BrNO₄, [M + H]⁺ = 372, C₁₆H₂₂^{80.9}BrNO₄, [M + H]⁺ = 374.

Ethyl 2-tert-butyl-1-3-(2-methoxyphenyl)-4,5,6,7-tetrahydro-2H-isoin-dole-1,2-dicarboxylate

(6)



Boc-protected bromopyrrole **5** (0.500 g, 1.35 mmol), 2-methoxyphenyl boronic acid (0.307 g, 2.02 mmol, 1.5equiv), tetrakis (triphenylphosphine) palladium (0) catalyst (0.156 g, 0.135mmol, 10% mol), and cesium carbonate (1.32 g, 4.04 mmol, 3.0equiv) were placed in a flask. The resulting solid mixture was subjected to 3 vacuum/argon cycles. Degassed 1, 4-dioxane (40mL) was added and the reaction mixture was heated to 70°C for 30 minutes and to 80°C for 4h. The reaction mixture was cooled to room temperature, diluted with EtOAc (200 mL), and filtered through a 1 inch pad of silica gel. The filtrate was then concentrated.

Purification by flash column chromatography (silica gel/ Hexanes/EtOAc 10:1) afforded

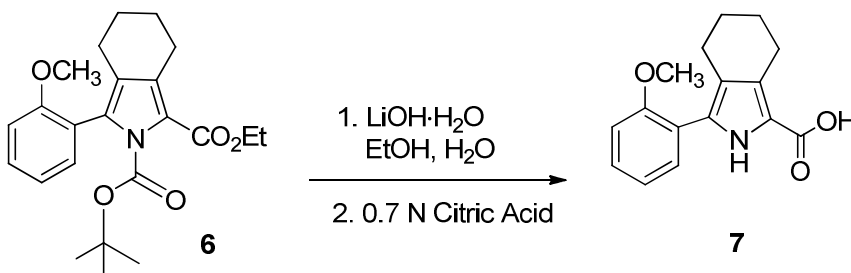
0.461 g of **6** (86% yield) as a light yellow solid: TLC (silica gel) $R_f = 0.24$ (10:1

Hexanes/Ethyl Acetate): $^1\text{H NMR}$ (CDCl_3): δ 7.33 (ddd, $J=8.20, 7.30, 1.80$ Hz, 1 H), 7.19 (dd, $J=7.40$ Hz, 1.40 Hz, 1 H), 6.96 (dt, $J=7.80$ Hz, 0.9 Hz, 2 H), 6.88 (dd, $J=8.2, 0.9$ Hz, 2 H), 4.29 (q, $J=7.33$ Hz, 2 H), 3.72 (s, 3 H), 2.79 (ABq of t, $\Delta\nu = 8.64\text{Hz}$, $J=17.9, 5.00$ Hz, 2 H), 2.28 (ABq of t, $\Delta\nu = 8.88\text{Hz}$, $J=16.0, 7.30$ Hz, 2 H), 1.32 (t, $J=6.90\text{Hz}$, 4 H), 1.28 (s, 9 H). $^{13}\text{C NMR}$ (CDCl_3): δ 161.4, 157.3, 149.2, 144.1, 138.6, 131.6, 131.5, 130.7, 129.7, 123.4, 121.7, 119.6, 120.3, 110.3, 83.4, 60.2, 55.3, 27.3, 23.4, 23.2, 23.1, 21.8, 14.6.

LCMS (75-95% acetonitrile in 0.05%TFA over 10 minutes) retention time = 5.60 min,

$\text{C}_{23}\text{H}_{29}\text{NO}_5$ $[\text{M} + \text{H}]^+ = 400$.

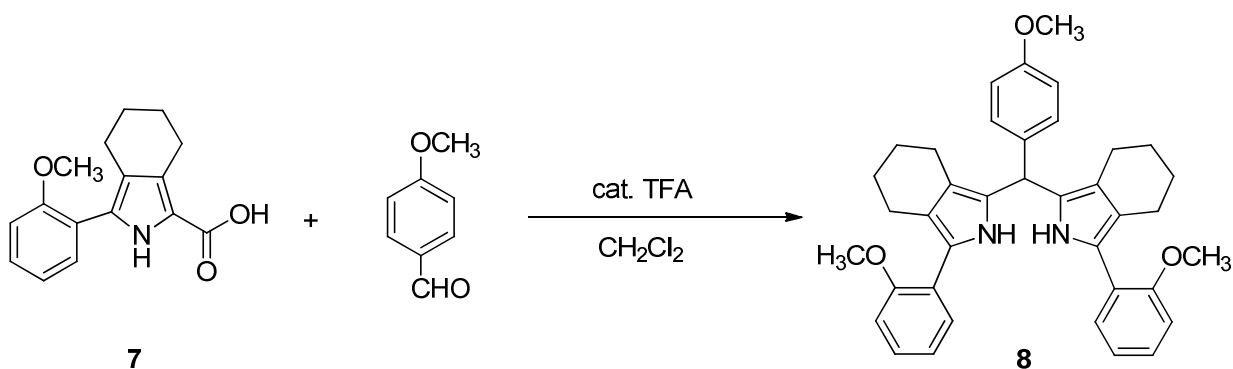
3-(2-Methoxyphenyl)-4,5,6,7-tetrahydro-2H-isoindole-1-carboxylic acid (7)



A solution of Suzuki coupling product **6** (3.50 g, 8.76 mmol) in ethanol (150 mL) and water (50 mL) was treated with lithium hydroxide monohydrate ($\text{LiOH}\cdot\text{H}_2\text{O}$) (4.34 g, 103 mmol, 11.8 equiv). The reaction mixture was heated at 75°C under argon atmosphere overnight. The mixture was then cooled in ice bath ($0\text{-}5^\circ\text{C}$) and treated with 0.7N citric acid (150mL) dropwise to lower the pH of the solution to approximately 3. Filtration afforded 1.99g of the desired product **7** (84% yield) as a grey solid: $^1\text{H NMR}$ (CDCl_3): δ 9.92 (bs, 1 H), 7.54 (dd, $J=7.79, 1.37$ Hz, 1 H), 7.35-7.23 (m, 2 H), 7.05-6.96 (m, 2 H), 3.94 (s, 3 H), 2.92 (t, $J=6.18$ Hz, 2 H), 2.72 (t, $J=5.72$ Hz, 2 H), 1.84-1.72 (m, 4 H). $^{13}\text{C NMR}$ (CDCl_3): 166.6,

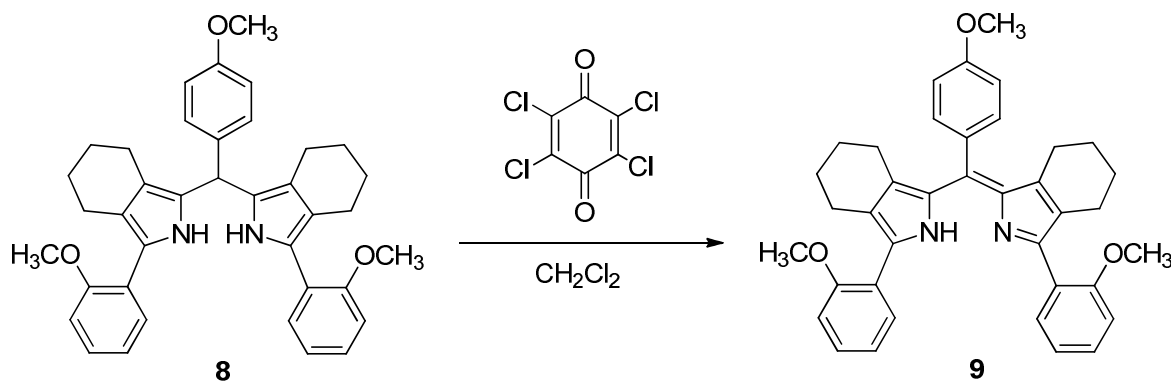
156.2, 131.1, 129.2, 128.5, 121.2, 121.0, 120.3, 111.4, 55.8, 24.5, 23.8, 23.4, 23.0. LCMS (75-95% acetonitrile in 0.05%TFA over 10 minutes) retention time = 2.75 min, $C_{16}H_{17}NO_3$ $[M + H]^+ = 272$.

3,3'-((4-Methoxyphenyl)methylene)-bis(1-(2-methoxyphenyl)-4,5,6,7-tetrahydro-2H-isoindole) (8)



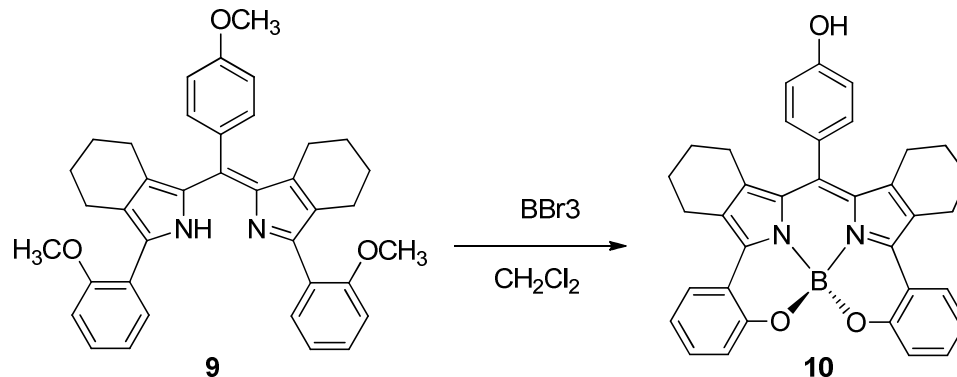
A mixture of compound **7** (0.900 g, 3.32 mmol) and 4-methoxybenzaldehyde (202 μ L, 0.226 g, 1.66 mmol, 0.5 equiv) in CH_2Cl_2 (100 mL) was stirred at room temperature under argon atmosphere for 10 minutes. Then 4 drops of trifluoroacetic acid (TFA) was added. The progression of the reaction was followed by LCMS. Additional TFA was added as follows: 5 drops after 1h, 5 drops after 2h, and 10 drops after 3h. The reaction was allowed to stir for another 6h. The mixture was transferred to a separatory funnel and washed with saturated $NaHCO_3$ (200 mL) and water (50 mL). The organic layer was separated, dried over (Na_2SO_4), filtered, and concentrated to afford 0.949 g (100% crude yield) as red amorphous solid **8**. LCMS (85-95% acetonitrile in 0.05% TFA over 10 minutes) retention time = 2.88min, $C_{38}H_{40}N_2O_3$ $[M + H]^+ = 571$. (A small sample was oxidized with DDQ to observe the presence of dipyrromethene due to the instability of dipyrromethane). The reaction was taken on directly to the next experiment without further purification.

(Z)-3-(2-methoxyphenyl)-1-((4-methoxyphenyl)-(3-(2-methoxyphenyl)-4,5,6,7-tetrahydro-2H-isoindol-1-yl)methylene)-4,5,6,7-tetrahydro-1H-isoindole (9)

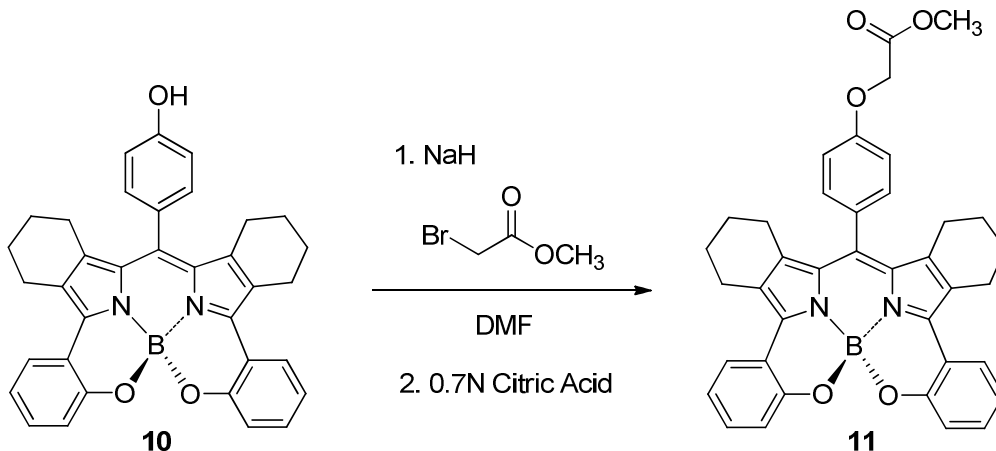


The dipyrromethane analogue **8** (0.949 g, 1.66 mmol) was dissolved in methylene chloride (100 mL) and the resulting mixture was stirred under argon atmosphere for 15 min.

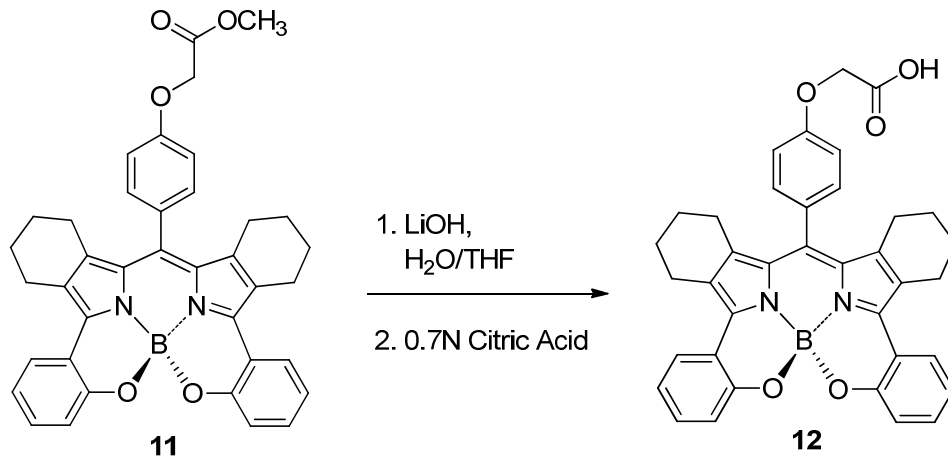
Tetrachloro-1,4-benzoquinone (*p*-chloranil) (0.488 g, 1.99 mmol, 1.2 equiv) was added and the reaction mixture was stirred at room temperature for 3h. LCMS at this time indicated full oxidation of dipyrromethane to the dipyrromethene. The reaction mixture was transferred to a separatory funnel and washed with saturated NaHCO₃ (100 mL) and water (50 mL). The organic layer was separated, dried over anhydrous Na₂SO₄, filtered, and concentrated. The crude product was purified by flash column chromatography (silica gel CH₂Cl₂/MeOH 20:1) to afford 0.651 g of **9** (69% yield) as a deep red solid. Due to hindered rotation, compound **10** displayed broadened NMR data at 25 °C. Variable temperature NMR studies indicated pure material at the near coalescence temperature of 75 °C: ¹H NMR (DMSO-*d*₆, 75 °C): δ 7.52 (d, *J* = 7.40, 2H), 7.45 (t, *J* = 7.80, 2H), 7.39 (d, *J* = 8.70, 2H), 7.16 (d, *J* = 8.20, 4H) 7.07 (t, *J* = 7.80, 2 H), 3.89 (s, 3H), 3.79 (s, 6H), 2.52 (t, *J* = 6.00, 4H), 2.06-1.98 (bm, 4H), 1.71-1.63 (bm, 4H), 1.58-1.50 (bm, 4H). LCMS (75-95% acetonitrile in 0.05% TFA over 10 minutes) retention time = 5.30min, C₃₈ H₃₈ N₂ O₃ [M + H]⁺ = 571.

meso-(4-Hydroxyphenyl)-(O,N)-chelated-BODIPY **10**

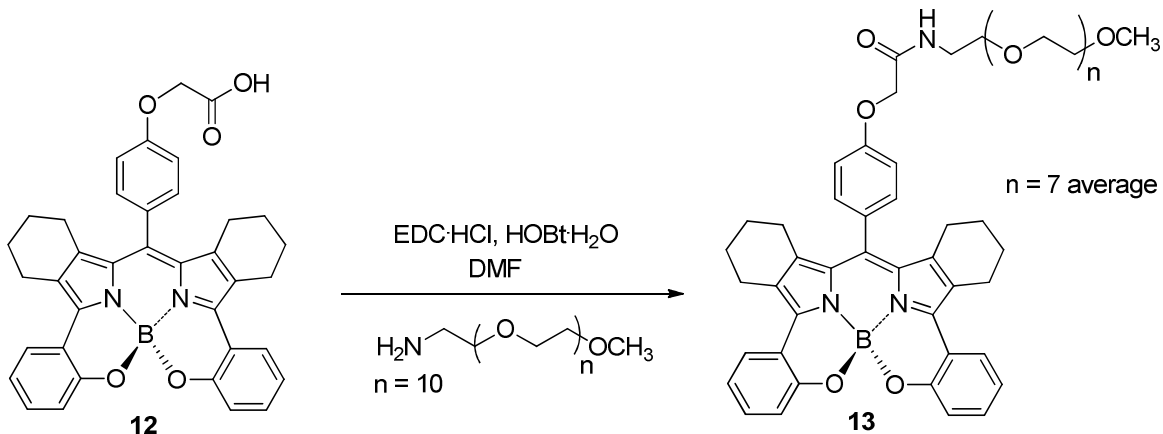
A solution of dipyrromethene **9** (0.651 g, 1.14 mmol) in CH_2Cl_2 (150 mL) was cooled in an ice bath (0-5°C) for 15 min. To this mixture was added 1.0M BBr_3 (11.4 mL, 11.4 mmol, 10 equiv) dropwise. The resulting reaction mixture was stirred at 0-5°C for 1h then allowed to warm to room temperature and stirred for an additional 30 min. After this time, LCMS indicated complete reaction. The mixture was cooled again in an ice bath and quenched by dropwise addition of saturated NaHCO_3 (50 mL) and then water (200 mL). The mixture was transferred to a separatory funnel and the organic layer was separated and washed with 1M NaHSO_4 (200 mL). The organic layer was separated, dried (Na_2SO_4), filtered and concentrated to afford 0.582 g of **10** (95% crude yield) as a dark green solid. This material was used directly in the next step. LCMS (75-95% acetonitrile in 0.05% TFA over 10 minutes) retention time = 7.25min, $\text{C}_{35}\text{H}_{29}\text{BN}_2\text{O}_3$ $[\text{M} + \text{H}]^+ = 537$.

meso-4-(Methyl phenoxyacetate)-(O,N)-chelated-BODIPY 11

The phenolic BODIPY **10** (0.582 g, 1.09 mmol) in DMF (90 mL) was stirred at 0°C for 15 min and treated with sodium hydride (60% dispersion in mineral oil, 0.344 g, 8.60 mmol, 7.93 equiv). The mixture was stirred for 30 min and treated with methyl bromoacetate (154 μ L, 1.63 mmol, 1.5 equiv) dropwise. The resulting reaction mixture was stirred at 0°C for an additional 2h and at room temperature for 3h. The reaction mixture was cooled in an ice bath (0-5°C) and quenched with 0.7N citric acid (50 mL) dropwise. The mixture was diluted with water (200 mL), partitioned with EtOAc (200 mL), and washed with water (5 x200 mL). The organic layer was separated, dried (Na₂SO₄), filtered, and concentrated. The isolated crude material was purified by flash column chromatography (silica gel/CH₂Cl₂) to afford 0.251g of **11** (38% yield) as a purple solid: ¹H NMR (CDCl₃): δ 7.74 (d, J = 7.80 Hz, 2 H), 7.33-7.25 (complex m, 4 H), 7.03-6.98 (m, 4 H), 6.90 (d, J = 8.2 Hz, 2H), 4.42 (s, 2 H), 4.08 (d, J = 6.90 Hz, 2 H), 3.84 (s, 3 H), 2.88-2.64 (complex m, 4 H), 2.09-1.75 (complex m, 4 H), 1.62-1.47 (complex m, 8 H). LCMS (75-95% acetonitrile in 0.05% TFA over 10 minutes) retention time = 8.12 min, C₃₈H₃₃BN₂O₅ [M + H]⁺ = 609.

meso-4-(Phenoxyacetic acid)-(O,N)-chelated-BODIPY **12**

Ester derivative **11** (0.321 g, 0.513 mmol) was dissolved in a 1:1 mixture of THF/H₂O (40 mL). This solution was treated with LiOH•H₂O (0.251 g, 5.13 mmol, 10 equiv) and stirred for 1h. The reaction mixture was quenched with 0.7N citric acid (140 mL) and diluted with distilled H₂O (300 mL). The mixture was transferred to a separatory funnel and extracted with EtOAc (200 mL). The EtOAc extract was dried over anhydrous Na₂SO₄, filtered, and concentrated. The residue was purified by flash column chromatography (silica gel/ CH₂Cl₂/ MeOH/3:1) to afford complex **12**. From NMR analysis, the final product was contaminated by a small quantity of citric acid. The product was dissolved in EtOAc, washed with water (5 x 200 mL), dried over anhydrous Na₂SO₄, filtered, and concentrated to afford 0.195g of pure complex **12** (56% yield) as a dark blue amorphous solid. This material was used directly in the next reaction. LCMS (75-95% acetonitrile in 0.05% TFA over 10 minutes) retention time = 6.38 min, C₃₇H₃₁BN₂O₅ [M + H]⁺ = 595.

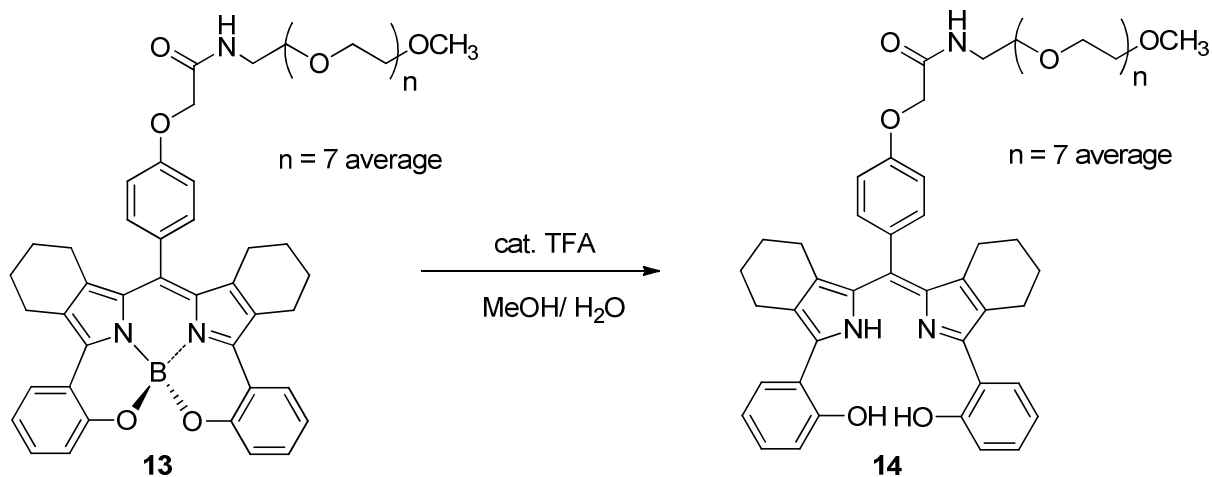
meso-(PEG-amide)-(O,N)-chelated-BODIPY 13

A solution of carboxylate **12** (0.157 g, 0.264 mmol) in DMF (20 mL) was stirred treated with EDC·HCl (0.066 g, 0.343 mmol, 1.3 equiv) and 1-hydroxybenzotriazole (0.040 g, 0.343 mmol, 1.3 equiv) and the resulting reaction mixture was stirred for 30 min. During this time, poly (ethyleneglycol) methyl ether amine (reported average molecular weight ~500, 0.135 g, 0.264 mmol, 1 equiv) was dissolved in DMF (5mL), placed under argon flow for 5 min, and then added to the reaction mixture. The PEG (amine) residue was rinsed with addition DMF (5mL) and added to the reaction mixture. The reaction mixture was allowed to stir overnight. The DMF solvent was evaporated and the residue was purified by flash column chromatography (silica gel $\text{CH}_2\text{Cl}_2/\text{MeOH}/10:1$ to $5:1$) to afford 0.150g of **13** (53% yield) as a dark green solid: ^1H NMR (CDCl_3): δ 7.74 (dd, $J = 7.79, 1.37$ Hz, 2 H), 7.34 (d, $J = 8.70$ Hz, 2 H), 7.27 (dt, $J = 8.70, 1.90$ Hz, 2 H), 7.18-7.13 (bt, 1 H), 7.05-6.97 (m, 4 H), 6.90 (dd, $J = 8.20, 0.9$ Hz, 2 H), 4.58 (s, 2 H), 3.68-3.57 (m, 14 H), 3.54-3.50 (m, 2 H), 3.36-3.34 (m, 3 H), 2.90-2.81 (m, 2 H), 2.70-2.62 (m, 2 H), 2.10-2.00 (m, 2 H), 1.82-1.72 (m, 2 H), 1.65-1.41 (complex m, 4 H). ^{13}C NMR (CDCl_3): δ 167.8, 157.9, 154.5, 145.6, 140.3, 135.9, 131.3, 131.1, 130.7, 128.5, 127.7, 126.6, 120.4, 120.0, 119.5, 115.0, 72.0, 70.6 (broad, overlapping PEG carbons), 70.4, 69.8, 67.3, 59.2, 39.0, 29.8, 24.5, 23.4, 22.8, 22.7. LCMS

(75-95% acetonitrile in 0.05% TFA over 10 minutes) retention time = 5.77 min,
 $C_{52}H_{62}BN_3O_{11} [M + H]^+ = 916$. UV-Vis (in MeOH): 305, 340, 577, 620. NMR and LCMS
data indicate that this molecule is a pure polydisperse pegylated compound with the average
number of ethylene glycol units = 7 for the major constituent.

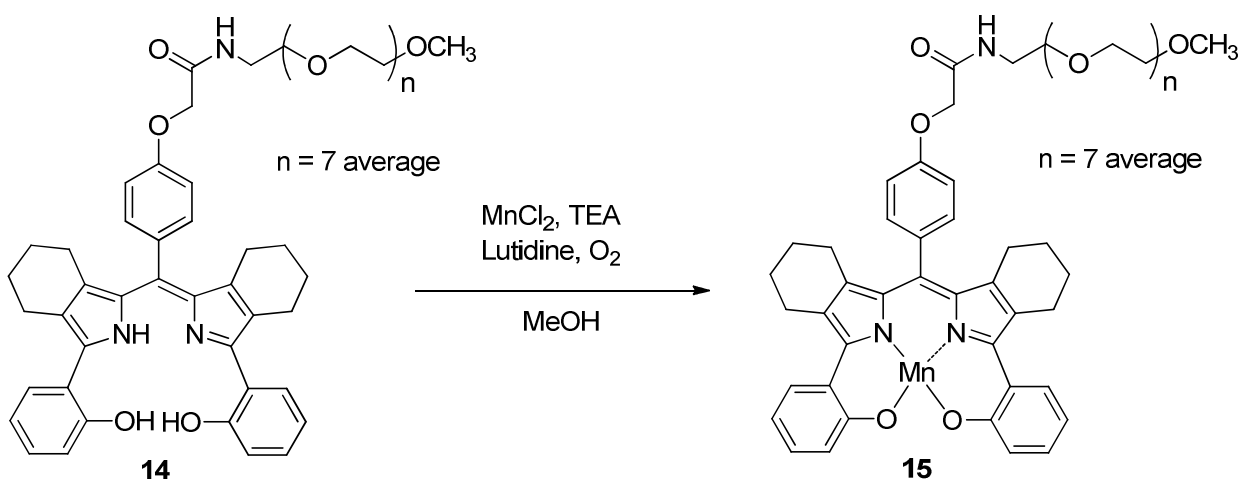
Wavelength, λ (nm)	Absorbance	Log ϵ
620	2.551	4.59
577	1.302	4.30
340	1.171	4.25
305	2.551	4.59

Table 5. UV-vis data for *meso*-(PEG-amide)-(O,N)-chelated-BODIPY **13** (concentration = 6.55×10^{-5} M in MeOH)

meso-(PEG-amide)-(O,N)-DPM **14**

Pegylated derivative **13** (0.080 g, 0.087 mmol) was dissolved in MeOH (25 mL) and water (20 mL). The solution was treated with TFA (2 mL) and stirred for 2h. At this time, LCMS indicated presence of the starting material. Additional TFA (1 mL) was added and the mixture was allowed to stir at room temperature overnight. The MeOH was evaporated via rotary evaporator and the residue was extracted with EtOAc (200 mL). The mixture was transferred to a separatory funnel and partitioned with EtOAc (200mL) and water (50 mL). The organic layer was dried over anhydrous Na_2SO_4 , filtered, and concentrated to afford 0.119 g of compound **14** (~100% crude yield) as dark blue solid: LCMS (75-95% acetonitrile in 0.05% TFA over 10 minutes) retention time = 2.20 min, $\text{C}_{52}\text{H}_{65}\text{N}_3\text{O}_{11}$ $[\text{M} + \text{H}]^+ = 908$. The material was used directly in the next step without further purification.

Mn(III) *meso*-(PEG-amide)-(*O,N*)-DPM **15**



A solution of pegylated dipyrromethene **14** (0.119 g, 0.131 mmol) dissolved in MeOH (80 mL) was treated with TEA (5 mL) and stirred for 15 min. Mn(II)Cl₂ (0.242 g, 1.92 mmol, 14.7 equiv) and 2,6 lutidine (5 drops) were added. The reaction mixture was stirred open to air (O₂) at room temperature overnight. The progression of the reaction was monitored by LCMS. Additional Mn(II)Cl₂ was added as follows: (0.153 g, 1.22 mmol, 9.27 equiv) after 24h and (0.204 g, 1.62 mmol, 12.4 equiv) after 24h. The reaction mixture was allowed to stir at 50° C for additional 2h. The mixture was treated with EtOAc (300 mL) and water (200 mL) and transferred to a separatory funnel. The organic layer was separated, dried over anhydrous Na₂SO₄, and concentrated. The residue was purified by flash column chromatography (silica gel/ CH₂Cl₂/MeOH/10:1) to afford 0.073 g of complex **15** (53% yield) as dark green amorphous solid: LCMS (50-95% acetonitrile in 0.05% TFA over 10 minutes) retention time = 5.58 min, C₅₂H₆₂MnN₃O₁₁ [M + H]⁺ = 960.20. UV-Vis (in MeOH): 303, 369, 432, 601, 650.

Wavelength, (nm)	Absorbance	Log ϵ
303	1.145	4.34
369	0.636	4.09
432	0.354	3.83
601	0.479	3.96
650	1.026	4.29

Table 6. UV-vis data Mn(III) *meso*-(PEG-amide)-(O,N)-DPM **15** (concentration = 5.21×10^{-5} M in MeOH)

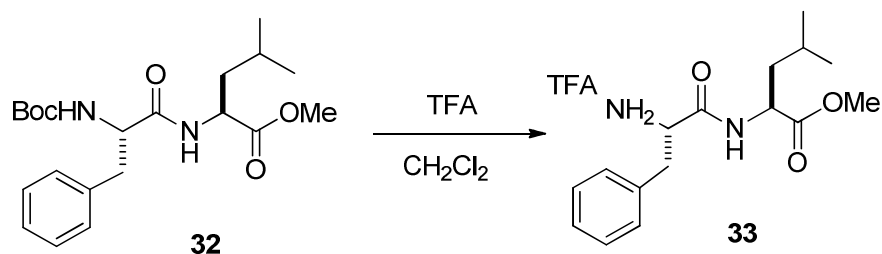
Boc-Phe-Leu-OMe (32)

A solution of Boc-phe (1.00 g, 3.77 mmol) in DMF (25mL) was stirred and treated with EDC·HCl (0.867 g, 4.52 mmol, 1.2 equiv) and HOBT·H₂O (0.693 g, 4.52 mmol, 1.2 equiv).

The resulting reaction mixture was stirred at room temperature for 30 min. At this time, Leu-OMe·HCl (0.754 g, 4.15 mmol, 1.1 equiv) and TEA (0.6 mL) and then the pH was adjusted to ~ 8 with additional TEA. The mixture was diluted with EtOAc (100 mL), transferred to a separatory funnel, and washed with 1N sodium bisulfate (100 mL), H₂O (100 mL), brine (50mL), and saturated NaHCO₃, respectively. The organic layer was dried over anhydrous Na₂SO₄, filtered, and concentrated to afford 1.32 g of **32** (89 % crude yield) as a white solid:

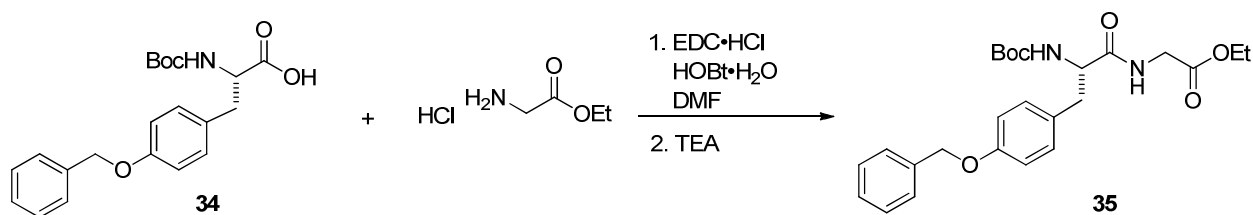
¹H NMR (DMSO-*d*₆): δ 8.24 (d, *J* = 7.80 Hz, 1 H), 7.30-7.12 (m, 5 H), 6.89 (d, *J* = 8.70 Hz, 1 H), 4.30 (ddd, *J* = 10.1, 7.80, 5.10 Hz, 1 H), 4.16 (dt, *J* = 10.1, 4.1 Hz, 1 H), 3.32 (s, 3H), (ABq of d, Δ*v* = 13.1 Hz, *J* = 13.8, 4.10 Hz), 1.67-1.41 (complex m, 3 H), 1.25 (s, 9 H), 0.86 (d, *J* = 7.00 Hz, 3 H), 0.80 (d, *J* = 6.40 Hz, 3 H). ¹³C NMR (DMSO-*d*₆): δ 173.4, 172.5, 155.7, 138.7, 129.7, 128.5, 126.7, 78.5, 56.0, 52.4, 50.7, 40.6, 37.7, 28.6, 24.6, 23.4, 21.7. LCMS (15-95% acetonitrile in 0.05% TFA over 10 minutes) retention time = 8.05 min, C₂₁H₃₂N₂O₅ [M + H]⁺ = 393.

Phe-Leu-OMe (33)



Compound **32** (1.32 g, 3.37 mmol) was dissolved in CH₂Cl₂ (40 mL) and treated with TFA (10 mL) and stirred at room temperature for 30 min. The reaction mixture was concentrated to a viscous material and dissolved with diethyl ether (16 mL). The solution was concentrated to afford 1.09 g of **33** (80% crude yield) a brown solid: ¹H NMR (DMSO-*d*₆) δ 8.88 (d, *J* = 2.3 Hz, 1 H), 8.20 (bs, 2 H), 7.31-7.23 (m, 5 H), 4.32 (ddd, *J* = 9.10, 7.70, 5.5 Hz, 1 H), 4.08-3.98 (m, 1 H), 3.00 (ABq of d, Δ*v* = 11.5 Hz, *J* = 13.7, 5.5 Hz, 2 H), 2.46 (s, 3 H), 1.66-1.44 (complex m, 3H), 0.84 (dd, *J* = 17.9, 6.90 Hz, 6 H). ¹³C NMR (DMSO*d*₆): δ 172.7, 168.8, 135.3, 130.1, 129.0, 127.7, 53.7, 52.6, 50.9, 37.4, 24.5, 23.2, 21.7. LCMS (15-95% acetonitrile in 0.05% TFA over 10 minutes) retention time = 6.27 min, C₁₈H₂₅F₃N₂O₅ [M + H]⁺ = 293.

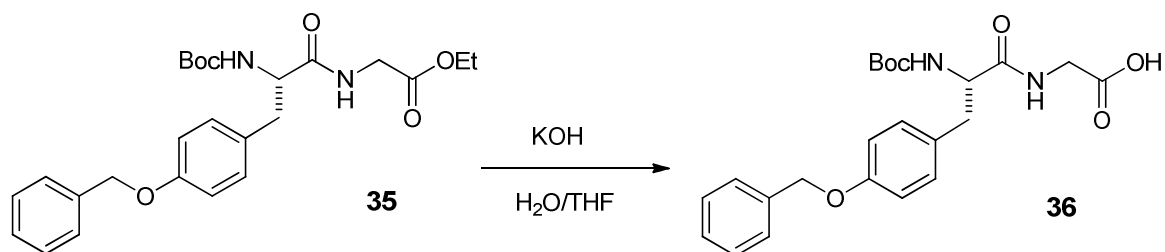
Boc-Tyr(OBn)-Gly-OEt (35)



A solution of Boc-Tyr(OBn)-OH **34** (0.800 g, 2.15mmol) in DMF was treated with EDC·HCl (0.495 g, 2.58mmol, 1.2equiv) and HOBT·H₂O (0.395g, 2.58 mmol, 1.2equiv) and the reaction was stirred at room temperature for 30 min. Gly-OEt (0.300 g, 2.37mmol, 1.1equiv) and TEA (0.60mL) were added and then, the pH of the reaction mixture was adjusted to ~ 8

with addition TEA. The solvent was evaporated and the residue was partitioned with EtOAc (200 mL) and washed with 1N NaHSO₄ (100mL), H₂O (50mL), brine (50mL), and saturated NaHCO₃ (100 mL), respectively. The organic material was dried over anhydrous Na₂SO₄, filtered, and concentrated to afford 0.920 g of compound **35** (96% crude yield). ¹H NMR (DMSO-*d*₆): δ 8.34 (t, *J* = 6.00 Hz, 1 H), 7.40-7.26 (complex m, 5 H), 7.15 (d, *J* = 8.20 Hz, 2 H), 6.88 (q, *J* = 5.9Hz, 2 H), 5.72 (bs, 1 H), 5.01 (s, 2 H), 4.11 (t, *J* = 5.30 Hz, 1 H), 4.05 (q, *J* = 7.03 Hz, 2 H), 3.81 (ABq of d, Δ*v* = 8.59 Hz, *J* = 17.8, 5.90 Hz, 2 H), 2.75 (ABq of d, Δ*v* = 14.4 Hz, *J* = 13.8, 3.70 Hz 2 H), 1.25 (s, 9 H), 1.16 (t, *J* = 7.10 Hz, 3 H). ¹³C NMR (DMSO-*d*₆): 172.7, 168.8, 159.1, 158.7, 135.3, 130.1, 129.0, 127.7, 118.0, 53.7, 52.6, 50.9, 36.3, 37.4, 24.5, 23.2, 21.7. LCMS (15-95% acetonitrile in 0.05% TFA over 10 minutes) retention time = 6.43 min, C₂₅H₃₂N₂O₆ [M + H]⁺ = 457.

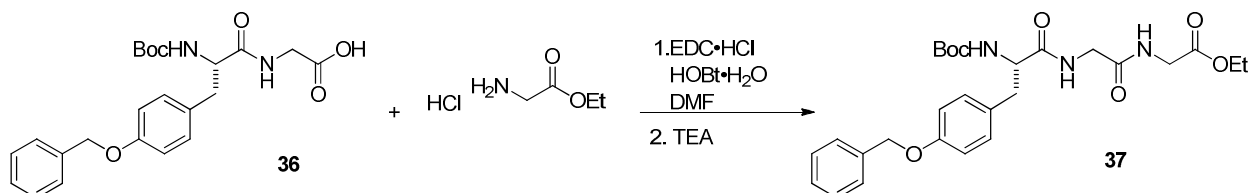
Boc-Tyr-(OBn)-Gly-OH (**36**)



Compound **35** (0.700 g, 1.53mmol) dissolved in a 2:1 mixture of THF/H₂O (30 mL). The solution was treated with KOH (0.172 g, 3.07 mmol, 2.0 equiv) and stirred at room temperature for 30 min. TLC at this time confirmed that the reaction was complete. The pH of the mixture was adjusted to ~ 2 with HCl dropwise. The solution was transferred to a separatory funnel and partitioned with EtOAc (50mL) and with water (50 mL). The organic layer was separated, dried over anhydrous Na₂SO₄, and concentrated to afford 0.333 g of

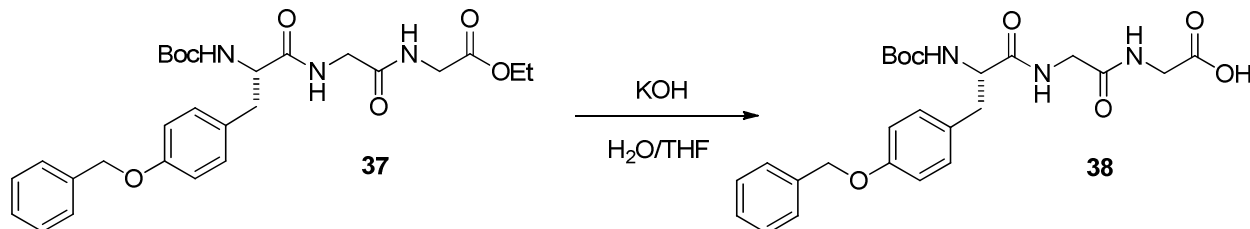
compound **36** (51% crude yield) as a white solid: LCMS (15-95% acetonitrile in 0.05% TFA over 10 minutes) retention time = 5.08 min, $C_{23}H_{28}N_2O_6$ $[M + H]^+ = 429$.

Boc-Tyr(OBn)-Gly-Gly-OEt (**37**)



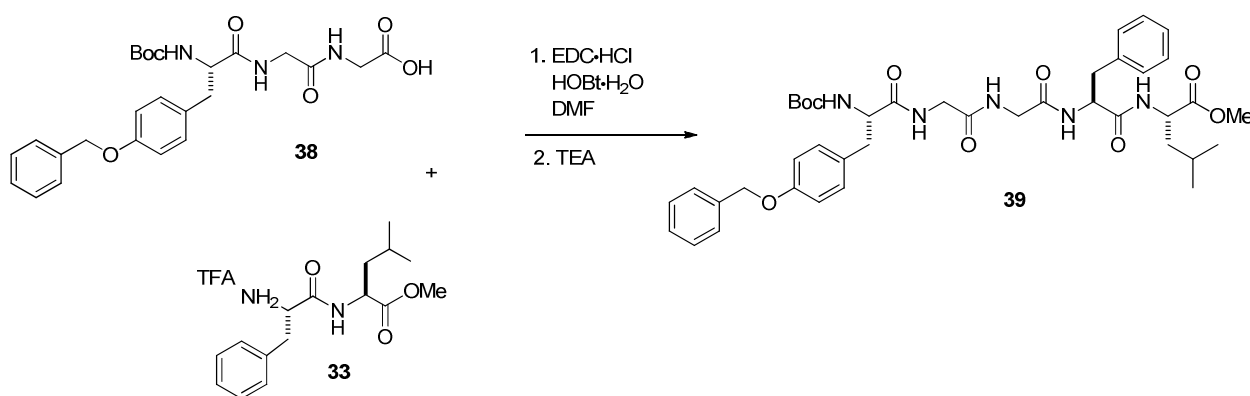
The Boc-Tyr(OBn)-Gly-OH **36** (0.333 g, 0.777 mmol) in DMF (30 mL) was treated with EDC·HCl (0.179 g, 0.932 mmol, 1.2equiv) and HOBT·H₂O (0.143 g, 0.932mmol, 1.2 equiv) and stirred at room temperature for 20 min. At this time, Gly-OEt (0.119 g, 0.855mmol, 1.1 equiv) and TEA (0.60 mL) were added and the pH of mixture was adjusted to ~ 8 with additional TEA. The resulting reaction mixture was stirred for 24h. The solvent was evaporated and the brownish residue was partitioned with EtOAc (50 mL) and 1N NaHSO₄ (50 mL) and washed with H₂O (30 mL), saturated NaHCO₃ (50 mL), and brine (50mL), respectively. The organic layer was dried over with anhydrous Na₂SO₄, filtered, and concentrated to afford 0.482 g of **37** (~100% crude yield) as a white solid: LCMS (50-95% acetonitrile in 0.05% TFA over 10 minutes) retention time = 5.72 min, $C_{27}H_{35}N_3O_7$ $[M + H]^+ = 514$.

Boc-Tyr(OBn)-Gly-Gly-OH (**38**)



Compound **37** (0.482 g, 0.939 mmol) was dissolved in 2:1 mixture of THF/H₂O (30 mL) and treated with KOH (0.105 g, 1.88 mmol, 2 equiv). The resulting reaction mixture was stirred at room temperature for 30 min. At this time, LCMS indicated that the reaction was complete. The pH of the mixture was adjusted to ~ 2 with HCl dropwise. The mixture was transferred to a separatory funnel and partitioned with EtOAc (200 mL) and H₂O (200 mL). The organic layer was separated, dried with anhydrous Na₂SO₄ and concentrated to afford 0.326 g of **38** (71% crude yield). LCMS (50-95% acetonitrile in 0.05% TFA over 10 minutes) retention time = 4.12 min, C₂₅H₃₁N₃O₇ [M + H]⁺ = 486.

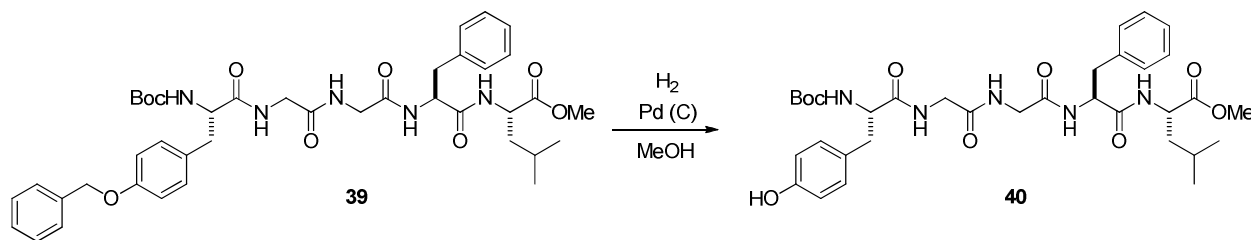
Boc-Tyr(OBn)-Gly-Gly-Phe-Leu-OMe (**39**)



The Boc-Tyr(OBn)-Gly-Gly-OH **38** (0.326 g, 0.672 mmol) in DMF (25 mL) was treated with EDC·HCl (0.155 g, 0.806 mmol, 1.2 equiv) and HOBT·H₂O (0.123 g, 0.806 mmol, 1.2 equiv) and stirred at room temperature for 45 min. Phe-Leu-OMe **33** (0.300 g, 0.739 mmol, 1.1

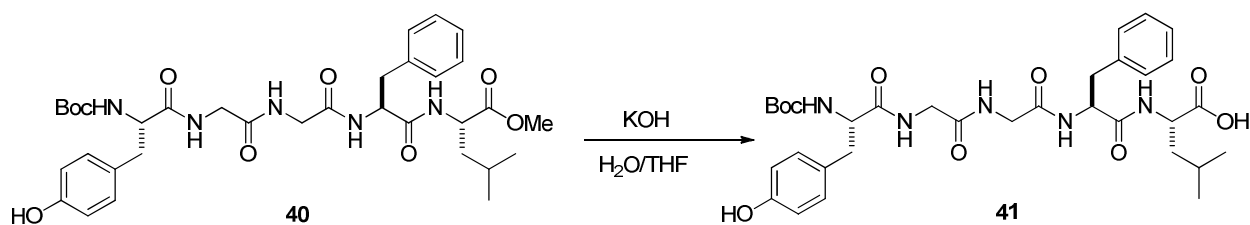
equiv) and TEA (0.6 mL) were added and the resulting reaction mixture was stirred at room temperature for 24h. At this time, LCMS indicated that the reaction was complete. The reaction solvent was evaporated. The brown viscous crude was dissolved with EtAOc (200 mL), transferred to a separatory funnel, and washed with 1M NaHSO₄ (200 mL), H₂O (200 mL), saturated NaHCO₃ (200 mL) and brine (200 mL), respectively. The organic layer was separated, dried over anhydrous Na₂SO₄, filtered and concentrated. The residue was combined with another batch and recrystallized with acetonitrile to afford 0.442 g of compound **39** (87% crude yield). LCMS (15-95% acetonitrile in 0.05% TFA over 10 minutes) retention time = 8.15 min, C₄₁H₅₃N₅O₉ [M + H]⁺ = 760.

Boc-Tyr-Gly-Gly-Phe-Leu-OMe (40)



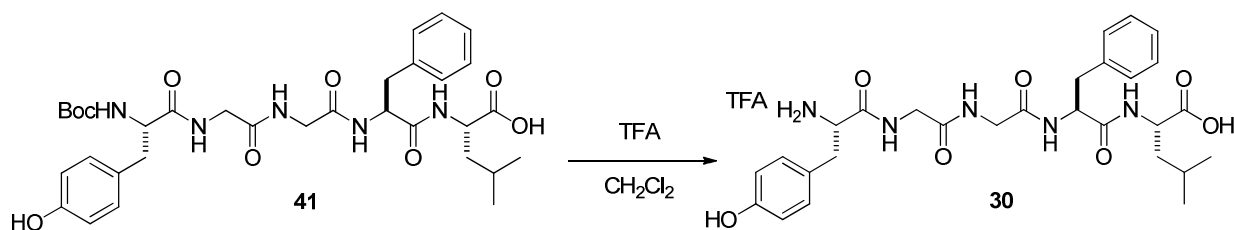
A solution of compound **39** (0.442 g, 0.582 mmol) in MeOH (30 mL) was treated with palladium on carbon catalyst (5%wt, 0.90 g) and stirred under a balloon filled with hydrogen gas at room temperature for 72h. At this time, LCMS indicated that the reaction was complete. The reaction mixture was filtered through 2 inch pad of celite with MeOH (3 x100 mL) as the eluent. The organic material was concentrated to afford 0.347 g of **40** (89% crude yield). LCMS (15-95% acetonitrile in 0.05% TFA over 10 minutes) retention time = 7.17 min, C₃₄H₄₇N₅O₉ [M + H]⁺ = 670.

Boc-Tyr-Gly-Gly-Phe-Leu-OH (41)



Compound **40** (0.347 g, 0.518 mmol) was dissolved in 2:1 mixture of THF/H₂O (30 mL) and treated with KOH (0.058 g, 1.04 mmol, 2.0 equiv). The resulting reaction mixture was stirred at room temperature for 30 min. The pH of the reaction mixture was adjusted to ~ 3 with concentrated HCl dropwise and then transferred to a separatory funnel. The mixture was partitioned with EtOAc (200 mL) and water (50 mL) and the extracted was separated, dried over anhydrous Na₂SO₄, and concentrated to afford 0.308 g of compound **41** (92 % crude yield). LCMS (15-95% acetonitrile in 0.05% TFA over 10 minutes) retention time = 6.82 min, C₃₃H₅₅N₅O₉ [M + H]⁺ = 656.

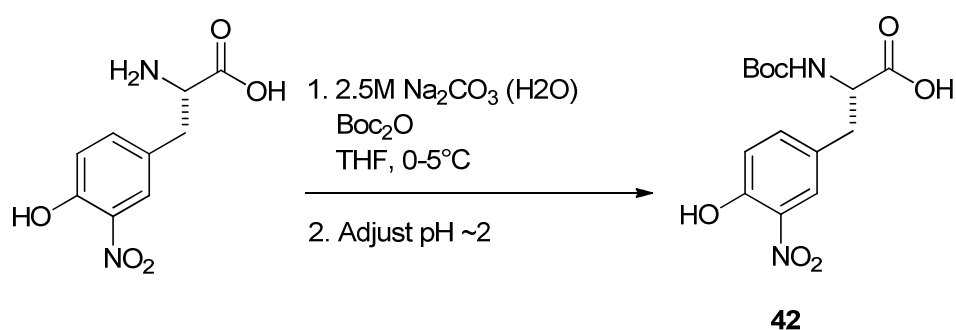
Tyr-Gly-Gly-Phe-Leu-OH (**30**)



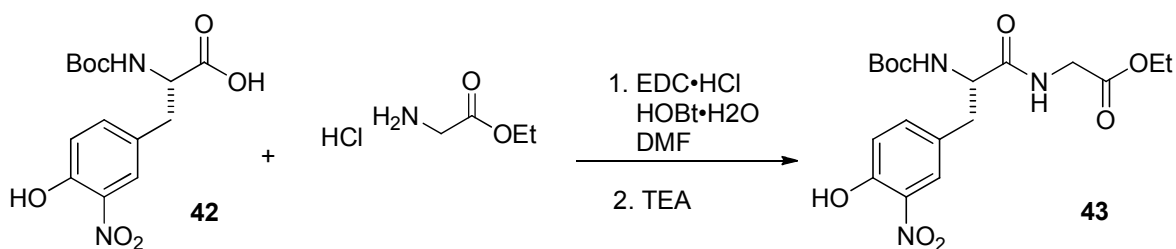
Compound **41** (0.308 g, 0.470 mmol) dissolved in CH₂Cl₂ (16 mL) was treated with TFA (4 mL) and stirred at room temperature for 30 min. At this time, LCMS indicated complete deprotected *N*-terminus of the pentapeptide product. The CH₂Cl₂ was evaporated and residue was dissolved with diethyl ether (20 mL) and concentrated to afford 0.267 g of compound **30** (85% crude yield) as a white solid: ¹H NMR (DMSO-*d*₆): δ 8.72 (t, *J* = 5.25 Hz, 2 H), 8.31 (d, *J* = 7.80 Hz, 1 H), 8.09 (d, *J* = 5.95 Hz, 1 H), 8.06 (d, *J* = 1 H), 7.22-7.13 (complex m, 5

H), 7.01 (d, $J = 8.20$ Hz, 2 H), 6.66 (d, $J = 8.20$ Hz, 2 H), 4.52 (dt, $J = 12.9, 3.70$ Hz 1 H), 4.19-4.14 (complex m, 1 H), 3.91 (dd, $J = 7.30, 6.00$ Hz, 1 H), 3.82-3.52 (m, 2 H), 3.01-2.91 (m, 2 H), 2.81-2.63 (m, 2 H), 1.64-1.41(m, 3 H), 0.86 (d, $J = 6.40$ Hz, 3 H), 0.81 (d, $J = 6.40$ Hz, 3 H). LCMS (15-95% acetonitrile in 0.05% TFA over 10 minutes) retention time = 6.07 min, $C_{30}H_{38}F_3N_5O_9$ $[M + H]^+ = 556$.

Boc-Tyr(3-nitro)-OH (42)

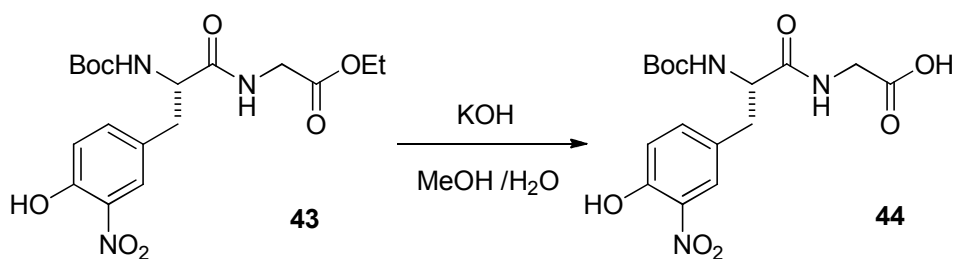


3-Nitro-tyrosine (2.00 g, 8.84 mmol) was dissolved in THF (200 mL) and 2.5M Na_2CO_3 (100 mL) and cooled to 0-5°C (ice bath) for 15 min. The solution was treated with di-*tert*-butyldicarbonate (2.31 g, 10.6 mmol, 1.2 equiv) and stirred at room temperature for 26h. The pH of the mixture was adjusted to 2.55 with concentrated HCl (~15 mL) and 1N $NaHSO_4$ (~5 mL) dropwise. The reaction mixture was extracted with EtOAc (150 mL) and the organic layer was separated, dried over anhydrous Na_2SO_4 , filtered, and concentrated to afford 2.61 g of compound **42** (91% crude yield) as a yellow solid: 1H NMR (DMSO- d_6) δ 10.8 (bs, 1 H), 7.73 (d, $J = 1.90$ Hz, 1 H), 7.40 (dd, $J = 8.30, 1.90$ Hz, 1 H), 7.14 (d, $J = 8.70$ Hz, 1 H), 7.01 (d, $J = 4.1$ Hz, 1 H), 4.05-3.95 (m, 1 H), 2.85 (ABq of d, $\Delta v = 13.3$ Hz, $J = 13.8, 4.60$ Hz, 2 H), 1.26 (s, 9 H). ^{13}C NMR (DMSO- d_6): 173.8, 156.0, 151.3, 136.8, 136.7, 129.8, 125.9, 119.4, 78.6, 60.3, 35.6, 28.6. LCMS (15-95% acetonitrile in 0.05% TFA over 10 minutes) retention time = 7.07 min, $C_{14}H_{18}N_2O_7$ $[M + H]^+ = 327$.

Boc-Tyr (3-nitro)-Gly-OEt (43)

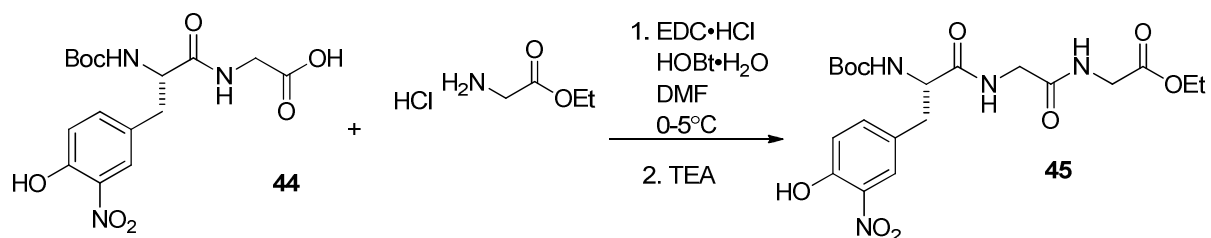
Boc-Tyr-(3-nitro)-OH **42** (2.40 g, 7.36 mmol), EDC·HCl (2.12 g, 11.0 mmol, 1.5 equiv) and HOBt·H₂O (1.69 g, 11.0 mmol, 1.5 equiv) were dissolved in DMF (70 mL) and cooled on ice bath (0-5°C) for 10 min. The reaction mixture was treated with Gly-OEt (1.13 g, 8.10 mmol, 1.1 equiv) and TEA (1.5 mL, 11.0 mmol, 1.5 equiv) and the mixture was stirred at room temperature for 24h. The solvent was evaporated and the residue was dissolved with EtOAc (100 mL) and transferred to a separatory funnel. The mixture was washed with 1M NaHSO₄ (50 mL), water (50 mL), and brine (50 mL), respectively. The organic layer was separated, dried over anhydrous Na₂SO₄, filtered and concentrated to afford 1.85g of compound **43** (61% crude yield) as a yellow solid: ¹H NMR (DMSO-*d*₆): δ 10.7 (bs, 1 H), 8.39 (t, *J* = 5.75 Hz, 1 H), 7.81 (d, *J* = 1.90 Hz, 1 H), 7.43 (dd, *J* = 8.20, 1.80 Hz, 1 H), 7.01 (d, *J* = 6.00 Hz, 1 H), 6.99 (d, *J* = 6.90 Hz, 1 H), 4.13 (td, *J* = 10.5, 3.70 Hz, 1 H), 4.05 (q, *J* = 7.17 Hz, 2 H), 3.83 (ABq of d, Δ*v* = 8.32 Hz, *J* = 17.4, 6.00 Hz, 2 H), 2.79 (ABq of d, Δ*v* = 15.1 Hz, *J* = 14.2, 4.20 Hz, 2 H), 1.22 (s, 9 H), 1.15 (t, *J* = 7.10 Hz, 3 H). LCMS (15-95% acetonitrile in 0.05% TFA over 10 minutes) retention time = 7.20 min, C₁₈H₂₅N₅O₅ [M + H]⁺ = 412.

Boc-Tyr(3-nitro)-Gly-OH (44)



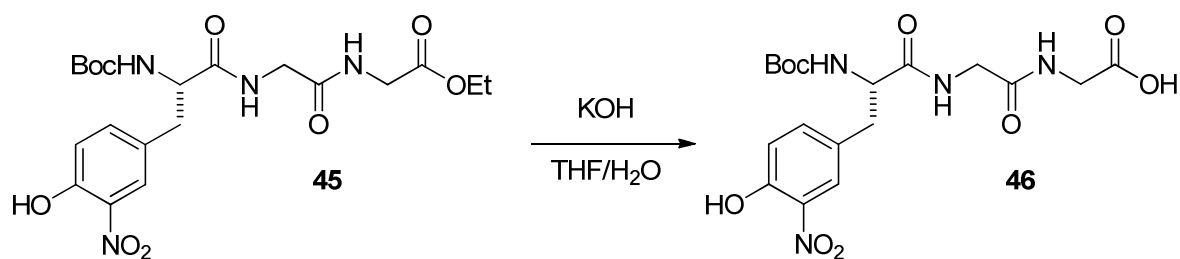
The boc protected Tyr(3-nitro)-Gly-OEt **43** (1.6 g, 3.89 mmol) was dissolved in MeOH (50 mL) and H₂O (17 mL) and treated with KOH (0.261 g, 4.67 mmol, 1.2 equiv). The resulting reaction mixture was stirred at room temperature for 2h. At this time, LCMS indicated that the reaction was complete. The pH of the mixture was adjusted to ~ 3 with 1N NaHSO₄ and partitioned with EtOAc (200mL). The organic layer was separated, dried over anhydrous Na₂SO₄, filtered, and concentrated to afford 1.16 g of compound **44** (78% crude yield) as a yellow solid: ¹H NMR (DMSO-*d*₆): δ 10.7 (bs, 1 H), 8.27 (t, *J* = 6.00 Hz, 1 H), 7.81 (d, *J* = 1.90 Hz, 1 H), 7.43 (dd, *J* = 8.70, 2.30 Hz, 1 H), 7.00 (d, *J* = 8.30 Hz 1 H), 6.96 (d, *J* = 8.70 Hz, 1 H), 4.12 (td, *J* = 11.0, 3.70 Hz, 1 H) 3.75 (ABq of d, Δ*v* = 8.18 Hz, *J* = 17.8, 5.90 Hz, 2 H), 2.79 (ABq of d, Δ*v* = 15.5 Hz, *J* = 13.8, 4.00 Hz, 2 H), 1.22 (s, 9 H). ¹³C NMR (DMSO-*d*₆): δ 172.3, 171.7, 155.8, 151.3, 136.5, 130.1, 127.0, 126.0, 119.3, 78.5, 55.9, 41.2, 36.8, 28.6. LCMS (15-95% acetonitrile in 0.05% TFA over 10 minutes) retention time = 6.72 min, C₁₆H₁₂N₃O₆ [M + H]⁺ = 484.

Boc-Tyr (3-nitro)-Gly-Gly-OEt (45)



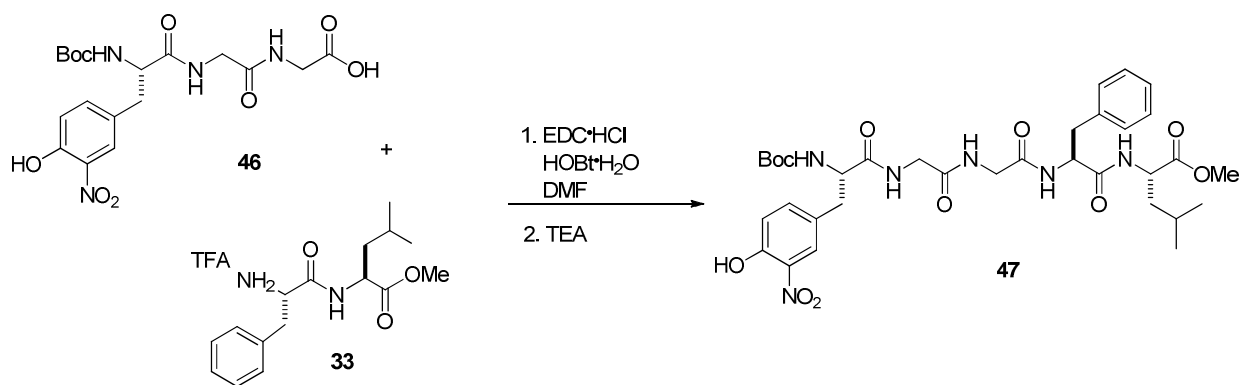
Compound **44** (0.980 g, 4.48 mmol) was dissolved in DMF (70 mL) and cooled to 0-5° C (ice bath). The solution was treated with EDC·HCl (0.713 g, 3.72 mmol, 1.5 equiv), and HOBT·H₂O (0.570 g, 3.72 mmol, 1.5 equiv) and the reaction mixture was stirred for 15 min. At this time, glycine ethyl ester (0.381 g, 2.73 mmol, 1.1 equiv) and TEA (516μL, 3.72 mmol, 1.5 equiv) were added and the resulting reaction mixture was stirred at room temperature for 24h. The solvent was evaporated and the crude was partitioned with EtOAc (300 mL) and 1N NaHSO₄ (100 mL), and washed with water (50 mL) and brine (50 mL). The organic layer was separated, dried over anhydrous Na₂SO₄, filtered, and concentrated to afford 0.884 g of compound **45** (76% crude yield). ¹³C NMR (DMSO-*d*₆): 172.2, 170.2, 169.8, 155.9, 151.3, 137.1, 130.1, 126.0, 119.7, 78.7, 61.0, 56.0, 42.3, 41.1, 36.6, 28.6, 14.6. LCMS (50-95% acetonitrile in 0.05% TFA over 10 minutes) retention time = 6.87 min, C₂₀H₂₈N₄O₉ [M + H]⁺ = 469.

Boc-Tyr(3-nitro)-Gly-Gly-OH (**46**)



Compound **45** (0.534 g, 1.25 mmol) dissolved in MeOH (25 mL) and H₂O (10 mL) was treated with KOH (0.084 g, 1.50 mmol, 1.2 equiv) and stirred at room temperature for 2h. At this time, LCMS indicated that the reaction was complete. The reaction mixture pH was adjusted with 1N NaHSO₄ to ~ 3. The organic material was extracted with EtOAc (100 mL), washed with water (90mL), dried over anhydrous Na₂SO₄, filtered, and concentrated to afford 0.486 g of **46** (88% crude yield) as a yellow solid: ¹H NMR (DMSO-*d*₆): δ 10.7 (bs, 1 H), 8.26 (t, *J* = 5.70 Hz, 1 H), 7.79 (d, *J* = 1.80 Hz, 1 H), 7.42 (dd, *J* = 8.70, 2.30 Hz, 1 H), 7.02 (d, *J* = 7.30 Hz, 1 H), 7.00 (d, *J* = 8.20 Hz, 1 H), 4.12 (td, *J* = 10.3, 4.10 Hz, 1 H), 3.74 (ABq of d, Δ*v* = 7.29 Hz, *J* = 17.8, 5.90 Hz, 4 H), 2.80 (ABq of d, Δ*v* = 15.6 Hz, *J* = 13.7, 4.10 Hz, 2 H), 1.23 (s, 9 H). ¹³C NMR (DMSO-*d*₆): δ 172.2, 171.6, 169.6, 155.9, 151.3, 137.1, 136.5, 130.1, 126.0, 119.7, 78.7, 60.3, 42.3, 41.1, 36.6, 28.6. LCMS (50-95% acetonitrile in 0.05% TFA over 10 minutes) retention time = 6.20 min, C₁₈H₂₄N₄O₉ [M + H]⁺ = 441.

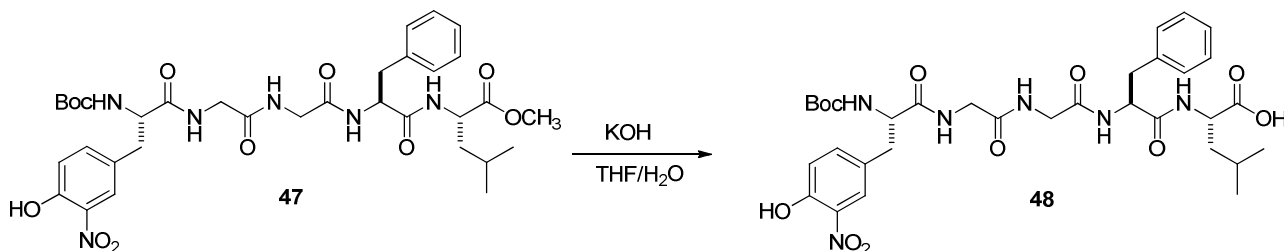
Boc-Tyr(3-nitro)-Gly-Gly-Phe-Leu-OMe (**47**)



Compound **46** (0.463 g, 1.05 mmol) dissolved in DMF (70 mL) was cooled to 5° C (ice-bath) and treated with EDC·HCl (0.302 g, 1.58 mmol, 1.5 equiv) and HOBT·H₂O (0.242 g, 1.58 mmol, 1.5 equiv). The reaction mixture was stirred for 10 min. and treated with TEA (219 μL, 1.58 equiv) and phe-leu-OMe **33** (0.497 g, 1.26 mmol, 1.2 equiv). The resulting mixture was stirred at room temperature for 24h. The solvent was evaporated and the residue was dissolved with EtOAc (100 mL), transferred to a separatory funnel, and washed with 1N NaHSO₄ (50 mL), water (50 mL), and brine (50 mL), respectively. The organic layer was separated, dried over anhydrous Na₂SO₄ and concentrated. The residue was purified by flash column chromatography (silica gel CH₂Cl₂/EtOH/100:1) to afford 0.334 g of **47** (44% crude yield) as a yellow solid: ¹H NMR (DMSO-*d*₆): δ 10.7 (bs, 1 H), 8.38 (d, *J* = 7.70 Hz, 1 H), 8.22 (t, *J* = 5.70 Hz, 1 H), 8.06 (d, *J* = 8.70 Hz, 2 H), 8.00 (t, *J* = 5.75 Hz, 1 H), 7.78 (d, *J* = 1.80 Hz, 1 H), 7.41 (dd, *J* = 8.70, 2.20 Hz, 1 H), 7.24-7.12 (complex m, 5 H), 4.52 (td, *J* = 9.20, 4.10 Hz, 1 H), 4.22 (ABq of d, Δ*v* = 4.73 Hz, *J* = 7.30, 5.00 Hz, 2 H), 4.14-4.08 (complex m, 2 H), 3.32 (s, 3 H), 2.96 (ABq of d, Δ*v* = 5.06 Hz, *J* = 9.60, 4.60 Hz, 2 H), 2.67 (ABq of d, Δ*v* = 8.10 Hz, *J* = 13.7, 9.60 Hz, 2 H), 1.62-1.42 (m, 3 H), 1.22 (s, 9 H), 0.85 (d, *J* = 6.50 Hz, 3 H), 0.80 (d, *J* = 6.40 Hz, 3 H). ¹³C NMR (DMSO-*d*₆): δ 173.3, 172.2, 171.8, 169.5, 168.8, 155.8, 151.3, 138.2, 137.1, 136.5, 130.1, 129.7, 128.6, 126.8, 126.0, 119.3, 78.6, 56.0, 54.1, 52.4, 50.8, 42.6, 42.2, 40.6, 39.4, 38.1, 28.5, 24.7, 23.3, 21.8. LCMS (50-

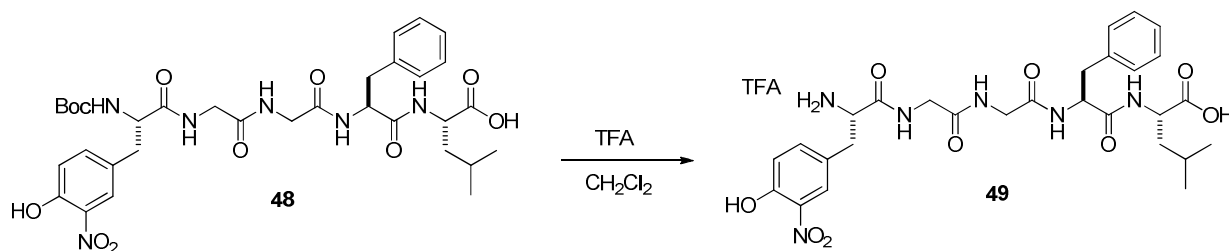
95% acetonitrile in 0.05% TFA over 10 minutes) retention time = 5.22 min, $C_{34}H_{46}N_6O_{11}$ $[M + H]^+ = 715$.

Boc-Tyr(3-nitro)-Gly-Gly-Phe-Leu-OH (**48**)



A solution of compound **47** (0.334 g, 0.468 mmol) in THF (45 mL) was treated with a solution of KOH (0.300 g, 5.36 mmol, 11.5 equiv) dissolved in water (25 mL). The resulting reaction mixture was stirred at room temperature for 2h. The solution was acidified with 1N NaHSO₄ to a pH of ~ 3. The mixture was partitioned with EtOAc (100 mL) and washed with water (50 mL), dried over anhydrous Na₂SO₄, and concentrated to afford 0.304 g of compound **48** (93% crude yield): ¹H NMR (DMSO-*d*₆): δ 10.7 (bs, 1 H), 8.27 (d, *J* = 7.80 Hz, 1 H), 8.22 (t, *J* = 5.50 Hz, 1 H), 8.05 (d, *J* = 2.70 Hz, 1 H), 7.99 (t, *J* = 5.75 Hz, 1 H), 7.78 (d, *J* = 1.80 Hz, 1 H), 7.41 (dd, *J* = 8.30, 1.80 Hz, 1 H), 7.22-7.12 (m, 5 H), 7.02 (d, *J* = 3.70 Hz, 1 H), 6.99 (d, *J* = 3.70 Hz, 1 H), 4.52 (td, *J* = 9.60, 3.60 Hz, 1 H) 4.30-4.08 (m, 4 H), 2.95 (ABq of d, Δ*v* = 7.38 Hz, *J* = 13.8, 3.70 Hz, 2 H), 2.73-2.59 (complex m, 2 H), 1.64-1.42 (m, 3 H), 1.21 (s, 9 H), 0.86 (d, *J* = 6.50 Hz, 3 H), 0.80 (d, *J* = 6.40 Hz, 3 H). ¹³C NMR (DMSO-*d*₆): 174.5, 172.2, 171.7, 169.4, 168.8, 155.9, 151.3, 138.3, 137.1, 136.5, 129.8, 128.5, 126.8, 126.0, 119.3, 78.6, 60.3, 56.0, 54.1, 50.8, 42.5, 42.1, 38.2, 28.5, 24.8, 23.4, 21.8, 21.3. LCMS (50-95% acetonitrile in 0.05% TFA over 10 minutes) retention time = 3.68 min, $C_{33}H_{44}N_6O_{11}$ $[M + H]^+ = 701$.

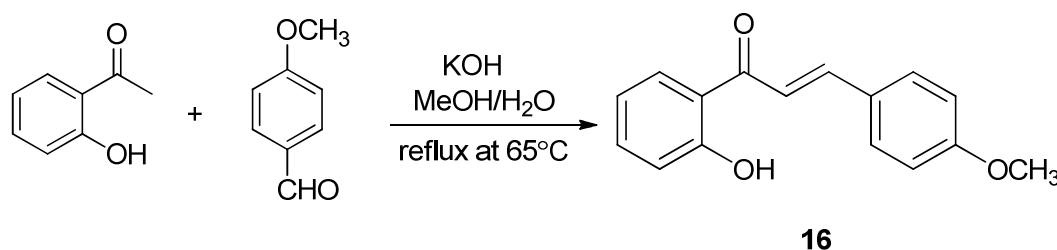
Tyr(3-nitro)-Gly-Gly-Phe-Leu-OH (**49**)



A solution of complex **48** (0.304 g, 0.430 mmol) in CH₂Cl₂ (16 mL) was treated with TFA (4 mL) and reaction mixture was stirred at room temperature for 3h. The progress of the reaction was followed by LCMS, which indicated presence of starting material. TFA (4 mL) was added and the reaction mixture was stirred for an additional 15 min and concentrated to afford 0.298 g of compound **49** (97% crude yield) as a yellow solid. LCMS (15-95% acetonitrile in 0.05% TFA over 10 minutes) retention time = 6.27 min, C₃₀H₃₆F₃N₆O₁₁ [M + H]⁺ = 601.

Synthesis of the oxidant-activated systems

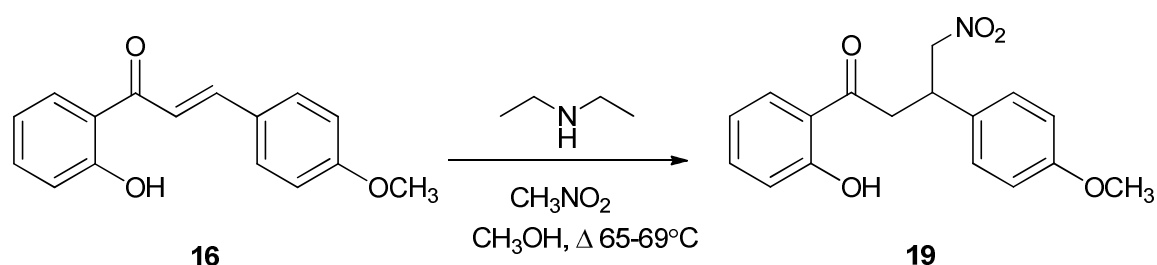
(E)-1-(2-Hydroxyphenyl)-3-(4-methoxyphenyl) prop-2-en-1-one (16**)**



2-Hydroxyacetophenone (10 mL, 11.3 g, 83.1 mmol), 4-methoxybenzaldehyde (10 mL, 11.3 g, 83.1 mmol), and KOH (9.31 g, 166 mmol, 2 equiv) were dissolved in MeOH (250 mL)/H₂O (50 mL). The reaction refluxed at 65°C for 48 h. Additional KOH (9.61 g) was

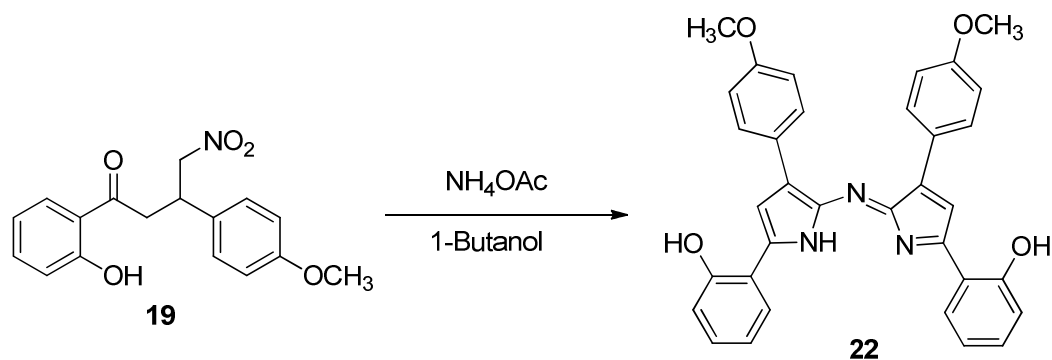
added and the mixture was stirred for 24h. The reaction mixture was cool on ice bath, acidified with concentrated HCl, which lead to the precipitation of product. The product was filtered and dried afford 10.7 g of compound **16** (51%) as yellow solid: $^1\text{H NMR}$ (DMSO- d_6) δ 12.72 (s, 1 H), 8.23 (dd, $J=8.47, 1.14$ Hz, 1 H), 7.85 (m, 2 H), 7.52 (m, 1 H), 6.98 (m, 2 H), 3.32 (s, 3 H). LCMS (50-95% acetonitrile in 0.05% TFA over 10 minutes) retention time = 7.15 min, $\text{C}_{16}\text{H}_{14}\text{O}_3$ $[\text{M} + \text{H}]^+ = 255$.

1-(2-Hydroxyphenyl)-3-(4-methoxyphenyl)-4-nitrobutan-1-one (**19**)



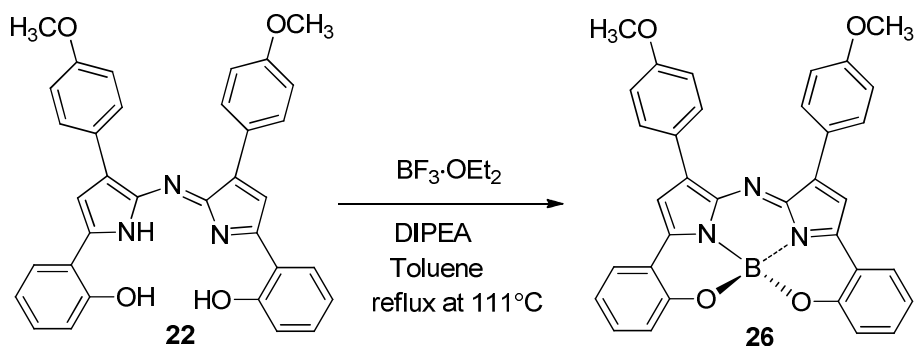
A mixture of hydroxychalcone **16** (2.00 g, 7.87 mmol), nitromethane (5.74 g, 5.09 mL, 94 mmol), and diethylamine (10 mL) were dissolve in MeOH (75 mL) and refluxed at 65°C for 12h. The reaction mixture was cooled on ice bath (0-5°C) and quenched with concentrated HCl (dropwise) until the vapor from the reaction had stopped. The organic material was extracted with CH_2Cl_2 (3 x200 mL), dried over anhydrous Na_2SO_4 , filtered, and concentrated. The residue was purified by flash column chromatography (silica gel/ CH_2Cl_2 / MeOH 10:1 to 5:1) to give 1.83 g of complex **19** (74%) as yellow solid: TLC (silica gel) $R_f = 0.40$ (5:1 Hexanes/EtOAc). LCMS (75-95% acetonitrile in 0.05% TFA over 10 minutes) retention time = 2.80 min, $\text{C}_{17}\text{H}_{17}\text{NO}_5$ $[\text{M} + \text{H}]^+ = 316$.

(Z)-2-(2-((5-(2-hydroxyphenyl)-3-(4-methoxyphenyl)-1H-pyrrol-2-yl) imino)-3-(4-methoxyphenyl)-2H-pyrrol-5-yl)phenol (**22**)



The nitro-compound **19** (6.54 g, 20.7 mmol) in 1-butanol (300 mL) was treated with ammonium acetate (13 g, 169 mmol, 8 equiv). The reaction mixture was refluxed at 120°C for 13h. During the course of the reaction, the product precipitated. The product was filtered and dried to afford 0.600 g of compound **22** (5%) as a blue solid: TLC (silica gel) $R_f = 0.29$ (3:1 Hexanes/EtOAc): $^1\text{H NMR}$ (DMSO- d_6) δ 8.00 (m, 7 H), 7.59 (s, 1 H), 7.31 (t, $J=7.56$ Hz, 1 H), 7.02- (m, 4 H), 3.31 (d, $J=0.92$ Hz, 6 H).

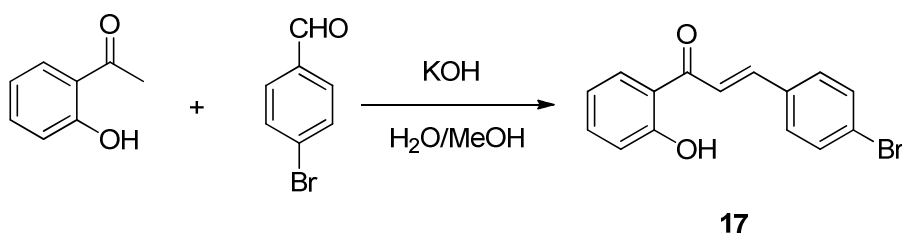
Bis(methoxyphenyl)-aza-(*O*, *N*)-chelated BODIPY (**26**)



Compound **22** (0.400 g, 0.738 mmol) was dissolved in toluene (200 mL) and added DIPEA (1.41 mL, 10.3 mmol, 14 equiv) and $\text{BF}_3 \cdot \text{OEt}_2$ (683 μL , 7.38 mmol, 10 equiv). The resulting mixture was refluxed at 111°C for 4h and monitored by LCMS. At this time there was still starting material present. Additional DIPEA (14 equiv) and $\text{BF}_3 \cdot \text{OEt}_2$ (10 equiv) were added.

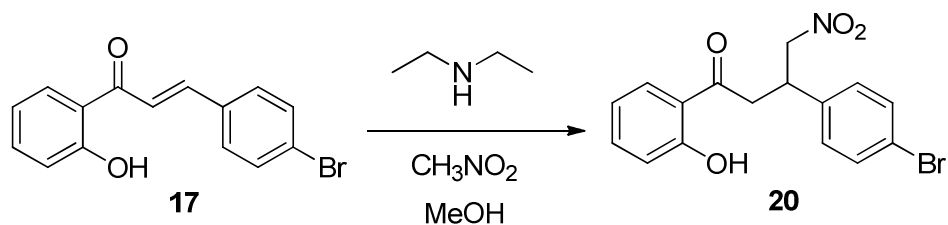
After 1 h, the reaction mixture was cooled, quenched with saturated NaHCO₃ (3 x200 mL) and partitioned with EtOAc (200 mL). The organic layer was separated, dried over anhydrous Na₂SO₄, filtered, and concentrated to give 0.344 g of compound **26** (85% crude yield): TLC (silica gel) R_f = 0.8 (20:1 CHCl₃/MeOH). LCMS (95-100 % acetonitrile in 0.1% ammonium acetate over 10 minutes) retention time = 3.40 min, C₃₄H₂₄BN₃O₄ [M + H]⁺ = 550.

(E)-3-(4-bromophenyl)-1-(2-hydroxyphenyl)prop-2-en-1-one (17)



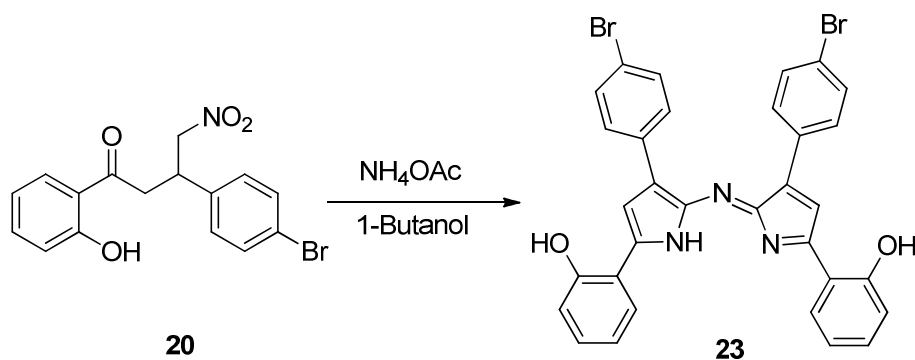
2'-hydroxyacetophenone (1.77 mL, 2.00 g, 14.7 mmol), 4-bromobenzaldehyde (2.72 g, 14.7 mmol, 1 equiv), and KOH (1.65 g, 29.4 mmol, 2 equiv) were dissolved in a mixture of 5:1 MeOH/H₂O (30 mL). The resulting mixture was stirred at room temperature for 24h. After this time, the mixture was cooled to 0-5°C (ice bath) and quenched with concentrated HCl dropwise until the fumes had stopped forming. During this process, the product precipitated, which was then filtered to afford 6.75 of complex **17** (~100% crude yield) as yellow solid. LCMS (75-95% acetonitrile in 0.05% TFA over 10 minutes) retention time = 4.73 min, C₁₅H₁₁BrO₂ [M + H]⁺ = 303.

3-(4-bromophenyl)-1-(2-hydroxyphenyl)-4-nitrobutan-1-one (20)



Compound **17** (3.50 g, 11.5 mmol) was dissolved in MeOH (60 mL) and treated with nitromethane (3.53 g, 3.13 mL, 57.7 mmol, 5 equiv), and diethylamine (4.24 g, 6.00 mL, 57.7 mmol, 5 equiv). The reaction mixture was refluxed at 65°C for 12h. The mixture was cooled on an ice bath (0-5 °C) and quenched with concentrated HCl dropwise until there was no smoke built up. The aqueous mixture was partitioned with CH₂Cl₂ (3 x200 mL), dried over anhydrous Na₂SO₄, and concentrated to afford 3.66 g of **20** (87% crude yield) as a brown solid. LCMS (75-95% acetonitrile in 0.05% TFA over 10 minutes) retention time = 3.33 min, C₁₆H₁₄BrNO₄ [M + H]⁺ = 364.

(Z)-2-(3-(4-bromophenyl)-2-((3-(4-bromophenyl)-5-(2-hydroxyphenyl)-1H-pyrrol-2-yl)imino)-2H-pyrrol-5-yl)phenol (**23**)

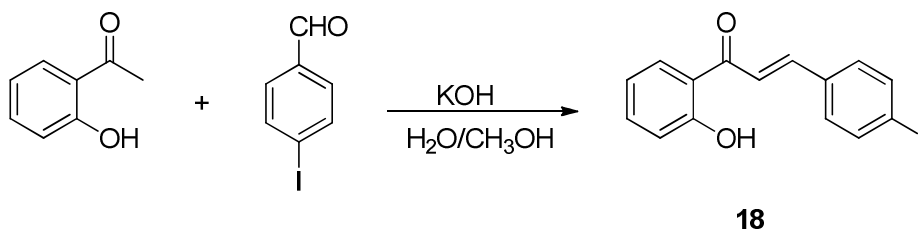


A solution of compound **20** (3.66 g, 10.1 mmol) in 1-butanol (150 mL) was treated with ammonium acetate (6.21 g, 80.5 mmol, 8 equiv) and the mixture was refluxed at 120°C for 20h. The product precipitated during the course of the reaction. After cooling, the reaction mixture was filtered to obtain 0.126 g of compound **23** (2% crude yield) as a brown product.

LCMS (95-95% acetonitrile in 0.05% TFA over 10 minutes) retention time = 5.48 min,

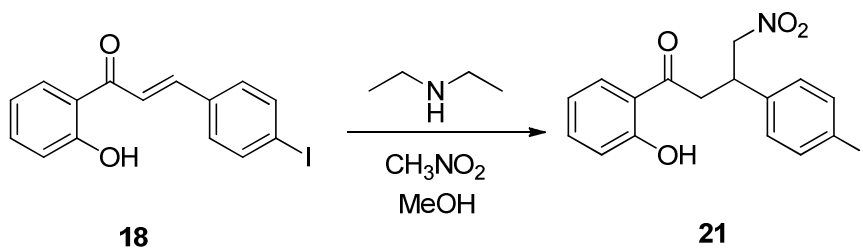
$C_{32}H_{21}Br_2N_3O_2$ $[M + H]^+ = 640$.

(E)-1-(2-hydroxyphenyl)-3-(4-iodophenyl)prop-2-en-1-one (18)



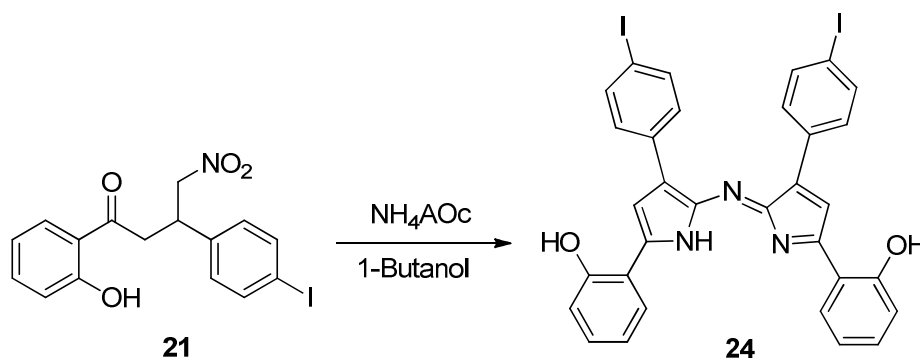
2'-hydroxyacetophenone (2.00 g, 1.77 mL, 14.7 mmol), 4-iodobenzaldehyde (3.41 g, 14.7 mmol, 1 equiv), and KOH (3.29 g, 58.7 mmol, 4 equiv) were dissolved in a 5:1 mixture of MeOH/H₂O (30 mL). The reaction mixture was stirred at room temperature for 25h. The mixture was quenched with concentrated HCl dropwise. During this process, the product precipitated, which was filtered, dried and collected to afford 6.72 g of **18** (~100% crude yield). LCMS (75-95% acetonitrile in 0.05% TFA over 10 minutes) retention time = 5.15 min, $C_{15}H_{11}IO_2$ $[M + H]^+ = 351$.

1-(2-hydroxyphenyl)-3-(4-iodophenyl)-4-nitrobutan-1-one (21)



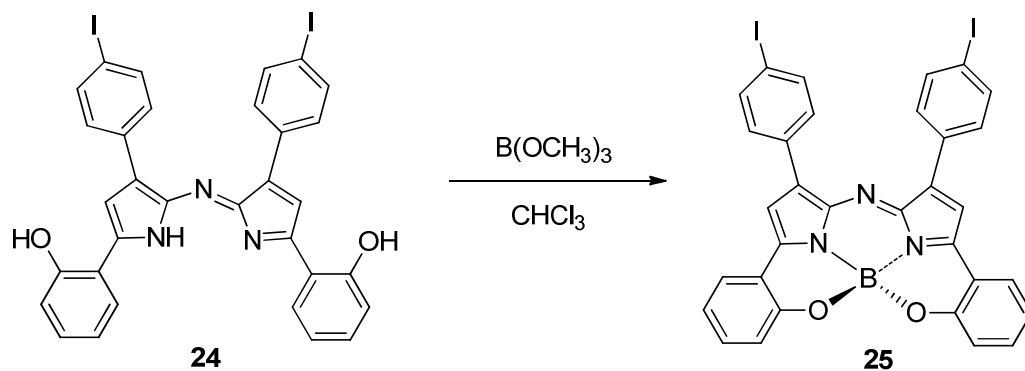
Compound **18** (3.0 g, 8.57 mmol) dissolved in MeOH (50 mL) was treated with nitromethane (2.49 g, 2.21 mL, 40.8 mmol, 5 equiv), and DEA (3.13 g, 4.43 mL, 5 equiv). The resulting reaction mixture was refluxed at 65°C for 19h. The mixture was cooled to 4°C (ice bath) and treated with concentrated HCl until there was no fume built-up. The aqueous solution was partitioned with CH₂Cl₂ (3 x200 mL). The organic layer was separated, dried over anhydrous Na₂SO₄, filtered, and concentrated to afford 2.70 g of compound **21** (77% crude yield). LCMS (75-95% acetonitrile in 0.05% TFA over 10 minutes) retention time = 3.52 min, C₁₆H₁₄INO₄ [M + H]⁺ = 412.29.

(Z)-2-(2-((5-(2-hydroxyphenyl)-3-(4-iodophenyl)-1*H*-pyrrol-2-yl)imino)-3-(4-iodophenyl)-2*H*-pyrrol-5-yl)phenol (**24**)



A solution of **21** (2.70 g, 6.56 mmol) in 1-butanol (100 mL) was treated with ammonia acetate (4.05 g, 52.4 mmol, 8 equiv). The reaction mixture was refluxed at 116 °C for 24h. During the course of the reaction, the product precipitated. After cooling, the product was filtered and dried to afford 0.555 g of compound **24** (12% crude yield) as a dark brown solid. LCMS (100% TFA over 10 minutes) retention time = 2.05 min, C₃₂H₂₁I₂N₃O₂ [M + H]⁺ = 734.

Bis(iodophenyl)-aza-(*O,N*)-chelated BODIPY **25**



Compound **24** (1.00 g, 1.36 mmol) dissolved in CH_2Cl_2 (75 mL) was treated with $\text{B(OCH}_3)_3$ (1.42 g, 1.52 mL, 13.6 mmol, 10 equiv). The reaction mixture was stirred at 37°C for 1h and 17h at room temperature. The progress of the reaction was followed by TLC. The reaction mixture was transferred to a separatory funnel and washed with H_2O (200 mL) and brine (100 mL). The organic layer was separated, dried over anhydrous Na_2SO_4 , filtered, and concentrated to afford 0.060 g of compound **25** (6% crude yield) as a dark blue solid. LCMS (100% isocratic acetonitrile over 10 minutes) retention time = 4.82, $\text{C}_{32}\text{H}_{18}\text{BI}_2\text{N}_3\text{O}_2$ $[\text{M} + \text{H}]^+$ = 742. (For the LCMS analysis, a small quantity of the isolated product was dissolved in 300 μL of DMSO due to the insolubility of the complex).

PNDC Activity: Boronate Oxidation Assay

Peroxonitrite in 0.1 N NaOH solution was prepared by the method of Pryor^x and frozen at -80°C (until needed for use). Stock solutions of 4-acetylphenylboronic acid and the catalyst (PNDC) were prepared in DMSO (in the range of 2-30 mM range). Small aliquots of PN solution were thawed, kept on ice, and the concentration was measured by UV/vis

spectroscopy (via Beer-Lambert Law, where $\epsilon_{\square} = 1670 \text{ M}^{-1}\text{cm}^{-1}$). PN concentrations ranged from 58-105 mM for these studies. In a typical procedure 3.00 mL of 100 mM phosphate buffer (pH = 7.4 or 7.2) which contained (concentration of 0.07% or 0.7%) surfactant (i.e. sodium docecyl sulphate, Brij® 35, or benzalkonium chloride) and 100 μM DTPA was pipetted into a cynalation vial equipped with a magnetic stir bar. 1.0×10^{-6} moles of 4-acetylboronic acid (24.4 μL of stock) was added followed by 1.0×10^{-6} moles of catalyst (aliquots from DMSO stock). The mixture was stirred at 600 rpm and retained at a temperature of 25 °C. To this rapidly stirred mixture, 1.0×10^{-6} moles of PN were added by a rapid injection. This reaction was allowed to stir for 1 minute. 1.00 mL of the reaction mixture was analyzed by LCMS (Waters Alliance-MS3100 system; 15% acetonitrile/ H_2O to 95% acetonitrile (0.05% TFA) over 10 minutes; Agilent Eclipse XD8-C-18 column, 5 μM , 4.6 x 150 mm, UV dection 280 nm for 4-hydroxyacetophenone oxidation product). Reactions were run in multiples ($n = 5$) and to standard control runs ($n = 5$) which contained everything except the catalyst (amounts of DMSO which were equivalent to those from aliquoted catalyst solutions were added to the control to compensate for the small effect of DMSO). The percent inhibition was determined by comparing the 4-acetylphenol peak areas for catalyst versus control. Sample calculations are shown below:

Control Runs: 1 eq PN + DMSO + BA	Peak (area) retention time = 5.48
1	89724
2	89298
3	85870
4	87877
5	86401
Average Oxidation Peak Area	87834
Standard Deviation (STDEV)	1705.0
Difference between the cat and control oxidation peak	41927.2
Percent Inhibition	47.7
Percent (\pm)	1.8
Reaction Runs: 1eq PN + BA + 1eq SR135	Peak (area) retention time = 5.45
1	45145
2	43759
3	47895
4	46708
5	46027
Average Oxidation Peak Area	45906.8
Standard Deviation	1565.46

Table 7. Example of SR135 activity in 0.7% Brij- 35 buffer at pH 7.4

Percent Inhibition Sample Calculations

A. Average Oxidation Peak Area:

$$\left(\frac{89724 + 89298 + 85870 + 87877 + 86401}{5} \right) = \mathbf{87834}$$

B. Difference between catalyst and control (oxidation peaks area):

$$87834 - 45906.8 = \mathbf{41927.2}$$

C. Percent Oxidation Inhibition:

$$(\text{Difference between } OX_{\text{catalyst}} \text{ and } OX_{\text{control}} / OX_{\text{control}}) * 100$$

$$\left(\frac{41927.2}{87834} \right) \times 100 = \mathbf{47.7}$$

D. Percent Oxidation STDEV:

$$\left(\frac{1565.46}{87834} \right) \times 100 = \mathbf{1.8}$$

E. Reported Value:

47.7 ±1.8 %

PNDC Activity: Prevention of Nitration Assay

Peroxyxynitrite in 0.1 N NaOH solution was prepared by the method of Pryor^x and frozen at -80 °C (until needed for use). Stock solutions of 4-acetylphenylboronic acid and the catalyst (PNDC) were prepared in DMSO (in the range of 2-30 mM range). Small aliquots of PN solution were thawed, kept on ice, and in alkaline solutions the concentration of PN was measured by UV/vis spectroscopy (absorbance at 302nm, where $\epsilon = 1670 \text{ M}^{-1}\text{cm}^{-1}$). PN concentrations ranged from 58-105 mM for these studies. In a typical procedure 2.00 mL of 100 mM phosphate buffer (pH = 7.4) which contained 0.7% surfactant (sodium dodecyl sulphate or Brij® 35) and 100 μM DTPA was pipetted into a cynalation vial equipped with a magnetic stir bar. 1.0×10^{-6} moles of LENK (168 μL of stock) was added followed by (1.0×10^{-7} , 2.0×10^{-7} , or 1.0×10^{-6} moles) of catalyst (aliquots from DMSO stock). The mixture was stirred at 600 rpm and retained at a temperature of 25 °C. To this rapidly stirred mixture, 1.0×10^{-6} moles of PN were added by a rapid injection. This reaction was allowed to stir for 1 minute. 1.00 mL of the reaction mixture was analyzed by LCMS (Waters Alliance-MS3100 system; 15% acetonitrile/H₂O to 95% acetonitrile (0.05% TFA) over 10 minutes; Agilent Eclipse XD8-C-18 column, 5 μM , 4.6 x 150 mm, UV detection 280 nm for 4-hydroxyacetophenone oxidation product). Reactions were run in multiples (n = 5) and compared to standard control runs (n = 5) containing everything except the catalyst (amounts of DMSO which were equivalent to those from aliquoted catalyst solutions were added to the control to compensate for catalyst vs control runs to determine percent inhibition. Another set of control runs (n=3) only contained buffer solution, LENK, catalyst, DMSO and no PN. This last set of controls were used to subtract a small buffer peak that overlapped with the nitro-LENK peak.

REFERENCES

1. Ma, Q. Advanced in Mechanism of Anti-Oxidation. *Discov. Med.* **2014**, *17*, 121-130.
2. Radi, R.; Szabo, C.; Ischiropoulos, H. Peroxynitrite: biochemistry, pathophysiology and development of therapeutics. *Na. Rev. Drug Discov.* **2007**, *6*, 662-680.
3. Peluffo, G.; Rafael, R. Biochemistry of protein tyrosine nitration in cardiovascular pathology. *Cardiovasc. Res.* **2007**, *75*, 291-302.
4. Kagan, V.E. et al. Cytochrome c/cardiolipin relations in mitochondria: a kiss of death. *Free Radical Biol. Med.* **2008**, *46*, 1439-1453.
5. Calcerrada, P.; Pelluffo, G.; Radi, R. Nitric Oxide-Derived Oxidants with a Focus on Peroxynitrite: Molecular Targets Cellular Responses and Therapeutic Implications. *Curr. Pharm. Des.* **2011**, *17*, 3905-3932.
6. Radi, R. Nitric Oxide, oxidants, and protein tyrosine nitration. *Proc Natl Acad Sci.* **2004**, *101*, 4003-4008.
7. Ferrer-Sueta, G.; Radi, R. Chemical Biology of Peroxynitrite: Kinetics, Diffusion, and Radicals. *ACS Chem. Biol.* **2009**, *4*, 161-177.
8. Radi, R. Protein Tyrosine Nitration: Biochemical Mechanisms and Structural Basis of Functional Effects. *Acc. Chem. Res.* **2013**, *46*, 550-559.
9. McKenna, R.; Silverman, D.N. et al *Free Radical Biol. Med.* **2006**, *40*, 453.
10. Surmeli, N.B.; Groves, N.K. et al. Peroxynitrite Mediates Active Site Tyrosine Nitration in Manganese Superoxide Dismutase. Evidence of a Role for the Carbonate Radical Anion. *J. Am. Chem. Soc.* **2010**, *132*, 17174-17185.
11. Souza, J.M.; Peluffo, G.; Radi, R. Protein tyrosine nitration-Functional alteration or just biomarker? *Free Radical Biol. Med.* **2008**, *45*, 357-366.

12. Godoy et al. Disruption of the M80-Fe ligation stimulates the translocation of cytochrome c to the cytoplasm and nucleus in nonapoptotic cells. *Proc Natl Acad Sci.* **2008**, *108*, 2653-2658.
13. Trujillo, M. Ferrer-Sueta, G.; Radi, R. Peroxynitrite Detoxification and Its Biologic Implications. *Antioxid. Redox Signaling* **2008**, *10*, 1607-1919.
14. Neumann, W.L. et al. Manganese (III) Complexes of Bis(hydroxyphenyl) dipyrromethenes Are Potent Orally Active Peroxynitrite Scavengers. *J. Am. Chem. Soc.* **2011**, *133*, 4200-4203.
15. Groves, J.T.; Maria, S.S. Peroxynitrite-Induced DNA Strand Scission Mediated by a Manganese Porphrin. *J. Am. Chem. Soc.* **1995**, *117*, 9578-9579.
16. Stern, M.K. et al. Peroxynitrite Decomposition Catalysts. *J. Am. Chem. Soc.* **1996**, *118*, 8735-8736.
17. Gross, Z. et al. Metalloporphyrins as cytoprotective agents against oxidative and nitritative stress in cellular models of neurodegeneration. *J. Neurochem.* **2010**, *113*, 363-373.
18. Kubota et al. Synthesis of Water-Soluble Dinuclear Mn-Porphyrin with Multiple Antioxidative Activities. *ACS Med. Chem. Lett.* [dx.doi.org/10.1021/ml400493f](https://doi.org/10.1021/ml400493f).
19. Wayman, N.S. et al. Ligand of the peroxisome proliferator-activated receptors (PPAR- γ and PPAR- α) reduce myocardial infarct size. *The FASEB Journal.* **2002**, *16*, 1027-1040.
20. Liu, K.G. et al. Synthesis and Biological Activity of L-Tyrosine-based PPAR γ Agonist with Reduced Molecular Weight. *Bioorg. Med. Chem. Lett.* **2001**, *11*, 311-3113.

21. Celi, F.S; Shuldiner, A.R. The Role of Peroxisome Proliferator-activated Receptor gamma in Diabetes and Obesity. *Curr. Diabetes Rep.* **2002**, *2*, 179-185.
22. Nelson, C.; Cox, M. Lehninger Principles of Biochemistry, 4th Ed.; W.H. Freeman and Company: New York, 2008.
23. Batinic-Haberle, I. et. al. Relationship among Redox Potentials, Proton Dissociation Constants of Pyrrolic Nitrogens, and in Vivo and in Vitro Superoxide Dismutating Activities of Manganese(III) and Iron(III) Water-Soluble Porphyrins. *Inorg. Chem.* **1999**, *38*, 4011-4022.
24. Batinic-Harberle, I. et. al. Superoxide Dismutase Mimics: Chemistry, Pharmacology, and Therapeutic Potential. *Antioxid. Redox Signaling.* **2010**, *13*, 877-918.
25. Neumann, W.L. et. al. Retooling Manganese(III) Porphyrin-Based Peroxynitrite Decomposition Catalysts for Selectivity and Oral Activity: A Potential New Strategy for Treating Chronic Pain. *J. Am. Chem. Soc.* **2011**, *54*, 8658-8669.
26. <http://www.sabiosciences.com/iapp/ppar.html#animdemo-ppar> (accessed 7/20/2014).
27. Ono, N. Barton-Zard pyrrole synthesis and its application to synthesis of porphyrins, polypyrroles, and dipyrromethenes dyes. *Heterocycles* **2008**, *75*, 243-284.
28. Radi, R.; Beckman, J.S.; Bush, K.M.; Freeman, B.A. *Proc. Natl. Acad. USA* **1990**, *87*, 1620-1624.
29. Lindsey, J.S.; Schreiman, I.C.; Hsu, H. C. Kearney, P. C.; Marguerettaz, A. M. Rothmund and Alder-Longo Reactions Revisited: Synthesis of Tetraphenylporphyrins under Equilibrium Conditions. *J. Org. Chem.* **1987**, *52*, 827-836.

30. Salvemini, D. et al. Targeting the Overproduction of Peroxynitrite for the Prevention and Reversal of Paclitaxel-Induced Neuropathic Pain. *J. Neurosci.* **2012**, *32*, 6149-6160.
31. Cammidge, A.N.; Öztürk, O. Controlled scrambling in porphyrin synthesis-selective synthesis of 5, 10-disubstituted porphyrins. *Tetrahedron Lett.* **2001**, *42*, 355-358.
32. Burgess, K. et al. Functionalized BF₂ chelated azadipyrromethene dyes. *Tetrahedron.* **2008**, *64*, 3642-3654.
33. http://www.waters.com/waters/en_US/HPLC---High-Performance-Liquid-Chromatography/nav.htm?cid=10048919&locale=en_US (last accessed: 8/1/2014)
34. O'Shea, D. F. et al. In Vitro Demonstration of the Heavy-Atom Effect for Photodynamic Therapy. *J. Am. Chem. Soc.* **2004**, *126*, 10619-10631.
35. Barnham, K. J.; Masters, C. L.; Bush, A. I. *Nat Rev Drug Discov* **2004**, *3*, 205-214.
36. Miyaura N.; Sakaki, M.; Saito, S. A synthesis of biaryl via nickel(0)-catalyzed cross-coupling reaction of chloroarenes with phenylboronic acid. *Tetrahedron Lett.* **1996**, *37*, 2993-2996.
37. Gujral, S. S.; Khatri, S.; Riyal, P.; Gahlot, V. Suzuki Cross-Coupling Reactions Review. *Indo Global J. Pharm. Sci.* **2012**, *2*, 351-367.
38. O'Shea, D.F. et al. B, O-chelated Azadipyrromethenes of Near-IR Probes. *Org. Lett.* **2008**, *10*, 4771-4774.
39. Ulrich, G. et al. The Chemistry of fluorescent Bodipy Dyes: Versatility Unsuppassed. *Angew. Chem. Int. Ed.* **2008**, *47*, 1184-1201.
40. Kalyanaraman, B. et al. Peroxynitrite is the Major Species Formed from Different Flux Ratio of Co-generated Nitric Oxide and Superoxide: Direct Reaction with Boronate-Based Fluorescent Probe. *J. Bio. Chem.* **2010**, *285*, 14210-14216.

41. Kalyanaraman, B. et al. Direct oxidation of boronates by peroxyxynitrite: Mechanism and implications in fluorescence imaging of peroxyxynitrite. *Free Radic. Biol. Med.* **2009**, *47*, 1401-1407.
42. Singer, M.M.; Tjeerdema, R.S. Fate and effects of the surfactant sodium dodecyl sulfate. *Rev. Environ. Contam. Toxicol.* 1993, *133*, 95-149.
43. Deo, S.K.; Daunert, S. An Immunoassay for Leu-enkephalin Based on C-terminal Aequorin-Peptide Fusion. *Anal. Chem.* **2011**, *73*, 1903-1908.
44. Krainev, A.G.; Williams, T.D.; Bigelow, D.J. Enzymatic Reduction of 3-Nitrotyrosine Generates Superoxide. *Chem. Res. Toxicol.* **1998**, *11*, 495-502.
45. Wang, B. et al. A BODIPY fluorescense probe modulated by selenoxide spirocyclization reaction for peroxyxynitrite detection and imaging in living cells. *Dyes Pigm.* **2013**, *96* , 383-390.
46. Villamena, F.A.; Zweier, J.L. Detection of Reactive Oxygen and Nitrogen Species by EPR Spin Trapping. *Antioxid. Redox. Signal.* **2004**, *6*, 619-629.
47. Gopalakrishnan, B. et al. Detection of Nitric Oxide and Superoxide Radical Anion by Electron Paramagnetic Resonance Spectroscopy from Cells using Spin Traps. *J. Vis. Exp.* **2012**, doi:10. 3791/2810.
48. Reaction between Peroxyxynitrite and Boronates: EPR Spin-Trapping, HPLC Analyses, and Quantum Mechanical Study of the Free Radical Pathway. *Chem. Res. Toxicol.* **2011**, *24*, 687–697.
49. Borberly, S. Aggregate Structure in Aqueous Solutions of Brij-35 Nonionic Surfactant Studied by Small-Angle Neutron Scattering. *Langmuir* **2000**, *16*, 5540-5545.

50. Dominguez, A. et al. Determination of Critical Micelle Concentration of Some Surfactants by Three Techniques. *J. Chem Educ.* **1997**, *74*, 1227-1231.
51. <http://www.who.int/mediacentre/factsheets/fs312/en/> (accessed 8/7/2014)
52. Duplain, H. et al. Stimulation of peroxynitrite catalysis improves insulin sensitivity in high fat diet-fed mice. *J. Physiol. Soc.* **2008**, *586*, 4011-4016.
53. Saha, T. K.; Yoshikawa, Y.; Sakurai, H. A [*meso*-Tetrakis(4-sulfonatophenyl) porphyrinato] zinc(II) Complex As an Oral Therapeutic for the Treatment of Type 2 Diabetic KKA^y Mice. *Chem. Med. Chem.* **2007**, *2*, 218-225.
54. Larsen, T.M.; Toubro, S.; Astrup, A. PPARgamma agonists in the treatment of type II diabetes: is increased fatness commensurate with long-term efficacy? *Int. J. Obesity.* **2003**, *27*, 147-161.
55. <http://www.piercenet.com/product/brij-35-detergent-solutions> (8/7/2014).
56. Groves, J. T.; Lee, J.; Hunt, J. A. Manganese Porphyrins as Redox-Coupled Peroxynitrite Reductases. *J. Am. Chem. Soc.* **1998**, *120*, 6053-6061.
57. Tahirat, N.; Luis, A.; Mindy, L. Determination of Critical Micelle Concentration Using UV-Visible Spectroscopy. *J. High School Res.* **2011**, *2*, 1-6.
58. Gross, Z. et al. Manganese Corroles Prevent Intracellular Nitration and Subsequent Death of Insulin-Producing Cells. *ACS Chem. Biol.* **2009**, *4*, 910-914.
59. http://openwetware.org/wiki/Critical_micelle_concentration_%28CMC%29 (accessed 9/23/2014).
60. Stadler, K. Peroxynitrite-Driven Mechanism in Diabetes and Insulin Resistance-the Latest Advances. *Curr. Med. Chem.* **2011**, *18*, 280-290.
61. Chinchilla, R.; Najera, C. *Chem. Rev.* **2007**, *107*, 874-922.